Sudan University of Science and Technology

College of Graduate Studies

Structural, Thermal and Optical Properties of PVA/$AgNO_3$ thin Films Using Gamma Irradiation Method

الخصائص التركيبية و الحرارية والضوئية لأفلام البولي فينايل الكحول المطعمة بنترات الفضة بإستخدام طريقة أشعة قاما

A thesis submitted for the fulfillment of the award of PhD in Physics

By:

Ibrahim Mohammed Osman Babiker

Supervisor:

Prof. Mubarak Dirar Abdalla

Co-supervisor:

Prof. Ahmed Elhassan Elfaki

November 2021

الآيـــــــــة

قـــــــــال تعالى :

بِسْمِ اللَّهِ الرَّحْمَنِ الرَّحِيمِ

اقْرَأْ بِاسْمِ رَبِّكَ الَّذِي خَلَقَ (1) خَلَقَ الْإِنْسَانَ مِنْ عَلَقٍ (2) اقْرَأْ وَرَبُّكَ الْأَكْرَمُ (3) الَّذِي عَلَّمَ بِالْقَلَمِ (4) عَلَّمَ الْإِنْسَانَ مَا لَمْ يَعْلَمْ (5) كَلَّا إِنَّ الْإِنْسَانَ لَيَطْغَى (6) أَنْ رَآهُ اسْتَغْنَى (7) إِنَّ إِلَى رَبِّكَ الرُّجْعَى (8) أَرَأَيْتَ الَّذِي يَنْهَى (9) عَبْدًا إِذَا صَلَّى (10) أَرَأَيْتَ إِنْ كَانَ عَلَى الْهُدَى (11) أَوْ أَمَرَ بِالتَّقْوَى (12) أَرَأَيْتَ إِنْ كَذَّبَ وَتَوَلَّى (13) أَلَمْ يَعْلَمْ بِأَنَّ اللَّهَ يَرَى (14) كَلَّا لَئِنْ لَمْ يَنْتَهِ لَنَسْفَعًا بِالنَّاصِيَةِ (15) نَاصِيَةٍ كَاذِبَةٍ خَاطِئَةٍ (16) فَلْيَدْعُ نَادِيَهُ (17) سَنَدْعُ الزَّبَانِيَةَ (18) كَلَّا لَا تُطِعْهُ وَاسْجُدْ وَاقْتَرِبْ (19).

سورة العلق

﴿وَيَسْئَلُونَكَ عَنِ الرُّوحِ قُلِ الرُّوحُ مِنْ أَمْرِ رَبّي وَما أُوتِيتُمْ مِنَ الْعِلْمِ إِلاَّ قَلِيلًا﴾

سورة الإسراء الاية ﴿85﴾

Dedication

Every challenging work needs self-efforts as well as guidance of elders especially those whom are very close to our heart.

I wish to dedicate this humble effort to the best mum in the world, to my brothers and sisters, their calls and prayers keep me strong, to the soul of my dad, you were the best father, rest in peace…

Acknowledgement

First of all, I would like to thank the almighty God, you have kept me alive and gave me power to do this work, I am so grateful. Secondly, I would like to thank everyone who has contributed in some way to my thesis. I am immensely grateful to Professor ***Mubarak Dirar*** *for his guidance, inspiration and patience during my thesis period. As my doctoral advisor, he gave me a research project to make my own and pushed me to keep moving on to the next step. When things didn't work well, that wasn't a dead end, it was a reason to read and discover more, but he always made me feel as if I was on the right track. I truly appreciate his enthusiasm for new information, and I am thankful for the time we spent discussing it. I am grateful to Dr.* ***Ahmed Elhassan Elfaki*** *for his motivation, monitoring, guidance, assistance and for his immense support.*

I express my appreciation to all my family and friends, thanks for your encouragement and your immense support, especial thanks to Dr. ***Abdalla Eldoma*** *from (SSMO). I also extend my appreciation to Mr.* ***Khalid Yagoub*** *from National Cancer Institute – Algazira University and Dr.* ***Eltaher Sam*** *from (SUST). I appreciate my friend's encouragement* ***Suliman, Waleed, Yasir, Virginie, François, Ariane, Margot, Yaseen, Anne*** *and* ***Osman****.*

Abstract

Polymeric materials are of great interest in scientific and technological research and play an important role in our modern daily life, they can be tailored to meet specific requirement for vast applications, and this is mainly due to their light weight, good mechanical strength, thermal stability and optical properties. Polyvinyl Alcohol (PVA) is one of the most important polymeric materials and the most utilized polymer in the last decades, due to its interesting applications in technology, biomedical and industry, it's also of relatively low cost and easy in manufacturing. Furthermore, it is well documented that structural, thermal, mechanical, electrical and optical properties of polymers can be improved to a desired limit through suitable doping. In this concern and since Ag^{+} ions is a fast conducting ion in a number of crystalline and amorphous materials, its incorporation within a polymeric system may be expected to enhance its thermal, mechanical, electrical and optical properties.

This present study intended to investigate the effects of γ-ray irradiation and the concentration of the inorganic dopants ($AgNO_3$) on the structural, thermal and optical properties of the composite material. PVA/Ag composites with different contents of inorganic filler i.e. (5, 10, 15 and 20) wt% Ag were prepared by reduction of Ag^{+} ions in PVA solution using gamma irradiation with different doses i.e. (0, 5 and 10) Gy. Structural studies of the synthesized PVA/Ag composites were carried out using X-ray diffraction (XRD) technique; thermal studies have been carried out using simultaneous thermal analysis (STA), i.e. thermogravimetric analysis (TGA) and differential scanning calorimetry (DSC). Furthermore, the dependence of the optical properties of PVA on the concentration of the filler as well as the effects of γ-irradiation has been studied through UV-Vis spectroscopy.

The results showed that the irradiation of the PVA/Ag films with γ-ray doses induces color change and the color intensity increases with increasing γ-ray doses. Measurements of the onset temperature of thermal decomposition showed that the composite material of PVA/Ag was more thermally stable than its pristine components, i.e. pristine PVA and $AgNO_3$ and the thermal stability improved with the increment of $AgNO_3$ concentrations and the applied radiation doses. DSC thermograms show that melting points shift to higher temperatures with increasing radiation dose and filler concentration. UV-Vis analysis of the films showed absorption band peaking at the wavelengths around 230 and 450 nm and the intensity of peaks in proportional increment with radiation dose. In addition, the specific absorbance and the absorption coefficient of the films were found to be directly proportional to the applied γ-ray doses. Moreover, γ- irradiation of PVA/Ag samples leads to the formation of Ag nanoparticles, and chain scission and/or cross-linking in the polymer as confirmed by XRD analysis, these consequently improved the thermal, optical and mechanical properties of the prepared films.

المستخلص

تحظى المواد البوليميرية باهتمام كبير في البحث العلمي والتكنولوجي وتلعب دورًا مهمًا في حياتنا اليومية الحديثة، ويمكن تصميمها لتلبية متطلبات محددة للتطبيقات الواسعة، ويرجع ذلك أساسًا إلى وزنها الخفيف وخصائصها الميكانيكية الجيدة واستقرارها الحراري والخصائص البصرية الجيدة. يعد مركب PVA (PolyVinylAlcohol) أحد أهم المواد البوليميرية والأكثر استخدامًا حاليا وخلال العقود الماضية، نظرًا لتطبيقاته المثيرة للاهتمام في التكنولوجيا والطب الحيوي والصناعة، كما أنه منخفض التكلفة نسبيًا وسهل التصنيع. علاوة على ذلك، من الموثق جيدًا أن الخصائص التركيبية والحرارية والميكانيكية والكهربائية والبصرية للبوليمرات يمكن تحسينها إلى الحد الأقصى المطلوب من خلال إضافة بعض المنشطات المناسبة. في هذا الصدد، وبما أن أيونات +Ag هي أيون سريع التوصيل في عدد من المواد البلورية وغير المتبلورة، فمن المتوقع أن يؤدي دمجها في نظام بوليمري إلى تعزيز خصائصها الحرارية والميكانيكية والكهربائية والبصرية.

تهدف هذه الدراسة إلى معرفة تأثير أشعة جاما وتركيز المادة غير العضوية ($AgNO_3$) على الخواص التركيبية والحرارية والبصرية للمادة المركبة (PVA/Ag). تم تحضير مركبات (PVA/Ag) بتراكيز مختلفة من الإضافات غير العضوية بنسبة (5 ، 10 ،15 و 20)% بالنسبة للوزن الكلى عن طريق إضافة أيونات Ag^+ في محلول PVA و باستخدام تشعيع جاما بجرعات مختلفة من (0 ، 5 ، 10) Gy. تمت دراسة الخصائص الحرارية لمركبات PVA / Ag باستخدام التحليل الحراري المتزامن (STA)، والذى يشتمل التحليل الحراري الوزني (TGA) والقياس الحراري للمسح التفاضلي (DSC). علاوة على ذلك ، تمت دراسة اعتماد الخواص البصرية للـ PVA على تركيز المادة المالئة وكذلك تأثيرات التشعيع وذلك باستخدام مقياس الطيف الضوئي للأشعة المرئية وفوق البنفسجية (UV-Vis).

أظهرت النتائج أن تشعيع أغشية PVA/Ag بجرعات γ-ray يؤدي إلى تغير اللون وزيادة كثافة اللون مع زيادة الجرعات المسلطة. أظهرت قياسات درجة حرارة بداية التحلل الحراري أن المادة المركبة لـ PVA/Ag كانت أكثر ثباتًا حرارياً من مكوناتها الأصلية، أي PVA و $AgNO_3$ البكر، و قد تحسن الاستقرار الحراري مع زيادة تركيز $AgNO_3$ وجرعات الإشعاع المطبقة. كما بينت الرسوم البيانية الحرارية (DSC) أن نقاط الانصهار تتحول إلى درجات حرارة أعلى مع زيادة جرعة الإشعاع وتركيز $AgNO_3$. أظهر تحليل مقياس الطيف الضوئي للأشعة المرئية وفوق البنفسجية للأفلام أن نطاق الامتصاص يبلغ ذروته عند الأطوال الموجية حول 230 و 450 نانومتر وشدة قمم الإمتصاص في زيادة طردية مع جرعة الإشعاع المطبقة. بالإضافة إلى ذلك، فإن الامتصاص النوعي ومعامل الامتصاص للأفلام يتناسبان طرديا مع جرعات أشعة جاما المطبقة. إلى ذلك، يؤدي التشعيع بأشعة γ-ray إلى تكوين الجسيمات النانوية (Ag nanoparticles) وانفصال السلسلة والربط المتبادل (chain scission and/or cross-linking) في جزيئات البوليمر وبالتالي تحسين الخصائص الحرارية البصرية والميكانيكية للمادة الجديدة.

Contents

List of Tables

List of figures

List of Abbreviations

Abbreviation	statement
PVA	Polyvinyl Alcohol
$AgNO_3$	Silver Nitrate
TLD	Thermos Luminescent Dosimeter
TGA	Thermogravimetric Analysis
DTGA	Derivative of TGA
DSC	Differential Scanning Calorimetry
DDSC	Derivative of DSC
STA	Simultaneous Thermal Analysis
NMR	Nuclear Magnetic Resonance
FTIR	Fourier Transform Infra-Red Spectroscopy
CPs	Conducting Polymers
ELF	Extremely Low Frequency waves
ICRU	International Commission of Radiation Units
ICRP	International Committee for Radiation Protection
Gy	Gray
amu	Atomic Mass Unit
CB	Conduction Band
CV	Valance Band
HOMO	Higher Occupied Molecular Orbital
LUMO	Lower Unoccupied Molecular Orbital
FSD	Focal to Skin Distance
SSD	Surface to Skin (Surface) Distance
SAD	Source Axial Distance technique

TPS	Treatment Planning System
UV-Vis	Ultraviolet-visible Spectroscopy
C.I	Crystallinity Index
FS	Field Size
XRD	X-ray Diffractometry
XRF	X-ray Fluorescence
SEM	Scanning Electron Microscope
TEM	Transmission Electron Microscope
IAEA	International Atomic Energy Agency
EURATOM	European Atomic Energy Community
ESAK	Entrance Surface Air Kerma
ESD	Entrance Skin (Surface) Dose
NRPB	National Radiation Protection Board
DOG	Degree of Grafting
SPR	Surface Plasmon Resonance
KERMA	Kinetic Energy Released per Unit Mass
OSL	optically stimulated luminescence
PPT	Part Per Thousand
FWHM	Full width at Half Maximum

Chapter one: Introduction

1.1 Preface

Polymer materials are of great interest in scientific and technological research. Solid polymer blends have been intensively studied due to their potential applications for novel systems and devices (Alan, 2002; Chiang et al., 1977; Long et al., 2012). By addition of dopants, blends, or copolymers to the main polymer matrix, the optical, electrical, thermal, mechanical and electrochemical properties of these materials could be selectively modified obtaining particular characteristics in various applications in different fields of science (Chiang et al., 1977; Chuange et al., 2008). This field of polymer additives has attracted strong interest in today's materials research, as it is possible to achieve impressive enhancements of material properties as compared with the pure polymers (Kros et al., 2007; Long et al., 2012; Reda et al., 2012). Furthermore, irradiation of polymers has established itself as one of the most acceptable, easy and non-toxic approach to alter polymer properties significantly (Alan, 2002; Chiang et al., 1977; Long et al., 2012). Irradiation of polymers destroys the initial structure by introducing defects inside the material which leads to changes in the properties of these polymers. Ionizing radiation effects on polymers include cross-linking of the molecular chains, degradation of macromolecules and changes in the number and nature of the double bonds (Alan, 2002; Chiang et al., 1977). This entire process can occur either in one or all together, depending on the chemical nature of the polymer, radiation dose applied and other external factors.

Polyvinyl alcohol (PVA) is the most studied polymer throughout the last few years in scientific research and continues to attract considerable attention due to its fascinating and desirable characteristics specifically for

various pharmaceutical and biomedical applications and also due to its relatively simple chemical structure with a pendant hydroxyl group (Chuang et al., 2008; Yamauchi et al., 2005). PVA is highly hydrophilic, non-toxic and biocompatible polymer with excellent film formation by casting (Alan, 2002; Chiang et al., 1977; Long et al., 2012). PVA has been of particular interest also due to its abundance, high absorption coefficients in the visible light, chemical stability, easy polymerization, and low cost of monomer (Bhadra et al., 2007; Goto, 2011; Khanna et al., 2005; Stejskal et al., 2002).

Inorganic additives, such as transition metal salts, have considerable effects on the optical, thermal and electrical properties of PVA (Bhadra et al., 2007; Kaeami et al., 2003; Reda et al., 2012). PVA doped with inorganic metals such as silver (Ag) (Khanna et al., 2005; Wankhede et al., 2013), gold (Au) (Sridevi et al., 2011), Copper (Cu) (Athawale et al., 2003), TiO_2 (Nabid et al., 2008) and CeO_2 to form PVA/metal composite films and hydrogels have been used to improve physical, mechanical, and electrical properties of these composite materials. Since silver has a very good electrical conductivity among all the metals; the combination of PVA/Ag with uniform dispersion can yield functional composite material with enhanced electrical properties. The obtained composites have characteristic advantages compared to their single component counterparts and can have potential applications in new devices (Gao et al., 2005; G.A. Snook et al., 2011; J. Lui et al., 2014; S. Bhadra, 2009). In particular, transition metal particles dispersed/encapsulated within a polymer matrix can offer attractive and practicable routes for combining properties arising from metal particles and from that of polymers (Lee et al., 2007; Lin et al., 1998; Nabid et al., 2008). This could greatly improve the optical and dielectric properties of the PVA composites. These particles could act as conductive junctions between the PVA chains that resulted in an increase

of the electrical conductivity of the composites (Alan, 2002; Marija et al., 2004). Several methods have been employed to prepare polymer–metal composites such as blending of both components and irradiation (Chiang et al., 1977; Chuang et al., 2008; Long et al., 2012). All these metallic particles (Gold, Silver, Platinum...etc) exhibit unusual electrical, magnetic, optical and electrochemical properties due the near-free conduction electrons, which are dependent on their size, surface Plasmon, surface free energy and surface area, as well as on the surrounding dielectrics (Stakeev et al., 1999).

Among these important metal particles used, silver (Ag) particles are of great interest in today's materials world due to its special electronic, optical, and magnetic properties (Khanna et al., 2005; Reda et al., 2012; Wankhede et al., 2013) and its wide variety of applications in catalysis (Athawale et al., 2003), conducting inks, microelectronics, thick-film electrode material, and solar cells (Chiang et al., 1977; Long et al., 2012). These mentioned properties are dependent on the particle size, shape and the method of composites synthesis. Varieties of synthesis method have been developed, including reduction from metallic salts, ultrasonic irradiation technique, ion implantation, and thermal process and microwave technique (Reda et al., 2012; Sridevi et al., 2011; Stejskal et al., 2002). However, fabrication of PVA/Ag composite films without using of toxic chemical agents still remains highly challenging. This challenge may be surpassed by using irradiation technique which has a capability to produce polymer and metal particle components without using any chemical agents. The synthesis of silver composites by using γ- irradiation has been mentioned by Ali et al., (2007). The combination of PVA as polymer with silver as a noble metal may produce hybrid composed material that possesses very interesting behaviors (Reda et al., 2012).

1.2 Significance Of The Study

The following study will help in broadening and encouraging the applications of ionizing radiation and radiochromic films in industrial sector especially the food sector (food irradiation, dose monitoring, labels, ...etc) as well as its energy applications (solar cells, energy storage and electrodes for supercapacitors). It can helps also establish a local in vivo dosimeter system to measure the entrance and exit dose with local available materials in Sudan's radiotherapy centers and to the private clinics lacking the frequent radiation exposure assessment tools. Thus, it will be as fast, easy and cheap assessment tool with only a presence of software and/or a densitometer which are the cheapest equipment used in the radiation exposure assessment.

1.3 Problems Of The Study

Over the past decades, the use of nuclear irradiation for medical and industrial applications has rapidly increased. The irradiation processing is being used for several purposes, such as food irradiation, sterilization of surgical equipments, polymerization and cross-linking of polymers (Gao et al., 2005; Riyadh et al., 2011). This irradiation technique has been demonstrated on a large commercial scale to be a very effective means of improving end use properties of various polymers (Riyadh et al., 2011). It is a well-established and economical method of precisely modifying the properties of bulk polymer resins and formed polymer components (Alan, 2002; Reda et al., 2012; Riyadh et al., 2011). Therefore, it is important to accurately measure the radiation dose delivered during processing. The use of solutions as standards and the changes in the oxidation states and colours has been largely demonstrated. However, these solutions require careful handling and the changes need to be detected by some external auxiliary instruments such as UV-Vis spectrophotometer, ESR, NMR, FTIR and thermo-luminescence devices (TLD), etc. The field of dosimetry

is being changing rapidly, and dosimeters which can be read directly without the help of these auxiliary instruments are now a reality using polymeric films (Gao et al., 2005; Riyadh et al., 2011). Such light-weight, fast, cheap and portable detectors, which can be easily put at any location, are very much practicable and possess many medical, industrial and security applications. One of these practicable applications would be helping to detect pilfering of nuclear sources and carrying these devices by terrorist groups.

Ionizing radiation has significant capabilities to induce chemical and physical changes in the exposed materials. Studies on irradiated polymers show many advantages of induced radiation changes on which can be quantified and qualified to deduce the amount of radiation dose and exposure. This method relative to other methods such as film badge is very simple and easy. The advantages include no developer, no fixer, no other effecting factors, and the process occurred at a solid-site condition, fast method and inexpensive, environmental friendly and controllable acquisition (Attix et al., 1986; Reda et al., 2012).

1.4 Scope Of The Study

Ionizing radiation has significant capabilities to induce physical and chemical changes in the exposed materials. The following study will highlights the exposure dose based on the PVA/$AgNO_3$ composites change due to irradiation by using XRF and UV-Vis spectroscopy. The practical applicability of polymer/metallic composites and Conducting Polymers (CPs) depends on their electrochemical properties, environmental and thermal stabilities (Abthagir et al., 1998). Although their methods of preparation, morphology and electrochemical characterizations have been extensively studied, research on the evaluation of their thermal properties has received less attention. Only a small amount of work has been devoted to this subject (Mallakpour et al., 2009). Thermal stability of composite

and CPs is useful for their applicability to various technologies (Abthagir et al., 2004). In this study Thermogravimetric Analysis (TGA) is used to study the thermal stabilities of the PVA/$AgNO_3$ composites. Deferential scanning calorimetry (DSC) is also performed. XRD is used to study structural changes of the composite films.

1.5 Hypothesis Of The Study

The researcher hypothesize that Sudanese radiation therapy centers have high exposure dose to the skin of the patients during treatment with radiation which is incompatible with the policy of radiation therapy system. Also there is a lack in facilities for assessment and measuring the in vivo dosimetry especially entrance and exit doses. This malaise of over dose is also reported in the workers of the petroleum (NDT) and mining sectors. This study also hypothesize that the under valuation and utilization of irradiation, polymeric materials and radiochromic films in the industrial sector in Sudan, in particular the food industry. The study also hypothesize that composite films matrix could have underpinning behaviors between electrical property of PVA and optoelectronic property of silver particles for new devices and applications and that gamma irradiation could be used for further enhancement of its mechanical, thermal and optical properties.

1.6 Objectives Of The Study

The aim of this work is to study a simultaneous synthesis of polyvinyl alcohol (PVA) and silver nitrate ($AgNO_3$) composite films using gamma irradiation method. The effects of dose and silver nitrate concentration on structural, mechanical, thermal and optical properties of the final PVA/$AgNO_3$ composite films will be carefully examined. The composite film matrix could have underpinning behaviors between electrical property of PVA and optoelectronic property of silver particles for new devices and applications. The aim is also to investigate the feasibility of modifying its

mechanical, thermal and optical properties to study the possibility of further enhancement of these properties using gamma irradiation.

The Specific Objectives Of This Work are to:

- Fabricate functional composite material with enhanced mechanical, thermal and optical properties.
- Measure the activation energy of thermal decomposition for PVA/$AgNO_3$ composite films.
- Measure glass transition temperatures and melting temperatures for PVA/$AgNO_3$ composite films.
- Measure the onset temperature of thermal decomposition for PVA/$AgNO_3$ composite films.
- Evaluate and assess the effect of $AgNO_3$ concentration on the thermal stability of the PVA/$AgNO_3$ composite films.
- Evaluate and assess the effect of radiation dose on the thermal stability of the PVA/$AgNO_3$ composite films.
- Explore the synthetic of PVA/$AgNO_3$ films to be used as chemical radiation dosimeter.
- Study the possibility of using PVA/$AgNO_3$ composite films as radiation monitor.
- Evaluate and assess the effect of radiation dose in PVA/$AgNO_3$ composite films and measure the absorption spectra post irradiation.
- Evaluate and assess the effect of $AgNO_3$ concentration in PVA/$AgNO_3$ composite films.
- Determine the absorption coefficients of the PVA/$AgNO_3$ composite films.
- Find the correlation between the absorption coefficients and the applied radiation doses.
- Determine the optical band gap (E_g) of the PVA/$AgNO_3$ composite films.

1.7 Thesis Layout

The backbone of the following thesis is formed of five chapters. The first chapter deals with the general introduction about the research background, scope of the study, problem statement, and hypothesis of the study as well as its objectives. The second chapter introduces the literature review, the theoretical background and previous studies. The third chapter contains the methodology of the study, including materials used, samples preparation, equipment and measurements. The fourth chapter covers the results in details while the last chapter contains discussion, conclusion and recommendations. Appendices are listed at the end of this thesis.

Chapter two

Theoretical Background and Literature Review

2.1 Theoretical Background

2.1.1 Ionizing Radiation

Ionizing radiation refers to a broad energetic spectrum of electromagnetic waves or high velocity atomic or subatomic particles. This radiation can be categorized according to their ability to ionize the media. Non-ionizing radiation is electromagnetic radiation that does not have sufficient energy to remove an electron from the atom. The various types of non-ionizing radiation are ultra violet (UV), visible light, infrared (IR), microwaves and extremely low frequency (ELF) waves. On the other hand, ionizing radiation is electromagnetic radiations, such as X-rays, γ-rays and charged particles (electrons, α-particles and β-particles) which possess sufficient energy to ionize an atom by removing at least an orbital electron. According to the 1996 European Guideline of the European Atomic Energy Community (EURATOM), electromagnetic radiation with a wavelength of 100 nm or less is considered as ionizing radiation, this is corresponding to ionizing potential of 12.4 eV or more (Smith, 2000). The ionization potential is dependent on the electronic structure of the target material and is generally in the range of 4 – 25 eV.

The International Commission of Radiation Units (ICRU) has classified the ionizing radiation based on the mechanisms by which they ionize the atom. Direct ionizing radiations are fast charged particles, such as alpha particles, electrons, beta particles, protons, heavy ions, and charged mesons; these particles transfer their energy to the orbital electron directly and ionize the atom by means of Columbic force interactions along their track. Indirect ionizing radiations are uncharged quantum, such as

electromagnetic radiations (X-rays and γ-rays), neutrons, and uncharged mesons; these particles undergo interactions with matter by indirectly releasing secondary charged particles which then take turn to transfer energy directly to orbital electrons and ionize the atom. Some properties of ionizing radiation are shown in Table (2.1) (Smith, 2000).

Table (2.1): Some properties of different ionizing radiation

Characteristics	Alpha	Proton	Beta or electron	Photon	Neutron
Symbol	$_{2}^{4}\alpha$ or $_{2}^{4}He^{+2}$	$_{1}^{1}p^{+}$ or $_{1}^{1}H$	$_{-1}e$ or β	γ- or X-rays	$_{0}^{1}n$
Charge	+2	+1	-1	Neutral	Neutral
Ionization	Direct	Direct	Direct	Indirect	Indirect
Mass (amu)	4.00277	1.007276	0.000548	-	1.008665
Velocity (m/s)	6.944×10^{6}	1.38×10^{7}	2.82×10^{8}	2.998×10^{8}	1.38×10^{7}
Speed of light	2.3%	4.6%	94%	100%	4.6%
Range in air	0.56 cm	1.81 cm	319 cm	820 m	39.25 cm

1 atomic mass unit (amu) = 1.6×10^{-27} kg.
Speed of light c = 3.0×10^{8} m/sec.

2.1.2 Radiation Sources

The sources of ionizing radiation can be divided into two categories namely as natural and man-made sources. The first natural source is cosmic radiation which is the radiation coming from outside our solar system as positively charged ions (protons, alpha, heavy nuclei), these ions interact with atmosphere to produce secondary radiations such as x-rays, muons, protons, alpha particles, pions, electrons and neutrons. The second natural source is external terrestrial sources which represent the radioactive materials found naturally in the earth crust, rocks, water, air and vegetations. The major radionuclides found in the earth crust are

Potassium-40, Uranium-235, and Thorium-210. Main sources of man-made radiations are in the form of medical diagnostic X-ray, radiation therapy, nuclear medicine and sterilization. The common radioactive sources are ^{131}I, ^{99m}Tc, ^{60}Co, ^{192}Ir, ^{90}St and ^{137}Cs. Other man-made sources include occupational and consumption products that originated in mines, combustible fuel (gas, coal), ophthalmic glasses, televisions, luminous, X-rays scanners at the airports, smoke detectors (Americium-241) and fluorescent lamp starters, nuclear fuels, nuclear accidents and nuclear weapons. The yield of artificial sources is represented either as quantum in X-rays and γ- rays or as high energy particles such as beta particles (β), alpha particles (α), neutrons and electrons (Smith, 2000). Most types of radiation sources discussed above are used in medicine, industry, and research. Today the most common radiation sources used in Sudan is ^{60}Co, which is an artificial source of γ radiation as well as linear accelerators for photon and electron beams having potential energy ranging from 0.3-10 MeV to 20 MeV. Table (2.2) shows the radiation sources commonly used in industry and research.

Table (2.2): Common sources of ionizing radiation (Smith, 2000).

Category	Source
Nuclear power	^{235}U fission products, ^{90}Sr, ^{137}Cs
Occupational exposure	X-ray, isotopes for γ- rays
Weapons tests	^{235}U, ^{239}Pu, fission products
Every day sources	Coal, Tobacco and Air-travel
Medical tests & treatment	X-ray, γ-rays & electrons
Cosmic rays	Protons, electrons, neutrons
Food	^{40}K, ^{137}Cs, ^{14}C and ^{131}I
Rocks & building	^{235}U, ^{238}U, and ^{232}Th
Atmosphere	^{222}Rn and ^{137}Cs

2.1.3 γ- Radiation Sources

Γ-rays are produced by the nuclear transitions that occur within the nuclei of radioactive elements. The emitted photons are mono-energetic with specific energy to the isotope from which they originate. By far the most

commonly employed radioactive isotope for γ-rays is cobalt-60 (^{60}Co), an isotope with a half-life of 5.272 years. ^{60}Co emits two γ-photons of equal intensity at 1.17 and 1.33 MeV. It is produced in nuclear reactors by a neutron-capture reaction involving ^{59}Co. Due to the long half-life, high penetrating power and ease of production, ^{60}Co sources have become sources of choice in both industrial and research institutions. The activity of the sources prepared in nuclear reactors can be made high up to 40 Ci/g (1.5 TBq/g), however sources with activities from 1 to 5 Ci/g are typically common for use. Over 80% of the ^{60}Co produced world-wide is manufactured by the Canadian company, Ontario Hydro and marketed by another Canadian company, MDS Nordion.^{60}Co radioisotope decays to stable nickel-60 by a nuclear transition (β-decay) in which a neutron is converted into a proton via the emission of β-particle with energy of 312 keV and two γ-photons, one of 1.17 MeV and another of 1.33 MeV. The decay scheme of this isotope is illustrated in figure (2.1) (Attix, 1986; Choppin et al., 1995).

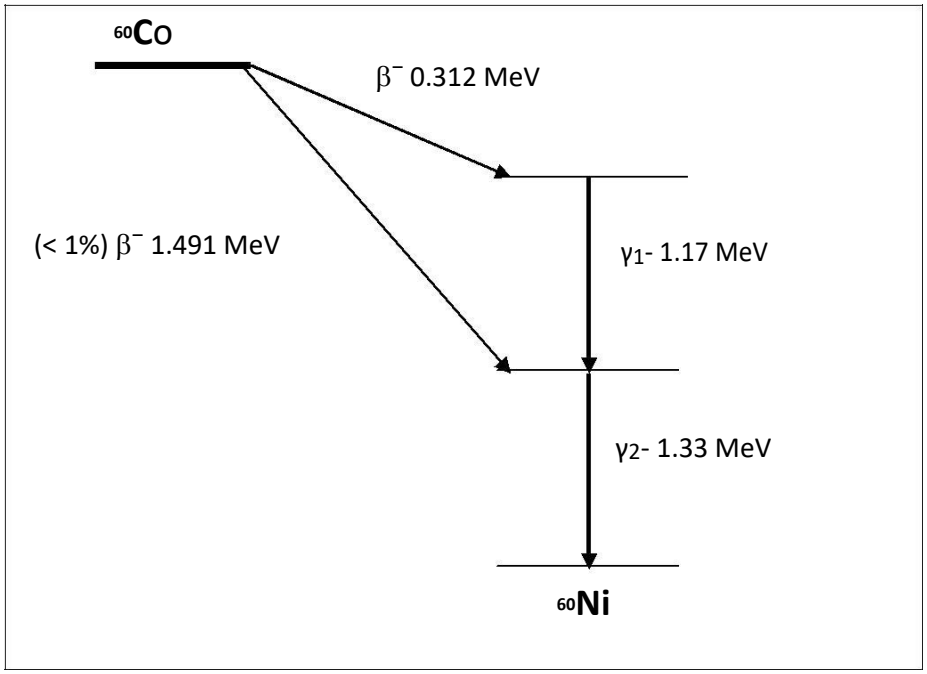

Figure (2.1): The decay scheme of ^{60}Co radioisotope which ends by Nicle-60 stable.

Another frequently used γ-ray source is cesium-137, a fission product from nuclear reactors. The energy of the emitted photon is 662 keV and the half-life is 30.17 years. Nuclear reactors themselves are potential sources of γ-rays.

2.1.4 Interaction of Radiation with Matter

Ionizing radiation interacts with matter depending on its nature: directly ionizing radiation (charged particles) and indirectly ionizing radiation (uncharged particles). Charged particles interact with nearly every atom along its path, depositing their energy in the medium through direct Coulomb-force interactions with the nearby atoms and losing their energy gradually. These Coulomb-force interactions are characterized in terms of the relative sizes of the impact parameter and the atomic radius into soft and hard collisions, and bremsstrahlung radiation (Andreo et al., 2017). Uncharged particles, by contrast, may pass through matter with no interactions at all. They deposit their energy by a two-step process: first they transfer their energy to charged particles, and then these charged particles will deliver their energy to matter (Glenn F. Knoll, 2010).

2.1.5 γ-Radiation Interaction with Matter

When photons of γ-radiation interact with matter, they undergo attenuation and hence lose their energy and intensity. Various processes are involved in this regard including photoelectric absorption (photoelectric effect), Compton scattering (inelastic scattering), pair production and Rayleigh scattering (elastic scattering) (Evan, 1952).

2.1.5.1 Photoelectric Absorption

Absorption of γ-rays occurs when the γ-ray photon is absorbed by an electron resulting in ejection of the electron from the inner shell of the atom and ionization of atom takes place. Subsequently, the ionized atom returns to the neutral state with emission of characteristic X-ray of the

atom as in figure (2.2). This subsequent emission of lower energy photons is generally absorbed and does not contribute to the secondary ionization. Photoelectron absorption is the dominant process for γ-ray absorption up to energies of about 500 keV. This phenomenon was explained by Einstein in 1905, in which an incident photon gives up all its energy (hν) to a bound electron, usually K shell (probability equal 90%), where subsequently part of the energy is used to overcome the electron binding energy (E_b) and the extra energy is converted as kinetic energy (K_e) for the photoelectron. This can be expressed as in equation (2.1).

$$h\upsilon = K_e + E_b \tag{2.1}$$

The atom that is left in an excited state will emit fluorescent x-rays or Auger electrons. The characteristic X-rays may escape especially for high-energy photons and high atomic number of absorbing material unless the absorber is thick enough to stop the γ-rays. The ranges of the Auger electrons are short and locally absorbed. The cross-section (probability) for photoelectric effect in K shell of an atom with atomic number Z for photon energy (hν) is given by equation (2.2). It is clear that the photoelectron absorption is dominant for atoms of high atomic numbers and for photons of low energies (Bushberg et al., 2002).

$$\sigma_k = 4\varphi_0\sqrt{2}\left\{\frac{mc_0{}^2}{h\nu}\right\}^{7/2}\frac{Z^5}{137^4} \tag{2.2}$$

Where $\varphi_0 = \pi r_0{}^2$ and $r_0 = e^2/m_0c^2 = 2.818\times10^{-15}m$ is the classical electron radius, m_0 is the rest mass of electron and c is the speed of light. M_0c^2 is the rest energy of the recoil electron, according to mass-energy equation proposed by Einstein in 1905 in the relativity theory.

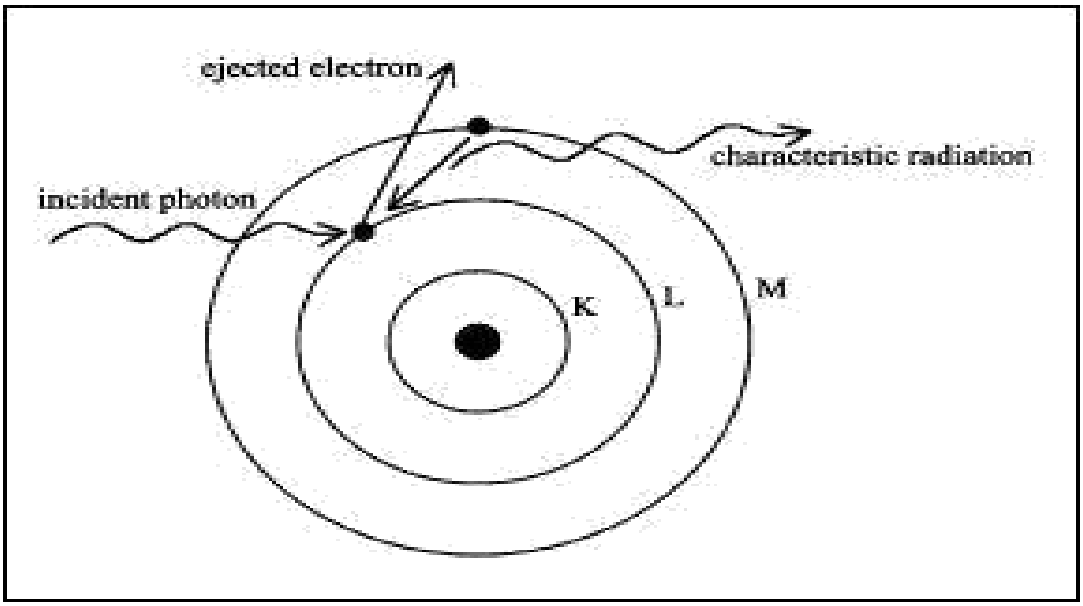

Figure (2.2): Schematic diagram of photoelectric absorption of γ-radiation resulting in ejection of orbital electron from L shell leading to ionization process of an atom (Bushberg et al., 2002).

2.1.5.2 Compton Scattering

Compton scattering process also known as incoherent scattering, occurs when the incident photon ejects free or weakly bonded electron from an atom and a photon of lower energy is scattered from the atom. Relativistic energy and momentum are conserved in this process and the scattered γ-ray photon has less energy and therefore greater wavelength than the incident photon as shown in figure (2.3). Compton scattering is important for low atomic number specimens. At energies from 100 keV to 10 MeV the absorption of radiation is mainly due to the Compton effects (McGervey, 1983). The change in wavelength of the scattered photon is given by equation (2.3).

$$\frac{c}{\nu'} - \frac{c}{\nu_o} = \lambda' - \lambda_o = \frac{h}{mc(1-\cos\theta)} \qquad (2.3)$$

Where λ is the wavelength of the incident photon, λ_0 is the wavelength of the scattered Photon, m is the mass of the electron and θ is the angle of scattering for the photon. Rearranging equation (2.3), we obtain equation (2.4) below

$$h\nu = \frac{h}{1+\alpha(1-\cos\theta)} \tag{2.4}$$

Where α is the ratio of the energy of the photon to the rest energy of the electron i.e. $\alpha = h\nu / m_0 c^2$. The kinetic energy T for the recoil electron is given by equation (2.5)

$$T = h\nu \frac{\alpha(1-\cos\theta)}{1+\alpha(1-\cos\theta)} \tag{2.5}$$

And the scattering angle of the electron is given by equation (2.6)

$$\cot\phi = (1+\alpha)\tan\frac{1}{2}\theta \tag{2.6}$$

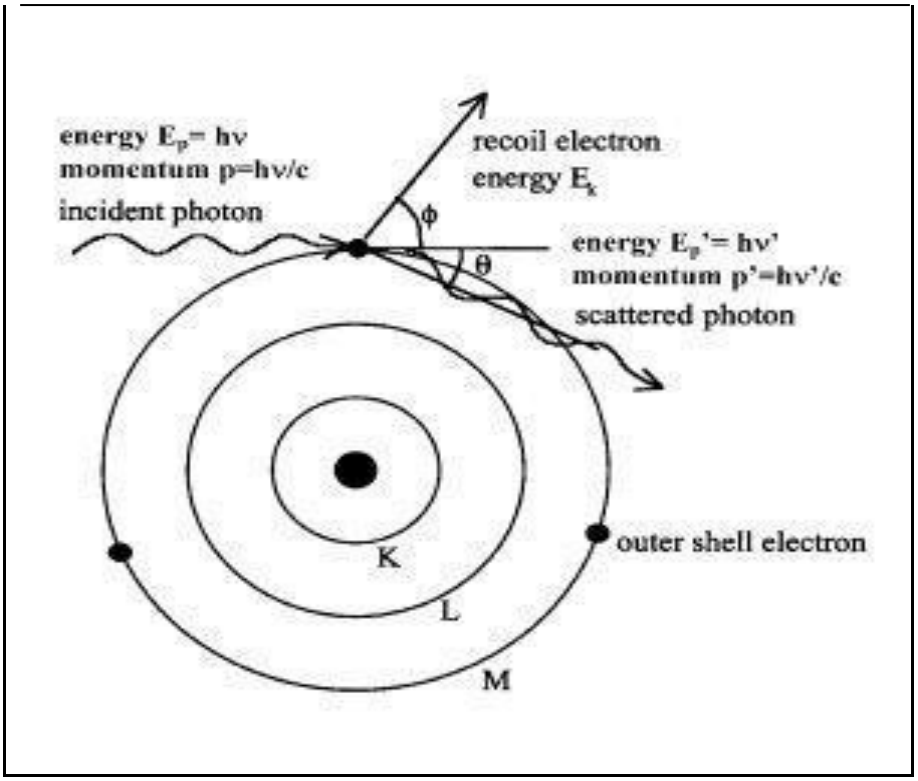

Figure (2.3): Schematic diagram of Compton scattering for γ-radiation resulting in ionization and scattering of the incident photon with less energy.

2.1.5.2 Pair Production

The production of a positive and negative electron pair is a process that can take place in the vicinity of the nucleus field of an atom or an electron field. Absorption of photons through the mechanism of pair production can occur when the energy of an incident photon is greater

than twice the rest mass of an electron, i.e. 2 m_0c^2 = 1.022 MeV (Johns and Cunningham, 1983). During pair production interactions, a photon has its energy converted to an electron–positron pair. The positron then interacts with matter by ionizing and exciting atoms through the same processes as electrons, thus losing energy and being brought to rest. At this point, the positron combines with an electron in an annihilation process producing two photons with energy equal to 0.511 MeV as shown in figure (2.4). Pair production is an absorption process in which a photon in the field of nucleus produces an electron-positron pair, where the total kinetic energy is equal to the energy of photon minus the rest energy of the two particles which have been created as shown in equation (2.7), thus the photon energy must be greater than 1.02 MeV for the interaction to take place. The electron and positron do not necessarily receive equal energy, but their average energy is given by equation (2.8).

$$h\upsilon = (m_0 c^2 + T_-) + (m_0 c^2 + T_+) \qquad (2.7)$$

$$\bar{T} = \frac{h\upsilon - 1.022}{2} \text{ MeV} \qquad (2.8)$$

The cross-section of the pair production in the field of nucleus is given by equation (2.9)

$$\sigma_{PP} = \frac{1}{137} r_0^2 Z^2 \left[\frac{28}{9} \ln\left(\frac{2h\upsilon}{m_0 c^2} \right) - \frac{218}{27} \right] \qquad (2.9)$$

The triplet production process is similar but the interaction takes place with one of the atomic electrons which receives sufficient energy to be set free. It occurs when incident photon have an energy of $4m_0c^2$, i.e. it implies both the pair production at the nucleus level plus triplet production. The total kinetic energy is equal to the energy of photon minus the rest energy of the three ejected particles as given by equation (2.10), from which the average kinetic energy can be deduced by equation (2.11) (Motz *et al*., 1969).

$$h\nu = \left(m_0 c^2 + T_-\right) + \left(m_0 c^2 + T_+\right) + \left(m_0 c^2 + T_*\right) \qquad (2.10)$$

$$\bar{T} = \frac{h\nu - mc^2}{3} \text{ MeV} \qquad (2.11)$$

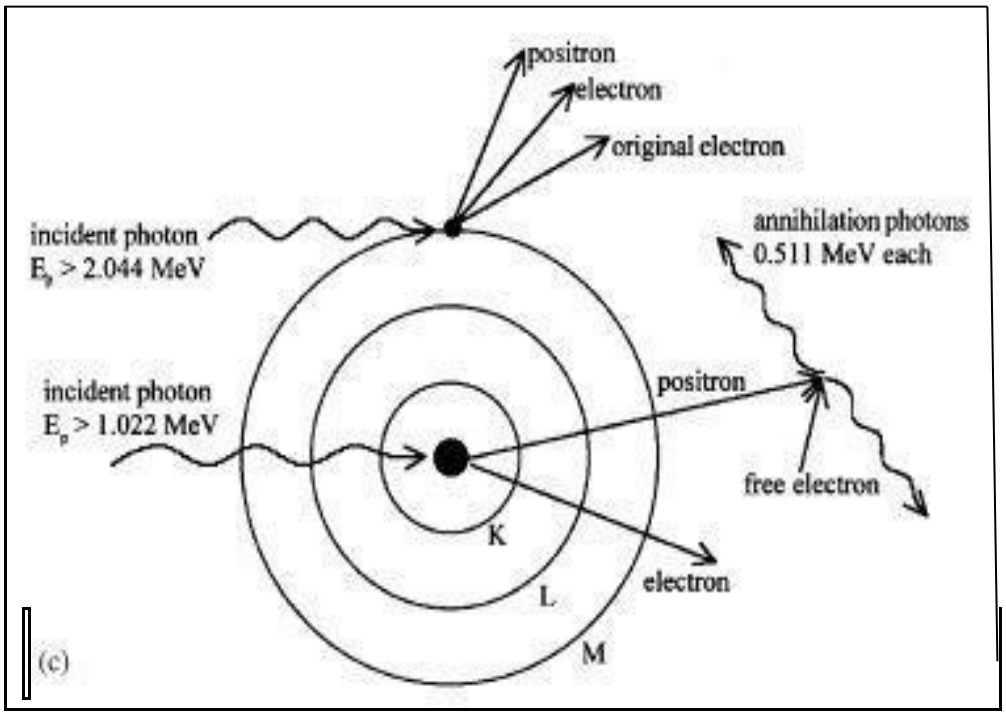

Figure (2.4): Schematic diagram of Pair Production process for γ-radiation being interfered in the nucleus field and orbital electron to produce triplet particles.

2.1.5.3 Raleigh Scattering

The coherent Rayleigh scattering is predominant for photons at low energy range from 1 keV to 100 keV. The Rayleigh scattering is a process in which a photon is deflected by a bounded electron of the atom and photon going off in different directions with no loss in energy. The atomic system may recoil as a whole under impact without the atom being ionized or excited. The probability of this process is large only for low energy photons and high atomic number materials. The differential cross-section of the coherent scattering of photon at deflection angle θ by a bounded electron is given by equation (2.12).

$$d\sigma_{coh} = \frac{1}{2} r_0^2 (1 + \cos^2\theta) \left[\frac{F(\alpha,\theta,Z)^2}{Z}\right] d\Omega \qquad (2.12)$$

Where F(α,ɵ,Z) is the atomic form function which varies from zero at large angles to Z at smaller angles.

2.1.6 γ-Ray Attenuation Coefficients

In general the characteristic of radiation interaction with matter is that each individual photon is absorbed or scattered from the incident beam in a single event. The photon number removed I is proportional to the thickness traveled through Δx and the initial photon number I_0, i.e. $\Delta I = -\mu I_o \Delta x$, where, μ is proportionality constant called the attenuation coefficient. By integration method, we have the following equation (2.13).

$$I = I_o e^{-\mu x} \tag{2.13}$$

The attenuation coefficient is related to the probability of interaction per atom, i.e. the atomic cross section σ_a which can be given by equation (2.14).

$$\mu = \frac{N}{A} \underline{\sigma^{a} \quad A} \ \underline{\rho} \tag{2.14}$$

Where A is the mass number and N_A the Avogadro's number (6.022×10^{23} mol/1), table (2.3) below briefly summarize the entire γ-radiation photon interactions with their possible energies required to initiate the reactions (Siegbahn, 1965; Smith, 2000).

Table (2.3): Types of γ-radiation interactions with matter (Siegbahn, 1965).

Process	Type of interaction	Other names	Approximate *E* of Maximum Importance.	Z dependence
Photoelectric	With bonded electrons, all *E* given to electron		Dominant at low *E* (1-500) KeV, cross section decrease as *E* increase	Z^3
Scattering from electrons	With bond atomic electron,	Rayleigh electron, resonance scattering,	<1MeV and greatest at small angles.	Z^2, Z^3
coherent	with free electrons	Thomson scattering	Independent of energy	Z
Incoherent	With bond atomic electron, with free electrons	Compton scattering	<1MeV least at small angle.	Z
			Dominate in region of 1 MeV, decreases as *E* increase	Z
Pair Production	In Coulomb field of Nucleus	Elastic Pair production	Threshold ~1MeV, *E*> 5MeV. Increase as *E* increase.	Z^2
Pair production	In coulomb field of electron & nucleus	Triplet production inelastic pair	Threshold at 2 MeV increases as *E* increases.	Z
Delbruk scattering		production. Nuclear potential scattering	Real Max > imaginary, below 3 MeV(both increase as *E* increases)	Z^4

2.1.7 γ-Radiation Interaction with Molecules

The essence of γ-radiation interaction with molecules changing its physical and chemical characteristics is ascribed to the amount of energy being transferred, which will create ions, free radicals and excited molecules. Such interaction process is termed ionization and excitation of the molecules, which can cause chemical changes to the irradiated molecules. This is due to the fact that all binding energy for organic compounds are in the range of 10 – 15 eV. In case of low energy transferred by the photon, the molecule moves to excitation state before returning to its natural state emitting X-ray photons or break down to release free radicals which in turn undergoes polymerization. The ejected electron from the irradiated molecule (A^+) is subjected to the strong electric field of the formed positive charge, therefore the recombination frequently occurs either during irradiation or after the end of irradiation creating energetic molecule (A^{**}). Such highly energetic excited molecule will break down into free radicals and new molecule (Denaro, 1972). The fundamental of this reaction can be shown in figure (2.5).

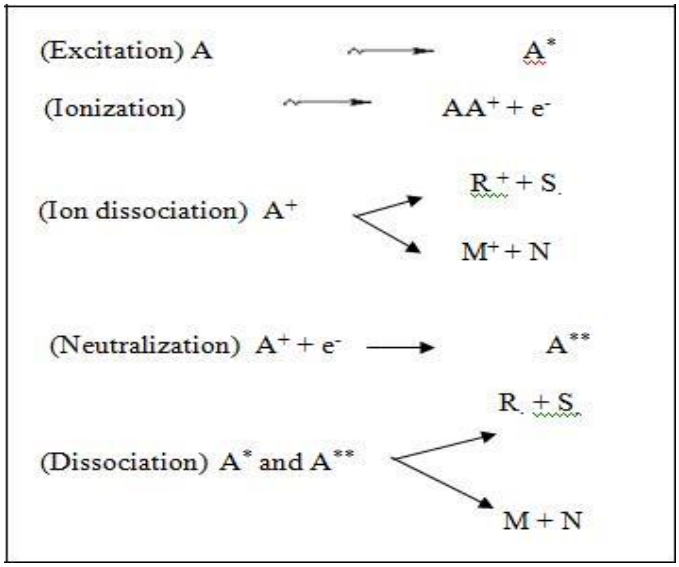

Figure (2.5): The expected irradiation results of the organic molecules, where R. and S. are free radicals and M and N are molecular products.

2.1.8 Radiation Dosimetry

Radiation dosimetry is the process of calculating the absorbed dose in matter and tissue resulting from the exposure to indirectly and directly ionizing radiation. It is a scientific subspecialty in the fields of health physics and medical physics that focus on the calculation of internal and external doses from ionizing radiation.

2.1.8.1 Radiation Quantities

There are many different physical quantities that can be used to express the amount of radiation delivered to a human body. Generally, there are advantages and applications as well as disadvantages and limitations for each of the quantities. There are two types of radiation quantities: those that express the concentration of radiation at some point, or to a specific tissue or organ, and there are also quantities that express the total radiation delivered to a body (IAEA, 2005).

2.1.8.1.1 Exposure

Exposure is a radiation quantity that expresses the concentration of radiation delivered to a specific point, such as the surface of the human body. There are two units for expressing exposure. The conventional unit is the roentgen (R) and the SI unit is the coulomb/kg of air (C/kg of air). The unit, roentgen, is officially defined in terms of the amount of ionization produced in a specific quantity of air. The ionization process produces an electrical charge that is expressed in the unit of coulombs. So, by measuring the amount of ionization (in coulombs) in a known quantity of air the exposure in roentgens can be determined (IAEA, 2005).

2.1.8.1.2 Air Kerma

Air kerma is a radiation quantity used to express the radiation concentration delivered to a point, such as the entrance surface of a patient's body. It is a quantity that fits into the SI scheme. The quantity,

kerma, originated from the acronym, KERMA, for Kinetic Energy Released per unit MAss (of air). It is a measure of the amount of radiation energy, in the unit of joules (J), actually deposited in or absorbed in a unit mass (kg) of air. Therefore, the quantity, kerma, is expressed in the units of J/kg which is also the radiation unit, the gray (Gy) (IAEA, 2005).

2.1.8.1.3 Absorbed Dose

Absorbed Dose is the radiation quantity used to express the concentration of radiation energy actually absorbed in a specific tissue. This is the quantity that is most directly related to biological effects. Dose values can be in the traditional unit of rad or the SI unit of gray (Gy). The rad is equivalent to 100 ergs of energy absorbed in a gram of tissue and the gray is one joule of energy absorbed per kilogram of tissue (IAEA, 2005).

2.1.8.1.4 Entrance Surface Dose

Entrance surface (skin) exposure is defined as the exposure in roentgens at the skin surface of the patient without the backscatter contribution from the patient. This measurement is popular because entrance skin exposure is easy to measure, but unfortunately the entrance skin exposure is poorly suited for specifying the radiation received by patients undergoing radiographic examination. The entrance skin exposure does not take into account the radio sensitivity of individual organs or tissues, the area of an x-ray beam, or the beam's penetrating power, therefore, entrance skin exposure is poor indicator of the total energy imparted to the patient (NRPB, 2000).

2.1.8.1.5 Entrance Surface Air Kerma (ESAK)

The entrance surface air kerma (ESAK) is defined as the kerma in air at the point where the central radiation beam axis enters the hypothetical object, i.e. patient or phantom, in the absence of the specified object

(Zoetelief et al., 1996). The entrance surface dose, or alternatively the entrance skin dose (ESD) is defined as the absorbed dose to air on the radiation beam axis at the point where radiation beam enters the patient or a phantom, including the contribution of the backscatter (NRPB, 1992). The ESD is to be expressed in mGy. Some confusion exists in the literature with regard to the definition of the ESD. That is, whether the definition should refer to the absorbed dose to the air as defined above or absorbed dose to tissue (NRPB, 2000).

2.1.8.1.6 Equivalent Dose (H_T)

Accounts for biological effect per unit dose

$$H_T = W_R \, xD \qquad (2.15)$$

2.1.8.1.7 Effective Dose (E)

Risk related parameter, taking relative radio sensitivity of each organ and tissue into account:

$$E(Sv) = \Sigma_T \, W_T \, x \, H_T \qquad (2.16)$$

W_T: tissue weighting factor for organ T

H_T: equivalent dose received by organ or tissue T

2.1.8.2 Radiation Units

2.1.8.2.1 Roentgen

The roentgen is a unit used to measure a quantity called exposure. This can only be used to describe an amount of gamma and X-rays, and only in air. One roentgen is equivalent to depositing in dry air enough energy to cause 2.58×10^{-4} coulombs per kg. It is a measure of the ionizations of the molecules in a mass of air. The main advantage of this unit is that it is easy to measure directly, but it is limited because it is only for deposition in air, and only for gamma and X-rays (Avenue, 2002).

2.1.8.2.2 Radiation Absorbed Dose (Rad)

The rad is a unit used to measure a quantity called absorbed dose. This relates to the amount of energy actually absorbed in some material, and is used for any type of radiation and any material. One rad is defined as the absorption of 100 ergs per gram of material. The unit rad can be used for any type of radiation, but it does not describe the biological effects of the different radiations (Avenue, 2002).

2.1.8.2.3 Roentgen Equivalent Man (Rem)

The rem is a unit used to measure a quantity called equivalent dose. This relates the absorbed dose in human tissue to the effective biological damage of the radiation. Not all radiation has the same biological effect, even for the same amount of absorbed dose. Equivalent dose is often expressed in terms of thousandths of a rem, or mill-rems. To determine equivalent dose in (rem), we multiply absorbed dose in (rad) by a quality factor (W) that is unique to the type of incident radiation.

2.1.8.2.4 Gray (Gy)

The gray is a unit used to measure a quantity called absorbed dose. This relates to the amount of energy actually absorbed in some material, and is used for any type of radiation and any material. One gray is equal to one joule of energy deposited in one kg of a material. The unit gray can be used for any type of radiation, but it does not describe the biological effects of the different radiations. Absorbed dose is often expressed in terms of hundredths of a gray, or centi-grays. One gray is equivalent to 100 rads.

2.1.8.2.5 Sievert (Sv)

The sievert is a unit used to measure a quantity called equivalent dose. This relates the absorbed dose in human tissue to the effective biological damage of the radiation. Not all radiation has the same biological effect,

even for the same amount of absorbed dose. Equivalent dose is often expressed in terms of millionths of a sievert, or micro-sievert. To determine equivalent dose in (Sv), we multiply absorbed dose in (Gy) by a quality factor (W) that is unique to the type of incident radiation. One sievert is equivalent to 100 rem (Thayalan, 2001).

2.1.9 Radiation Measurements

2.1.9.1 Thermo Luminescent Dosimetry

Many crystalline materials exhibit phenomena of thermo luminescence. When such a crystal is irradiated, a very minute fraction of the absorbed energy is stored in crystal lattice. Some of this energy can be recovered latter as visible light if the material is heated. This phenomenon of releasing visible photon by thermal means is known as thermos luminescence. (Thayland, 2001).

2.1.9.2 Radiochromic Dosimetry

Radiochromic films are a new type of films in radiotherapy dosimetry; the most commonly used is a (Gaf) Chromic film. It is a colorless film with a nearly tissue equivalent composition (9.0% hydrogen, 60.6% carbon, 11.2% nitrogen and 19.2% oxygen) that develops a blue color upon radiation exposure. Radiochromic film contains of a special dye that is polymerized upon exposure to radiation. The polymer absorbs light and the transmission of light through the film can be measured with a suitable densitometer. Radiochromic films are self-developing, requiring neither developer nor fixer. Since radiochromic film is grain less, it has a very high resolution and can be used in high dose gradient regions for dosimetry (e.g. measurements of dose distributions in stereotactic fields and in the vicinity of brachytherapy sources).

Dosimetry with radiochromic films has many advantages over radiographic films, such as ease of use; elimination of the need for darkroom facilities, film cassettes or film processing; dose rate

independence; better energy characteristics (except for low energy X-rays of 25 kV or less); and insensitivity to ambient conditions (although excessive humidity should be avoided). Radiochromic films are generally less sensitive than radiographic films and are useful at higher doses, although the dose response non-linearity should be corrected for in the upper dose region. Radiochromic film is a relative dosimeter, if proper care is taken with calibration and the environmental conditions; a precision better than 3% is achievable. Data on the various characteristics of radiochromic films (e.g. sensitivity, linearity, uniformity, reproducibility and post-irradiation stability) are available in the literature (E.B. Podgorsak, 2005).

2.1.10 Polymers

Polymer is a Greek word containing two syllables, (poly) and (mer) and they signify many parts. Polymer is a large molecule, or macromolecule, composed of many repeated subunits because of their broad range of properties (Painter et al., 1997). Both synthetic and natural polymers play essential roles in everyday life (McCrum et al., 1997). Polymers range from familiar synthetic plastics such as polystyrene to natural biopolymers such as DNA and proteins that are fundamental to biological structure and function. Polymers, both natural and synthetic, are created via polymerization of many small molecules, known as monomers. Their consequently large molecular mass relative to small molecule compounds produces unique physical properties, including toughness, viscoelasticity, and a tendency to form glasses and semi crystalline structures rather than crystals.

2.1.10.1 Polymer Properties

Polymer properties are broadly divided into several classes based on the scale at which the property is defined as well as upon its physical basis (S.A. Baeurle, 2009). The most basic property of a polymer is the identity

of its constituent monomers. A second set of properties, known as microstructure, essentially describe the arrangement of these monomers within the polymer at the scale of a single chain. These basic structural properties play a major role in determining bulk physical properties of the polymer, which describe how the polymer behaves as a continuous macroscopic material. Chemical properties, at the nano scale, describe how the chains interact through various physical forces. At the macro scale, they describe how the bulk polymer interacts with other chemicals and solvents.

2.1.10.2 Polymerization

Radiation polymerization is a process in which the free radicals interact with the unsaturated molecules of a low molecular unit known as monomer to form high molecular mass polymer. The formed polymer can be in different forms called homopolymer and copolymer depending on the monomer compositions linked together.

Radiation-induced polymerization process can be achieved in different media whether it is liquid or solid unlike the chemical polymerization which can only be accomplished in aqueous media, it is also temperature independent. Radiation polymerization often continues even after removing away from the radiation source; such condition is known as post-polymerization (Lokhovitsky and Polikarpov, 1980). Since radiation initiation is temperature independent, polymer can be polymerized in the frozen state around aqueous crystals. The mechanism of the radiation induced polymerization is concerning the kinetics of diffusion-controlled reactions and consists of several stages: addition of hydroxyl radicals and hydrogen atoms to carbon-carbon double bond of monomer with subsequent formation of monomer radicals; addition of hydrated electrons to carbonyl groups and formation of radical anion of a very high rate constant and the decay of radicals with parallel addition of monomer to the growing chain.

2.1.10.3 Crosslinking and Chain Scission

The process of crosslinking occurs due to interaction between two free radical monomers which combine to form intermolecular bond leading to three dimensional net of cross linked highly molecular polymer, more likely dominate in unsaturated compound or monomer. The cross-linked polymer shows strong mechanical strength and high thermal resistance. The most important reactions occurring during radiolysis of polymers are those that lead to permanent changes in their molecular weight. The reactions leading to either increase or decrease in molecular weight are referred to as crosslinking and chains scission, respectively. In general crosslinking and scission processes can occur simultaneously in any irradiated material; however, it is often observed that one tends to dominate over the other, and thus polymers can be broadly placed into the categories crosslinking or degrading. Some processes could be observed in irradiated polymer molecules, such as:

- **Evolution of Gas:** When polymers are exposed to high energy radiation, the reactions induced will lead to the formation of low molecular weight gaseous molecules. For example, when polyethylene $-(-CH_2-)-$ is irradiated, the scission of the C-H bond leads to the formation of thermally activated hydrogen atoms which are able to escape and form molecular hydrogen gas.
- **Formation of Unsaturated Groups:** When polymers are exposed to high energy radiation, chain scission leads to the formation of active atoms which leads to the evolution of gas and the formation of unsaturated groups. For example, the formation of main-chain unsaturation in irradiated polyethylene is proportional to the yield of hydrogen gas.
- **Color Centers:** Most polymers change colors during irradiation. This change depends on the structure of the polymer, the irradiation

temperature, the type of radiation and also varies for irradiations performed in vacuum and in air. The discoloration is attributed to the formation of conjugated double bonds in some polymers and also to trapped free radicals, electrons, and ions (David J.T. HILL, et al., 2005).

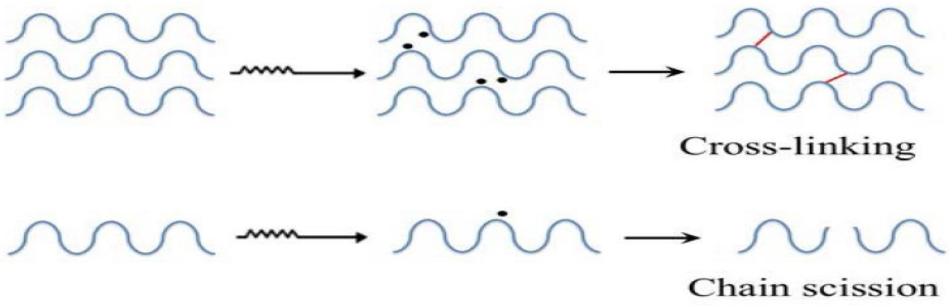

Figure (2.6): Schematic representation of competing radiation induced polymer scission and cross-linking (Saphwan et al., 2016).

2.1.10.4 Radiation Grafting

Radiation grafting is a process in which active radical sites are formed on or near the surface of an exciting polymer followed by polymerization of monomer on these sites. It is accompanied by homopolymerization of the monomer; the material to which the monomer is grafted is described as the backbone, trunk or support. Radiation grafting is used to modify the polymers texture such as films, fibers, fabrics and molding powders. This process can be explained as follow; suppose that the polymer A is exposed to γ-rays, thus the active free radical sites A^* is created randomly along the polymer backbone chain, this free radical initiates a free radical on the monomer B then undergoes grafting polymerization at that active site. The extension of the attached monomer B upon the base polymer A is termed as the degree of grafting (DOG) which refers to the mass of the grafted polymer as a percentage of the mass of the original base polymer. Such process can be expressed as in schematic figure (2.7).

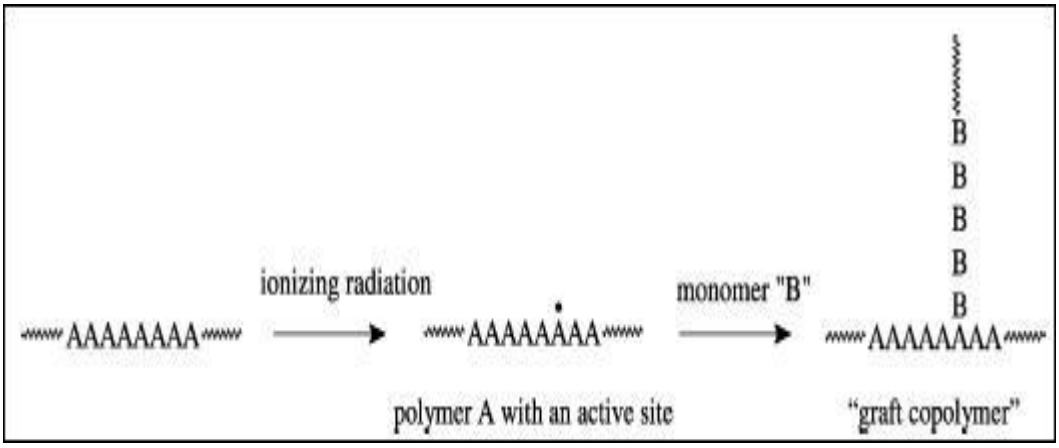

Figure (2.7): The scheme for grafting process for polymer A with monomer B using γ-radiation.

2.1.10.5 Polyvinyl Alcohol (PVA)

PVA is one of the most important polymers binders; it's available in forms of powders, fibers and films. It can be obtained from polyvinyl acetate (PVAc) by esterification and has distinct crystalline. The polymer has intermolecular chin of 2.5 Å and consists of 1, 3 glycol linkages, in which all hydroxyl groups are arranged along the same side of the chain. These in turn account for the mechanical strength and strong interactions between different chains. The unit cell of PVA consists of two monomer units of vinyl alcohol (CH2CHOH) (Bunn, 1948) as in figure (2.8).

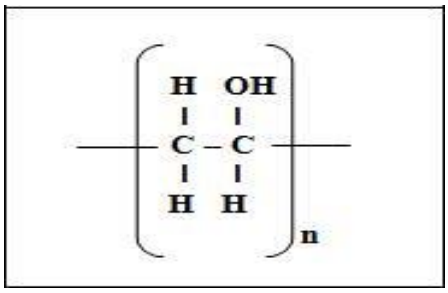

Figure (2.8): The chemical structure of polyvinyl alcohol (PVA) monomer.

It is non-ionic vinyl polymer, tough with film forming capacity due to hydrogen bonding (Ravve, 2000), fibers and tubes forming capability and highly resistant to hydrocarbon solvents (Molyneux, 1983). It is highly resistive to electrical conductivity with low dielectric loss. Its electrical conductivity and charge storage capability can be significantly influenced

by doping with suitable impurities (Nagaraja, et al., 2002). Due to its biocompatibility, PVA has been used in medical devises, materials for drug delivery system, carrier for cell signaling, sizing, adhesives, emulsification and bio-separation membranes (Yano, et al., 2003).

2.1.11 Silver Nitrate ($AgNO_3$)

Silver nitrate is a chemical compound with a chemical formula $AgNO_3$ shown in the figure below. This nitrate of silver is the light sensitive ingredient in photographic films and is a corrosive compound. Soluble silver salts tend to be very toxic to bacteria and other lower life species. The compound notably stains the skin giving a blackening color which is made visible after exposure to sunlight. Silver nitrate is one of the significant compounds in the field of industries due to its potential characteristics such as wider response to electromagnetic radiations i.e. optical properties in addition to electronic, magnetic and catalysis properties (Wang and Toshima, 1997). It has been used in wider applications as conductive ink, thick film pastes, adhesive for electronic compounds (Lin and Wang, 1996), in photonic and photographic applications (Jin et al., 2001). Silver nitrate has a molecular weight of 169.87, boiling point of 444 ^{0}C, melting point 212 ^{0}C as crystal structure rhombic, decomposed by heat to give Ag, NO_2 and O_2.

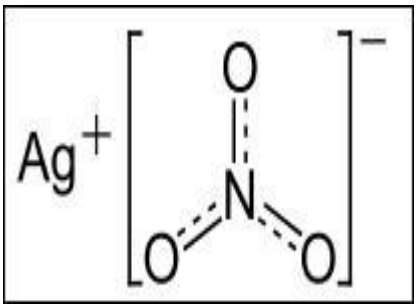

Figure (2.9): Chemical structure of the silver nitrate compound.

2.1.12 Absorption of Light and UV-Visible Spectrophotometry

2.1.12.1 Optical Absorption

The transmittance of light across the absorber accompanied with absorption of the light waves. Such absorption depends on the wavelength of the light, thickness of the absorber or the transmitted media and the nature of the media. Beer-Lambert law, successfully determines the absorption coefficient of the media as follows; supposing *I* is an incident light beam to an object whose area is a, α is its absorption coefficient, then the fraction absorption *dI* of light by this absorber in a thickness *dx* is given by the following equation (2.17).

$$dI = -\alpha I dx \tag{2.17}$$

or

$$\frac{dI}{I} = -\alpha dx \tag{2.18}$$

The integration of this equation (2.18) gives the absorbance *A* as in equation (2.19). In this case the light intensity *I* changed from 0 to *I* by crossing a distance from *x* = 0 to *x* = *x* in the absorber.

$$\int_{I=0}^{I=I} \frac{dI}{I} = -\alpha \int_{x=0}^{x=x} dx$$

$$\ln I /_{I_0} = -\alpha x /_0^x$$

$$\ln(I) - \ln(I_o) = -\alpha x$$

$$\ln \frac{I}{I_0} = -\alpha x$$

$$\log \frac{I}{I_0} = e^{-\alpha x} = A \tag{2.19}$$

From equation (2.19) of absorbance *A*, the absorption coefficient α can

be deduced as in equation (2.20).

$$\frac{\log \frac{I}{I_0}}{e^{-1}} = \alpha x$$

$$\frac{e \times A}{x} = \alpha \qquad (2.20)$$

As the value of $\log \frac{I}{I_0} = A$ and e is 2.303, then the absorption coefficient can be given by equation (2.21)

$$\alpha = \frac{2.303 \times A}{X} \qquad (2.21)$$

Where x is the distance crossed by the light, also can be the sample thickness in the case of UV-visible spectroscopy. The corrected absorption value known as the molar absorptivity (**ε**) is used for the comparison between different spectra of different compounds and can be expressed by the following equation:

$$\varepsilon = \frac{A}{cl} \qquad (2.22)$$

Where A is the absorbance, c is the sample concentration in moles/liter and l is the path length through the cuvette in cm.

2.1.12.2 Mechanism of Absorption Process

The absorption processes of microwaves in polymers, generally accompanied with energy reduction in the transition wave. Such reduction is due to the optical absorption constant of the media α which comes in the range of $10^5 – 10^6$ cm^{-1} (Richard, 1988). The variation of the absorption on the transition involves direct or indirect transitions. As the photon energy drops below the band gap energy, the energy levels are created if imperfections are present in the polymers; they lie

in forbidden gap. At energy less than the band gap energy it is still possible to excite electrons to the conduction band from imperfection levels occupied by electrons. Electrons also can be excited from the valence band to unoccupied imperfection levels. Each process will give rise to optical absorption. When the photon energy is less than the energy required to make a transition from the imperfection level to one of the bands, this absorption in turn comes to an end. The corresponding absorption constant α may have values as high as 10^3 cm^{-1} for very high imperfection densities, but in general is considerably less. Absorption of photons by free carriers causes a transition to higher energy states within the same band or to higher bands, this process can occur over a wide range of photon energies. It involves the absorption of both photons and phonons since both energy and k must be changed in the transition. There is also an optical absorption due to free carriers acting collectively as a kind of electron gas, which is known as plasma resonance absorption.

2.1.12.3 Absorption Edge

The transition of electrons between the valence and conduction bands in the polymers starts at the absorption edge which refer to the minimum or threshold energy at which the absorption coefficient started. The transition is called direct if it is extreme occur due to direct absorption of the incident photonic energy, or can be indirect transition in case of phonon assisted initiation. Mostly, all materials have discriminated absorption edge and the energy gap E_g, which related to their chemical properties, hence such criteria can be utilized as a fingerprint in materials characterization (Tauc, 1974).

The absorption constant $\alpha(\nu)$ within the range of ~1 cm^{-1} up to $10^4 cm^{-1}$, is described by the following equation (2.23)

$$\alpha(\nu) = \alpha_0 \exp\left(\frac{h\nu}{E_e}\right) \quad (2.23)$$

Where, the energy (E_e) is the absorption edge in eV.

2.1.12.4 Optical Band Gap

At high enough absorption levels ($\alpha > 10^4$ cm^{-1}), the absorption constant $\alpha(\nu)$ commonly takes place as frequency dependent from which the band gap energy between the conductive band CB and the valence band VB can be deduced, depending on Mott and Davis (1979) which is applicable for UV-spectrum. It correlates between energy band gap E_g and the absorption coefficient $\alpha(\nu)h\nu$ of the composites as in the following equation (2.24).

$$\alpha(\nu)\, h\nu = A\,(h\nu - E_g)^r \quad (2.24)$$

Where $h\nu$ is the energy of the incidence photon, h is the Planck constant, E_g is the optical band gap energy, A is a constant known as the disorder parameter which is dependent on composite composition and independent of photon energy. Parameter r is the power coefficient with the value that determined by the type of possible electronic transitions, such as direct allowed and indirect allowed (Tauc, 1974). The direct transition is the transition of electron from the band i via k band to the final conduction band f by the transition-dipole moments and the electric fields at the surface, while for the indirect transition the incident photon is absorbed in the substrate followed by scattering of a photo-excited electron trapped into the intermediate state k band then transferred to the final band f, as being illustrated in figure (2.10) below. All electrons of the valence band can connect to the empty states of the conduction band by indirect transition process; however phonons, could also participate in the transition process (Pankove, 1971).

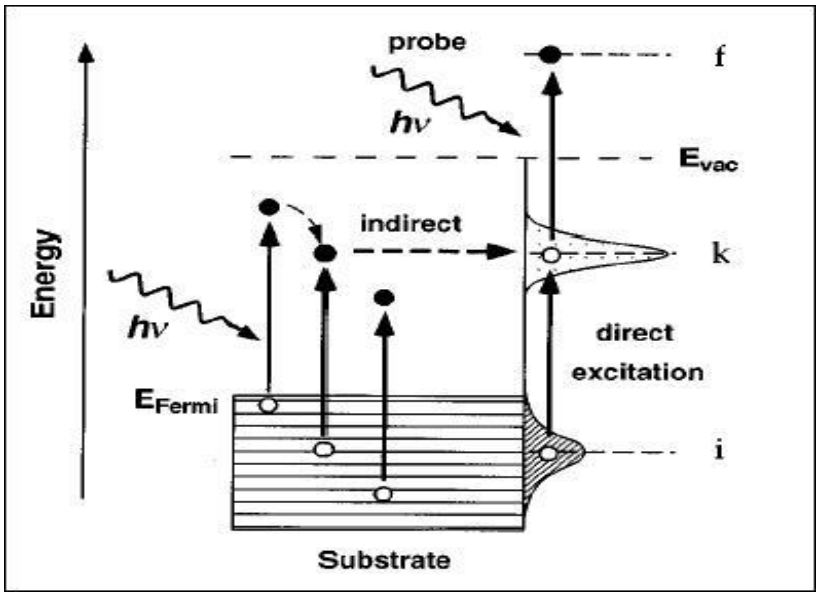

Figure (2.10): Schematically illustrates the sequence of direct electronic transitions from the initial state *i* to the final state *f*, or by an indirect process in which the intermediate state *k* is populated by scattering and relaxation of (hot) electrons, which are photo-excited in the substrate (Pankove, 1971).

2.1.12.5 UV-Visible Absorption Spectrophotoscopy

The following figure (2.11) explains the UV-visible spectroscopy principles, in which a beam of light from a UV-visible light source is separated into its component wavelengths by a prism or diffraction grating. Each monochromatic (single wavelength) beam in turn is divided into two equal intensity beams by a half-mirrored device. One beam of the sample (colored magenta), passes through a small transparent container (cuvette) as a sample chamber. The other beam, for reference (colored blue), passes through an identical cuvette. The intensities of these light beams are then measured by electronic detectors and compared. The intensity of the reference beam, with no light absorption, is defined as I_0 and the intensity of the sample beam is defined as I. Over a short period of time, the spectrometer automatically scans all the component wavelengths in the manner described. The UV region scanned is normally from 200 to 400 nm, and the visible portion is from 400 to 800 nm (Whiffen, 1971).

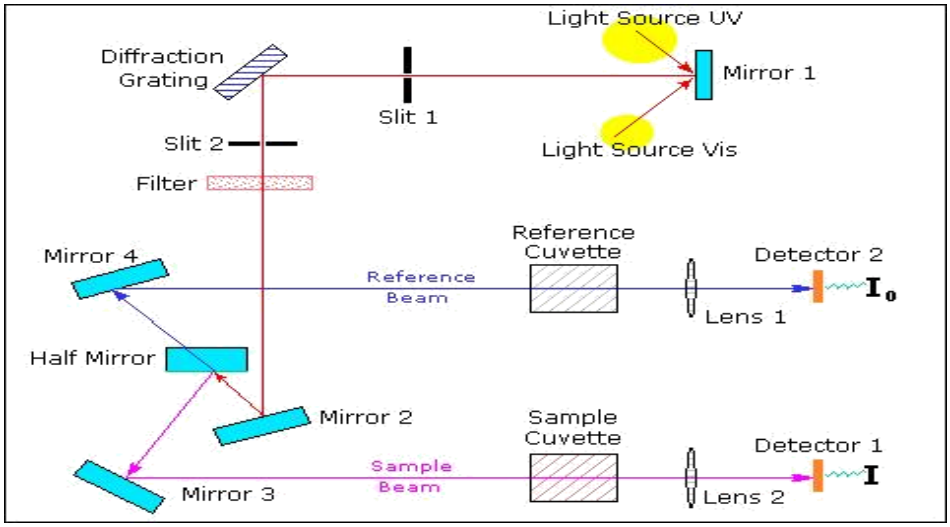

Figure (2.11): Schematic representation for UV-visible spectroscopy principle and steps of taking the spectra.

If the sample compound does not absorb light of a given wavelength then $I = I_0$. However, if the sample compound does absorb light then I is less than I_0, and this difference may be plotted on a graph versus wavelength. Absorption may be presented as transmittance ($T = I/I_0$) or absorbance ($A = \log I_0/I$). If no absorption has occurred, $T = 1.0$ and $A = 0$. Most spectrometers display absorbance on the vertical axis, and the commonly observed range is from 0 (100% transmittance) to 2 (1% transmittance). The wavelength of maximum absorbance is a characteristic value, designated as λ_{max}. Different compounds have very different absorbance. The reference absorption intensity for the system is based on a completely transparent standard compound (non-absorbing), the most commonly used compounds are water, ethanol, hexane and cyclohexane. The compounds with double or triple bonds and heavy atoms are generally avoided, because the absorbance of a sample will be proportional to its molar concentration in the sample cuvette.

2.1.12.6 Origin of UV-Visible Spectra

When radiation interacts with matter, number of processes occur, including reflection, scattering, absorbance, phosphorescence & fluorescence (reemission and absorption), and photochemical reaction

(absorbance and bond breaking). In general, when measuring UV-visible spectra, we want only absorbance to occur. Because light is a form of energy, absorption of light by matter causes the energy content of the molecules (or atoms) to increase. The total potential energy of a molecule generally is represented as the sum of its electronic, vibrational, and rotational energies:

$$E_{total} = E_{electronic} + E_{vibrational} + E_{rotational}$$

The amount of energy a molecule possesses in each form is not a continuum but a series of discrete levels or states. The differences in energy among the different states are in the order:

$$E_{electronic} > E_{vibrational} > E_{rotational}$$

In some molecules and atoms, photons of UV and visible light have enough energy to cause transitions between the different electronic energy levels. The wavelength of light absorbed is that having the energy required to move an electron from a lower energy level to a higher energy level. (A Primer, 1996).

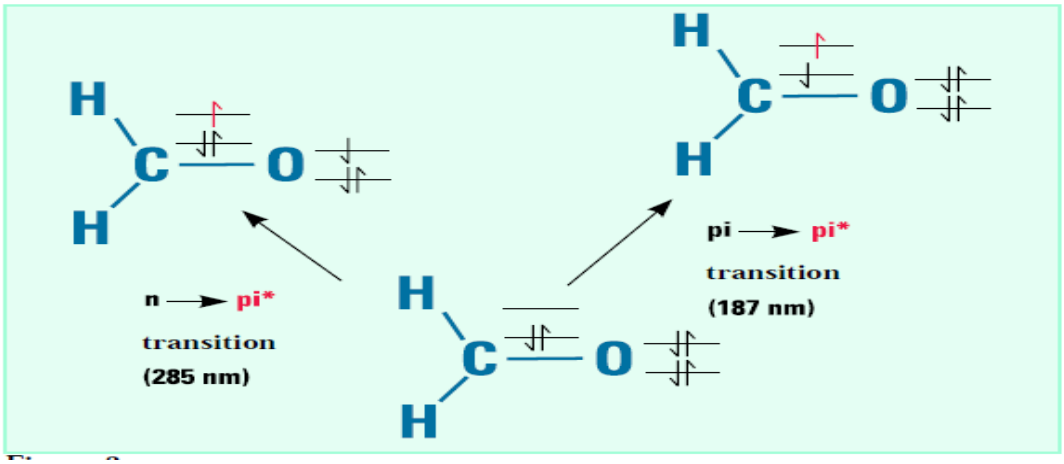

Figure (2-12): An example of electronic transitions in formaldehyde and the wavelengths of light that cause them (A Primer, 1996).

These transitions should result in very narrow absorbance bands at wavelengths highly characteristic of the difference in energy levels of the absorbing species. This is true for atoms, as depicted in figure (2.13).

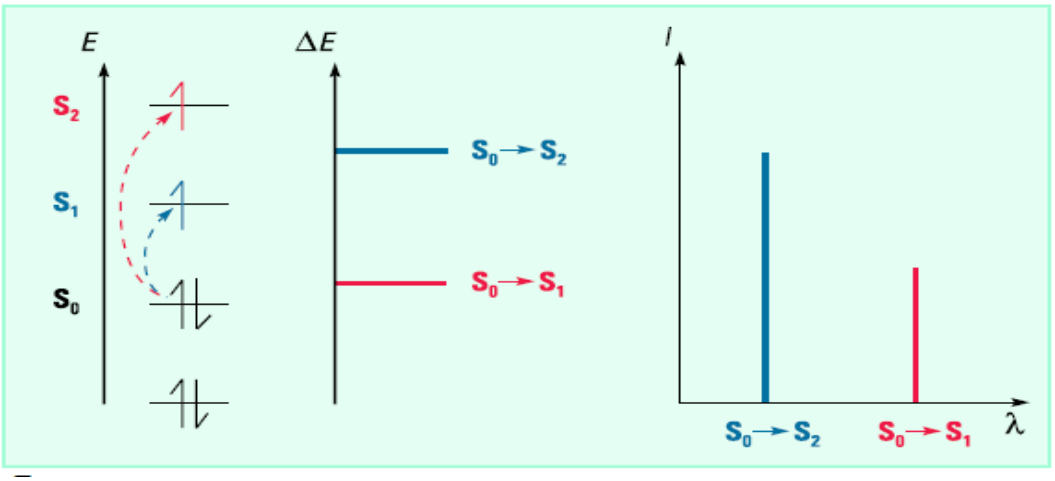

Figure (2.13): The electronic transitions and spectra of atoms. (A Primer, 1996).

However, for molecules, vibrational and rotational energy levels are superimposed on the electronic energy levels. Because many transitions with different energies can occur, the bands are broadened; the broadening is even greater in solutions owing to solvent-solute interactions (A Primer, 1996).

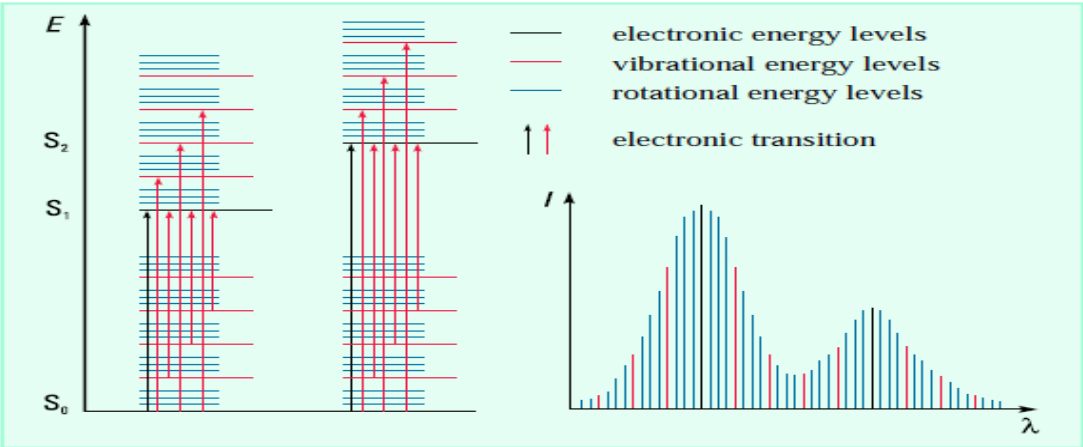

Figure (2.14): The electronic transitions and UV-visible spectra in molecules (A Primer, 1996).

2.1.12.7. Optics of Spectrophotometer

Either lenses or concave mirrors are used to relay and focus light through the instrument. Simple lenses are inexpensive but suffer from chromatic aberration, that is; light of different wavelengths is not focused at exactly

the same point in space. However, with careful design, the chromatic aberrations of individual lenses in an optical system can be used to cancel out each other, and an effective optical system can be constructed with these simple and inexpensive components. Achromatic lenses combine multiple lenses of different glass with different refractive indices in a compound lens that is largely free of chromatic aberration. Such lenses are used in cameras, they offer good performance but at relatively high cost. Concave mirrors are less expensive to manufacture than achromatic lenses and are completely free of chromatic aberration. However, the aluminum surface is easily corroded resulting in a loss of efficiency.

At each optical surface, including the interfaces between components in an achromatic lens, 5–10 % of the light is lost through absorbance or reflection; thus spectrophotometers ideally should be designed with a minimum number of optical surfaces (A. Primer, 1996).

2.1.13 Thermogravimetric Analysis (TGA)

Thermogravimetric Analyzer (TGA) is an essential laboratory tool used for material characterization. TGA is used in the research & development of various substances and engineering materials solid or liquid in order to obtain information about their thermal stability and composition. TGA is used as a technique to characterize materials used in various environmental, food, pharmaceutical, and petrochemical applications (Perkin Elmer guide, 2015). Recently, TGA has been used increasingly for the quality control and assurance of raw materials and incoming goods as well as for failure analysis of finished parts, especially in the polymer processing industry. In TGA, the mass of a substance is monitored as a function of temperature or time as the sample specimen is subjected to a controlled temperature program in a controlled atmosphere. A typical TGA apparatus consists of a sample pan that is supported by a precision balance; that pan resides in a furnace and is

heated or cooled during the experiment. The mass of the sample is monitored during the experiment. A sample purge gas controls the sample environment, this gas may be inert or a reactive gas that flows over the sample and exits through an exhaust as shown in figure (2.15) below.

These instruments can quantify loss of water, loss of solvent, loss of plasticizer, decarboxylation, pyrolysis, oxidation, decomposition, weight % filler, amount of metallic catalytic residue remaining on carbon nanotubes, and weight % ash. All these quantifiable applications are usually done upon heating, but there are some experiments where information may be obtained upon cooling. Both the TGA 8000 and the TGA 4000 are controlled by PerkinElmer's proprietary thermal software, Pyris software, and have auto-sampler accessories for unattended operations.

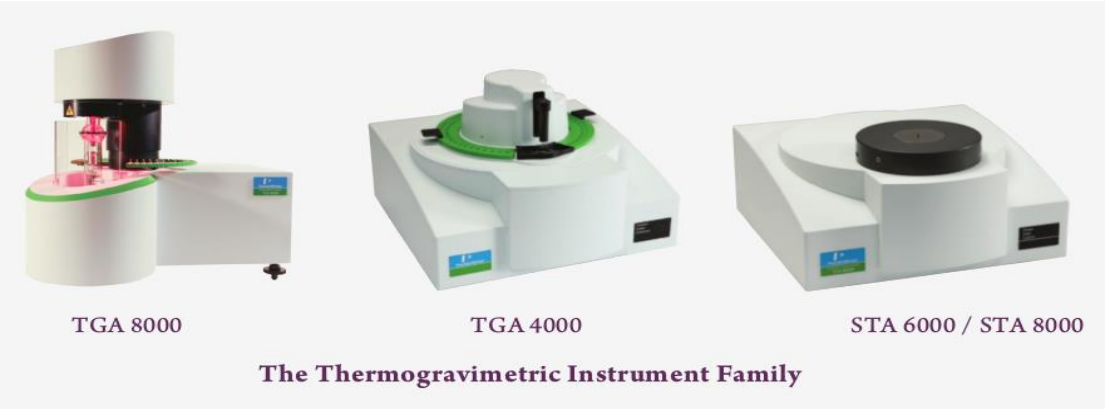

Figure (2.15): Various TGA models.

The thermogravimetric data collected from a thermal reaction is compiled into a plot of mass or percentage of initial mass on the y-axis versus either temperature or time on the x-axis. This plot, which is often smoothed, is referred to as a TGA curve. The first derivative of the TGA curve (the DTG curve) may be plotted to determine inflection points useful for in-depth interpretations as well as differential thermal analysis. Thermogravimetric kinetics may be explored for insight into the reaction

mechanisms of thermal (catalytic or non-catalytic) decomposition involved in the pyrolysis and combustion processes of different materials. Pyrolysis is the chemical decomposition of organic materials by heating in the absence of oxygen or any other reagents.

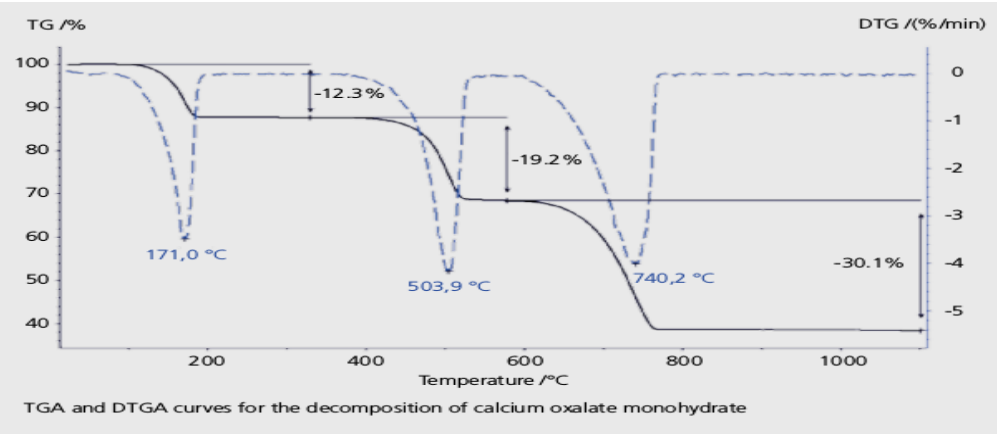

Figure (2.16): The decomposition of calcium oxalate monohydrate, CaC_2O_4. HO, in air at a heating rate of 10 K/min (NETZSCH Analysis & Testing publications, 2017).

2.1.13.1 Types of Thermal Gravimetric Analysis

- **Isothermal or Static Thermogravimetry:** In this technique, the sample weight is recorded as function of time at constant temperature.
- **Quasistatic Thermogravimetry:** In this technique the sample is heated to a constant weight at each of increasing temperatures.
- **Dynamic Thermogravimetry:** In this technique the sample is heated in an environment whose temperature is changed in linear manner.

2.1.13.2 TGA Characterizations

- Thermal stability of materials: Explicate decomposition mechanism, fingerprint materials for identification & quality control.
- Oxidative stability of materials: Oxidation of metals in air, oxidative decomposition of organic substances in air/O_2, thermal decomposition in inert atmosphere.
- Composition of multi-component systems: Behaviors sufficiently different on the temperature scale can be identified and reaction

mechanism formulated.

- ❖ Estimated lifetime of a product: Related to thermal stability.
- ❖ Decomposition kinetics of materials: Rate of reaction, activation energy.
- ❖ The effect of reactive or corrosive atmospheres on materials: Oxidation & corrosion studies.
- ❖ Moisture and volatiles content of materials: Loss of moisture, drying, desorption

2.1.13.3 Mechanisms of Weight Change in TGA

Weight Loss:

- ❖ Decomposition: The breaking apart of chemical bonds.
- ❖ Evaporation: The loss of volatiles with elevated temperature.
- ❖ Reduction: Interaction of sample to a reducing atmosphere (hydrogen, ammonia, etc).
- ❖ Desorption.

Weight Gain:

- ❖ Oxidation: Interaction of the sample with an oxidizing atmosphere.
- ❖ Absorption or Adsorption.

All of these are kinetic processes i.e. there is a rate at which they occur.

2.1.14 Differential Scanning Calorimetry (DSC)

A DSC measures the difference in the heat flow rate in (mW) between a sample and inert reference as a function of time and temperature. There are two types of DSC, namely; the heat flux DSC also known as qualitative differential thermal analysis which has only a single heat source, the second type is power compensated DSC with multiple heat sources that measure enthalpy change and compensates heat released or gained during thermal events. The heat flow is defined as:

$$\frac{dH}{dt} = c_p \frac{dT}{dt} \qquad (2.25)$$

Where dT/dt is the heating rate and c_p is sample heat capacity which is equal to the sample specific heat multiplied by its weight.

2.1.15 Simultaneous DSC-TGA Analyzer (SDT) Technique

Simultaneous DSC-TGA measures both heat flow and weight changes in a material as a function of temperature or time in a controlled atmosphere. Simultaneous measurement of these two materials properties not only improves productivity but also simplifies interpretation of the results. The complimentary information obtained allows differentiation between endothermic and exothermic events which have no associated weight loss (e.g., melting and crystallization) and those which involve a weight loss (e.g., degradation).

2.1.16 X-ray Diffraction (XRD)

It's all started in 1913 when Sir W.H. Bragg and his son Sir W.L. Bragg proposed the famous Bragg's law

$$2d \sin\theta = n\lambda \qquad (2.26)$$

Where they explained why the cleavage faces of crystals appear to reflect X-ray beams for certain incident angle (θ), here (n) is an integer (λ) is the wavelength of the X-rays and (d) is the distance between atomic layers in a crystal. This was the first example of X-ray interference known today as X-ray diffraction (XRD) and was direct evidence for the periodic atomic structure of crystals postulated several centuries before. Although Bragg's law was used to explain the interference patterns of X-rays scattered by crystals, diffraction method has been developed to study the structure of all states of matter with any beam such as ions, electrons, neutrons, and protons with a wavelength similar to the distance between the atomic or molecular structures of interest.

A crystal may be defined as a collection of atoms arranged in a pattern that is periodic in 3D. Crystals are necessarily solids, but not all solids are crystalline. In a perfect single crystal all atoms in the crystal are

related either through translational symmetry or point symmetry. Polycrystalline materials are made up of a great number of tiny single crystals. In powder diffraction method we can get the information from peak positions, crystal system, space group symmetry, translational symmetry, unit cell dimension, qualitative phase identification, from peak intensities, unit cell contents, point symmetry, peak shapes and widths, crystalline size, non-uniform microstrain and extended defects.

Deviations from ideal crystallinity, such as finite crystallite size and strain lead to broadening of the diffraction lines. By analyzing this broadening it is possible to extract information about the microstructure of a material. A perfect crystal would extend in all directions to infinity, so we can say that no crystal is perfect due to its finite size. This deviation from perfect crystallinity leads to a broadening of the diffraction peaks. However above a certain size (~ 0.1-1μm) this type of broadening is negligible.

In the present study, the Scherer equation was used to estimate the crystalline domain size (D) ***(Li et al., 2009)***:

$$D = \frac{k\lambda}{ß \cos ɵ} \qquad (2.27)$$

Where*:* k is a constant called shape factor which usually takes a value of about 0.94, *β is* full width at half maximum of the peak corresponding to a chosen plane for example (200), and ɵ is the angle obtained from 2ɵ value corresponding to maximum intensity peak in XRD pattern.

2.2 Previous Studies

In this section, previous studies concerning the utilization of PVA hybridized with silver nitrate ($AgNO_3$), in the field of radiotherapy as radiation detector and dosimeter as well as in other applications have been reviewed:

(Karthikeyan, 2005) prepared PVA/Ag films and the influence of annealing time upon the variation of cluster size were analyzed using optical absorption, emission and Fourier-transform infrared (FTIR) spectra. Measurements of optical spectra showed that the surface Plasmon resonance lays around 420 nm, and confirmed the growth of Ag clusters. Measurements of FTIR spectra were carried out to identify the role of chemical interface damping which influenced the broadening of the absorption band. The emission peak was observed at 540 nm for clusters which were annealed for 1 min as well as 2 min. The optical absorption spectra of PVA/Ag films annealed at 120 ^{o}C for different time duration are shown in figure (2.17). All the spectra showed the presence of a peak around 420 nm; this peak is a characteristic of silver's SPR. When the annealing time duration increases, the peak intensity also increases, and correspondingly the full width at half maximum (FWHM) becomes lesser. This clearly indicates that while increasing the time duration the mean size of Ag cluster formed also increases. At the same time, a red shift of the peak maximum and a noticeable broadening have been observed for the 10, 15 and 30 min annealed films.

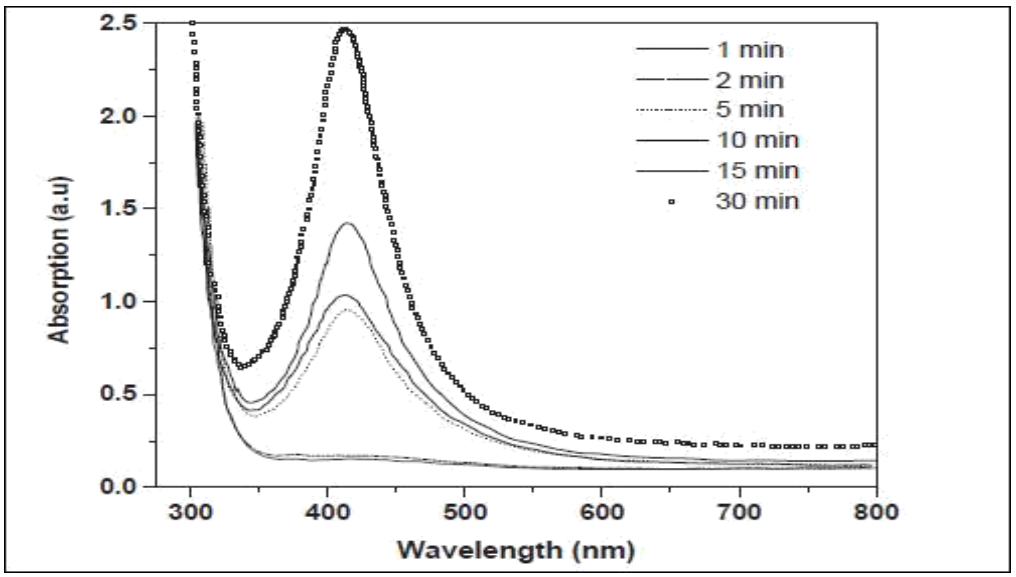

Figure (2.17): Optical absorption spectra of PVA/Ag films annealed at 120 ^{0}C for different durations.

(Aleksandra et al., 2007) prepared PVA/Ag nanocomposites with different contents of inorganic phase by reduction of Ag^+ ions in aqueous PVA solution by gamma irradiation followed by solvent evaporation. Optical properties of the colloidal solutions and the nanocomposite films were investigated using UV–Vis spectroscopy, an absorption peak at 420 nm corresponding to PVA/Ag films after irradiation with three different particle sizes were observed as shown in figure (2.18).

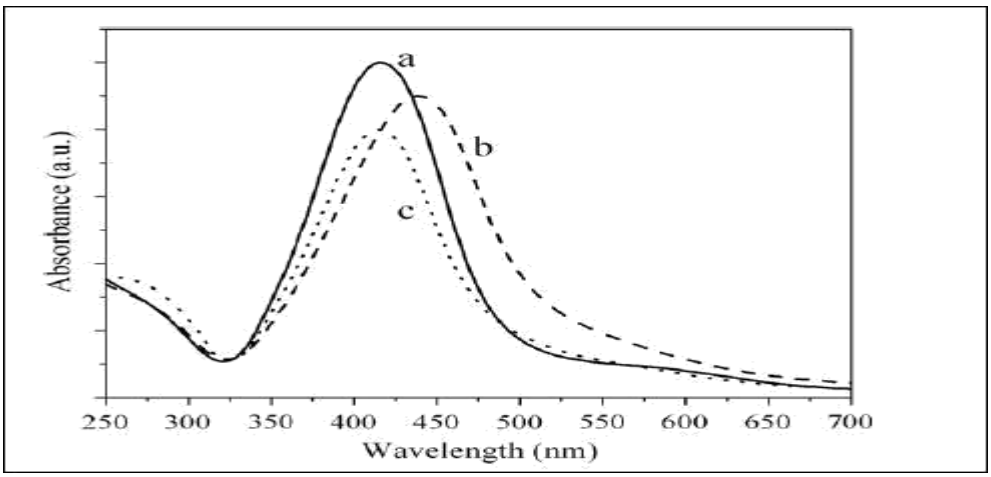

Figure (2.18): Absorption spectra of primary Ag colloid (a), corresponding PVA/Ag nanocomposite film (b), and colloid obtained after dissolution of PVA/Ag nanocomposite film(c).

Structural characterization of the Ag nanoparticles was performed by SEM and XRD. Interaction of the Ag nanoparticles with polymer matrix and the heat resistance of the nanocomposites were followed by IR spectroscopy and differential scanning calorimetry (DSC) analysis. IR spectra indicated that Ag nanofiller interact with PVA chain over OH groups. The changes of heat resistance upon the increase of the content of inorganic phase are correlated to the adsorption of polymer chains on the surface of Ag nanoparticles.

(Omer M. et al., 2011) prepared a poly vinyl-alcohol/silver composites in a form of a film by in situ irradiation doping technique up to 50 kGy. The effect of radiation upon the composites resulted in reducing the silver ions into black metallic silver, so the general film color changed

from white to golden-yellow then black color at 50 kGy. The UV-Vis spectroscopy revealed an absorption band peaking at 425 nm which was increased exponentially with dose increment. The study of UV-Vis spectrogram revealed that the maximum absorbance A_{max} increased with increasing particles radius. Scanning electron microscopy (SEM) revealed shiny nanoparticles of silver cored in PVA with homogeneous distribution and having an average size of 30 nm as well as the XRD spectrum that shows cubic center face of silver nanoparticles in the film and a crystalline peak for PVA reduced by radiation to amorphous phase**.**

(Muhammad Attique et al., 2014) investigated the dosimetric characterization and spectroscopic study of radiochromic films using natural dyes as dosimeters. Radiochromic films were prepared with PVA gel matrix and natural dyes (Turmeric, Walnut and Henna) with three concentrations, i.e. C_1=0.5 g/L, C_2=0.25 g/L and C_3=0.13 g/L having pH value of 4 for acidic samples and 10 for alkaline samples. The thickness of the film was fixed to be 0.05 mm. The behavior of the dyes was studied on the basis of change in specific absorbance with concentration, change in specific absorbance with absorbed dose; effect of pH on specific absorbance, electrical conductivity, molar extinction coefficients, and percentage discoloration. Absorption spectra for non-irradiated and γ-irradiated films were studied. λ_{max} of T= 451 nm, for W=340 nm and for H=320 nm was recorded. Absorbance at each λ_{max} was found by using spectrophotometer and specific absorbance was calculated. Response curve for specific absorbance versus concentration showed linear behavior for each dye. Plot of specific absorbance versus dose made the behavior of the dye clear and it was noticed that acidic samples of all the dye samples worked the best. Maximum degree of discoloration in the Turmeric, Walnut and Henna dye films was observed to be 94%, 51.5%

and 93.7% respectively. XRD analysis was performed and it was found that for Turmeric, %age crystallanity as well as C.I decreased while for Walnut and Henna both factors increased. Moreover, mechanical properties of dye films were studied which showed that due to irradiation some changes had occurred in the crystal structure which is the major reason of discoloration of the dye films.

(Zidan, 1999) prepared Polyvinyl alcohol films, with various $AgNO_3$ filler mass fractions ($\leq 5\%$). The structural and morphological variations due to filling and UV-irradiation were investigated using differential scanning calorimetry (DSC), UV-Vis optical absorption spectroscopy, X-ray diffraction and scanning electron microscopy (SEM). Two different crystalline phases (one is due to the PVA matrix and the other is attributed to the PVA/Ag+ chelates) were detected besides the PVA amorphous phase, for the non-irradiated and the UV-irradiated (for 2, 4 and 6 h) films as shown in figures (2.19), (2.20) and (2.21).

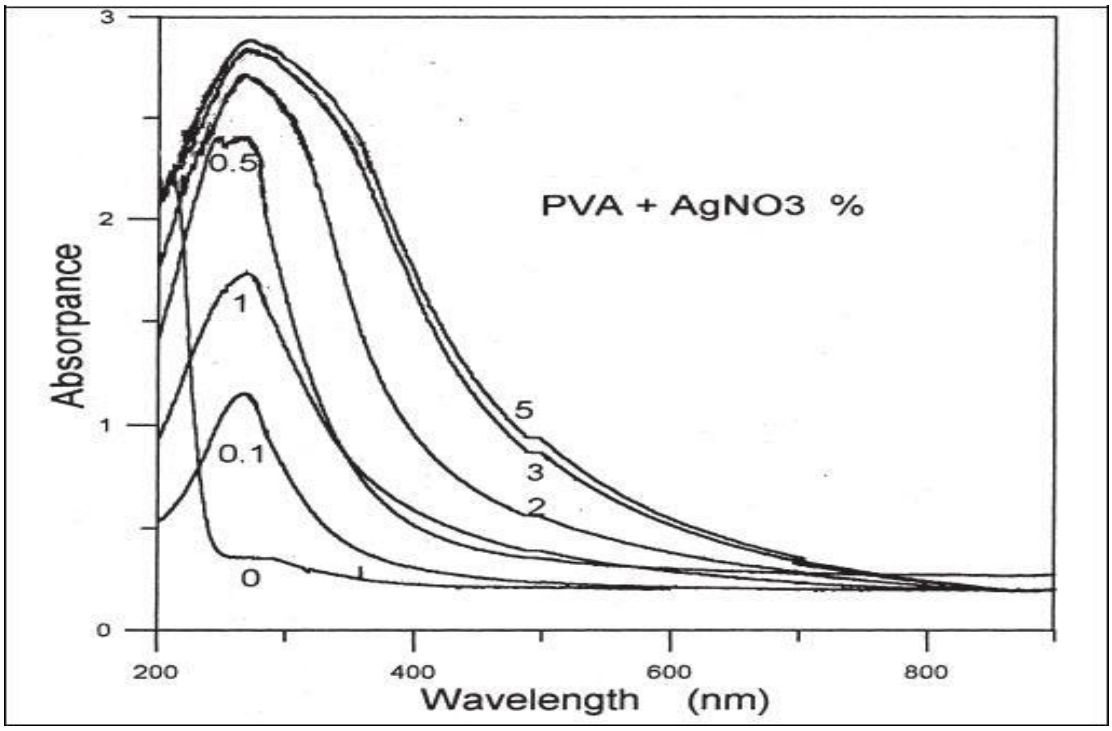

Figure (2.19): UV/Vis optical absorption spectra after IT 2 h for film of $AgNO_3$ filled with PVA system.

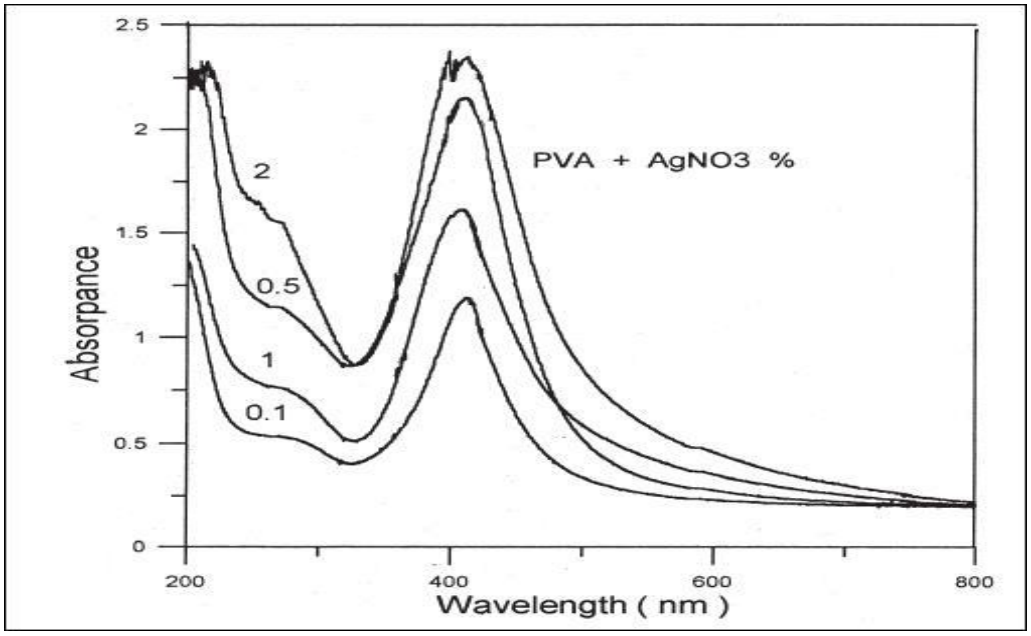

Figure (2.20): UV/Vis optical absorption spectra after IT 4 h for film of $AgNO_3$ filled with PVA system.

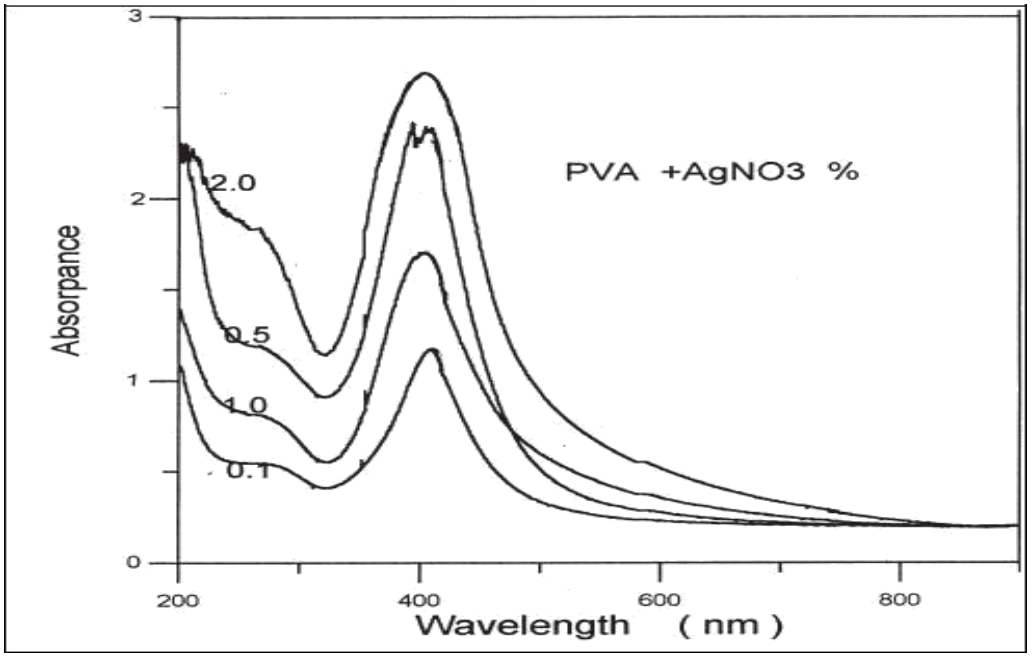

Figure (2.21): UV/Vis optical absorption spectra after IT 6 h for film of $AgNO_3$ filled with PVA system.

The PVA–Ag+ chelates disappeared at 2 h UV-irradiation implying that the structural morphology changes vastly due to the changes in filling level and/or UV-irradiation time. The observed morphological patterns were discussed.

(Abdo Mohd et al., 2014) prepared polyaniline (PANI) and nickel (Ni) nanoparticles embedded in polyvinyl alcohol (PVA) film matrix using gamma radiolytic method. The mechanism of formation of PANI and Ni nanoparticles were proposed via oxidation of aniline and reduction of Ni ions, respectively. The effects of dose and Ni ions concentration on structural, optical, and electrical properties of the final PVA/PANI/Ni nanocomposites films were carefully examined. The structural and morphological studies showed the presence of PANI with irregular granular microstructure and Ni nanoparticles with spherical shape and diameter less than 60 nm. The average particle size of Ni nanoparticles decreased with increasing dose and decreasing of precursor concentration due to increase of nucleation process over aggregation process during gamma irradiation. The optical absorption spectra showed that the absorption peak of Ni nanoparticles at about 390 nm shifted to lower wavelength and the absorbance increased with increasing dose. The formation of PANI was also revealed at 730 nm absorption peak with the absorbance increasing by the increase of dose. The electrical conductivity increased with increasing of dose and chlorine concentration due to number of polarons formation increase in the PVA/PANI/Ni nanocomposites. Optical absorption spectra showed a blue shift of the absorption peak of Ni nanoparticles due to decreasing particle size with increasing of dose. The optical band gap of PANI decreased with increasing of dose and chlorine concentration. Moreover, the absorbance of both PANI and Ni nanoparticles increased with dose due to increase of polarons and Ni nanoparticles formation. Finally, the electrical conductivity of the nanocomposites increased with the increase of dose and chlorine concentration corresponds to the increased amount of polarons.

(Mutahir et al., 2011) stated the International Commission of

Radiological Units (ICRU) sets a tolerance of ±5 % on dose delivery, with more recent data limiting the overall tolerances to ±3 %. One of the best methods for accurate dose delivery and quality check is in vivo dosimetry, while radiotherapy is performed. This study was carried out to test the applicability of diodes for performing in vivo entrance dose measurements in external photon beam radiotherapy for pelvic tumors and its implementation as quality assurance tool in radiotherapy. During November 2007 to December 2009, in 300 patients who received pelvic radiotherapy on a multileaf-collimator-assisted linear accelerator, the central axis dose was measured by in vivo dosimetry by p-Si diodes. Entrance dose measurements were taken by diodes and were compared with the prescribed dose. Totally 1000 calculations were performed, the mean and standard deviation between measured and prescribed dose was 1.26 ± 2.8 %. In 938 measurements (93.8 %), the deviation was <5 % (1.36 ± 2.9%); in 62 measurements (6.2 %) the mean deviation was >5 % (5.51 ± 2.3 %). Larger variations were seen in lateral and oblique fields more than anteroposterior fields. For larger deviations, patients and diode positional errors were found to be the common factors alone or in combination with other factors. After additional corrections, repeated measurements were achieved within tolerance levels. This study showed that diode-detector-based in vivo dosimetry was simple, cost–effective, provides quick results and can serve as a useful quality assurance tool in radiotherapy. The data acquired in this study can be used for evaluating output calibration of therapy machine, precision of calculations, effectiveness of treatment plan and patient setup.

(Farhat et al., 2011) measured the entrance and exit dose for patient treated for head and neck tumors. The target absorbed dose was determined from the exit and entrance dose measurement. Twenty patients were evaluated. The results were compared to the calculated

values and the midline dose was determinate and compared with the prescribed dose. 80 entrance doses and 80 exit doses measurements were performed. The average difference from expected values was 1.93% for entrance dose (SD 1.92%) and 0.34% for exit dose (SD 4.1%). The target absorbed dose differed from prescribed dose values by 2.94% (1.97%) for the results using the Noël method and 3.34% (SD: 2.29%) with the Rizzotti method. The total uncertainty budget in the measurement of the absorbed entrance and exit dose with diode, including diode reading, correction factors and diode calibration coefficient, is determined as 3.02%. Simple in vivo dose measurements are an additional safeguard against major setup errors and calculation or transcription errors that were missed during pre-treatment chart check.

(Mohammed et al., 2011) prepared PVA/Ag nanoparticles composites films by using in situ irradiation doping technique up to 50 KGy. The effect of radiation upon the composites resulted in reducing the silver ions into black metallic silver, so the general film color changed from white to golden-yellow then black color at 50 KGy as shown in figures (2.22) and (2.23).

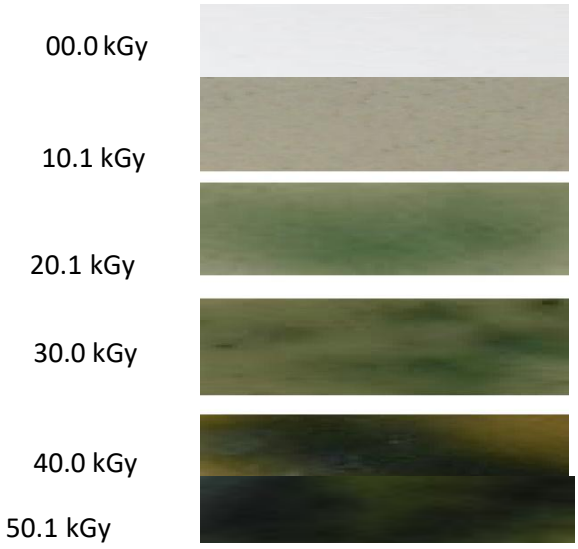

Figure (2.22): The color change of PANI nanoparticles polymerized by radiation doping at different doses in PVA blend for 28.6%-AniHCl monomer. The picture of the un-irradiated film was taken on a white background.

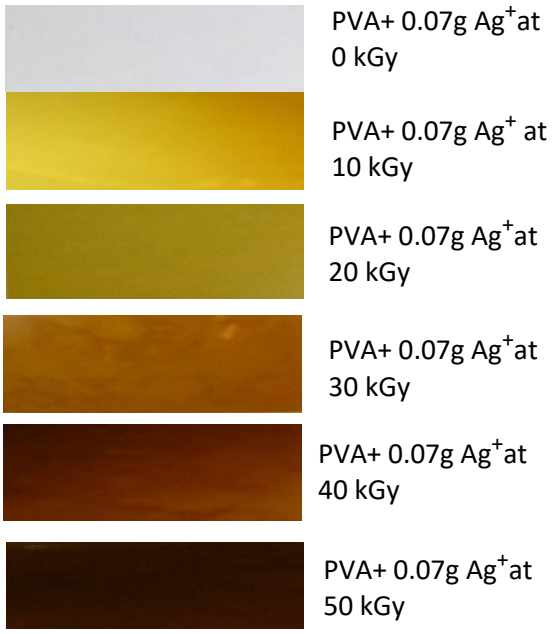

Figure (2.23): The color change to golden yellow of irradiated PVA/$AgNO_3$ composites due to reduction of $AgNO_3$ to Ag^+ nanoparticles induced by γ-rays. The picture of the un-irradiated film was taken on a white background.

The UV-visible spectroscopy revealed an absorbance band peaking at 425 nm which was increased exponentially with dose increment. The study of UV-spectrogram revealed that the maximum absorbance A_{max} increased following the particles radius. Scanning electron Microscopy (SEM) revealed shiny nanoparticles of silver cored in Polyvinyl-alcohol PVA with homogeneous distribution and having an average size of 30 nm as well as the XRD spectrum that showed cubic center face of silver nanoparticles in the film and a crystalline peak for PVA reduced by radiation to amorphous phase.

(Ramnani et al., 2007) synthesized Silver clusters on SiO_2 support using ^{60}Co gamma radiation, the irradiation of Ag^+ in aqueous suspension of SiO_2 in the presence of 0.2 moldm_3 isopropanol resulted in the formation of yellow suspension. The absorption spectrum showed a band at 408 nm corresponding to typical characteristic surface Plasmon resonance of Ag nanoparticles. The effect of Ag^+ concentration on the formation of Ag cluster indicated that the size of Ag clusters vary with Ag^+ concentration, which was varied from 4-10-4 to 5-10-3 moldm-3. The results showed that Ag clusters are stable in the pH range of 2–9 and start agglomerating in the alkaline region at pH above 9. The effect of radiation dose rate and ratio of Ag^+/SiO_2 on the formation of Ag clusters have also been investigated. The prepared clusters have been characterized by X-ray diffraction (XRD) and transmission electron microscopy (TEM), which showed the particle size of Ag clusters to be in the range of 10–20 nm, as shown in figure (2.24).

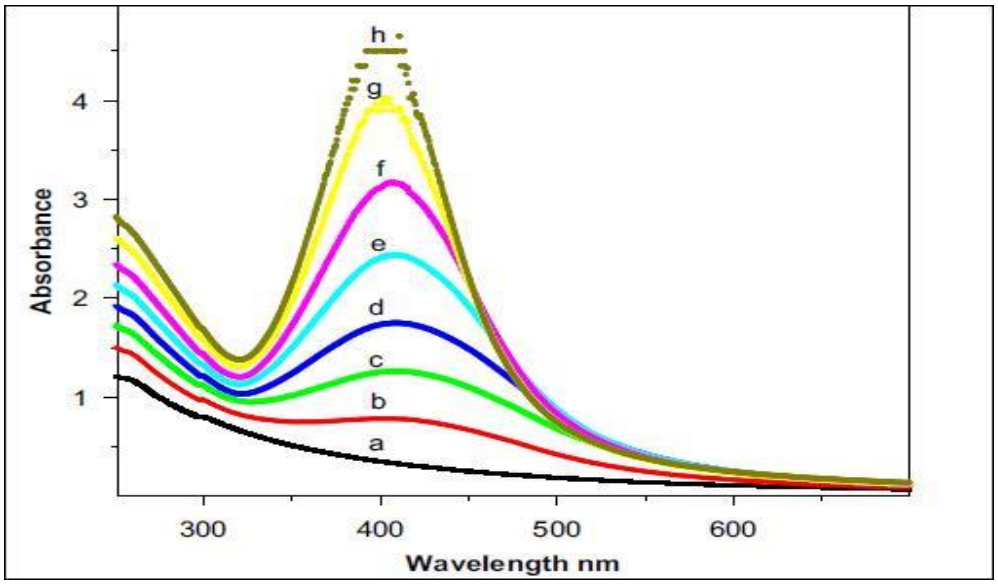

Figure (2.24): UV spectra with various radiation doses (a) 0 kGy, (b) 0.12 kGy, (c) 0.24 kGy, (d) 0.36kGy, (e) 0.54 kGy, (f) 0.66 kGy, (g) 0.72 kGy and (h) 0.78 kGy.

Chapter Three
Materials and Methodology

3.1Materials

3.1.1 Polyvinyl Alcohol (PVA)

Polyvinyl alcohol powder supplied by TECHNO PHARMCHEM (Mol. wt = 85000 to 124000 g/mol, Degree of hydrolysis 86-89%).

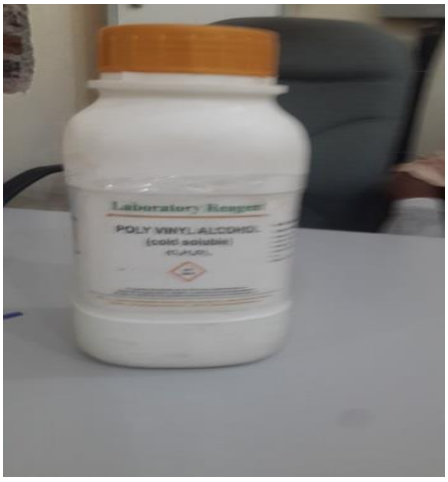

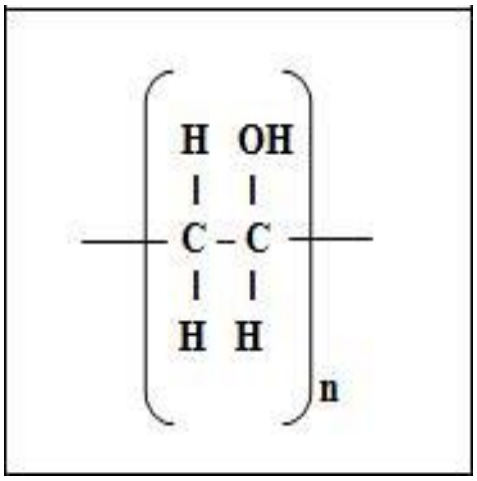

Figure (3.1): Polyvinyl alcohol used in this study and its monomer.

3.1.2 Silver Nitrate ($AgNO_3$)

Silver nitrate chemical compound (in powder) supplied by laboratory reagents and fine chemicals Ltd, sensitive to sun light in photographic films.

3.1.3 Other Experimental Tools

Distilled water, volumetric flask, Petri dish, beakers, bottles and cutter.

Figure (3.2): Various tools used during films preparation.

3.1.4 ^{60}Co Teletherapy Unit

TERABALT radiotherapy unit type 80/100 containing a powerful gamma radiation source (Cobalt-60 isotope) has been used for samples irradiation. General cobalt-60 teletherapy unit specifications are briefly discussed below.

3.1.4.1 The Source

The ^{60}Co source is produced by irradiating ordinary stable ^{59}Co with neutron in a reactor. The nuclear reaction can be represented by ^{59}Co (n,γ) ^{60}Co. The ^{60}Co source, usually in the form of a solid cylinder disc or pallets, is contained inside stainless capsule and sealed by welding. The double welded seal is necessary to prevent any leakage of the radioactive material. The ^{60}Co source decay to ^{60}Ni with the emission of β particles (E_{max} = 0.32 Mev) and two photons per disintegration of energies 1.17 and 1.33 Mev, these two photons constitute the useful treatment beam.

The β particles are absorbed in the cobalt metal and the stainless-steel capsules resulting in the emission of Bremsstrlung X-ray and small amount of characteristic X-ray. A typical teletherapy ^{60}Co source is a cylinder of diameter ranging from 1.0 to 2.0 cm and is positioned in the cobalt unit with its circular end facing the patient. The fact that the radiation source is not a point source complicates the beam geometry and gives rise to what is known as the geometric penumbra.

3.1.4.2 Source Housing

The housing for the source is called the source head figure (3.3). It consists of a steel shell filled with lead for shielding purposes and a device for bringing the source in front of an opening in the head from which the useful beam emerges. Also, a heavy metal alloy sleeve is provided to form an additional primary shield when the source is in the OFF position. A number of methods have been developed for moving the

source from the off position to the on position. These methods have been discussed in detail by (Johns and Cunningham, 2010). It will suffice here to mention briefly four different mechanisms: (a) the source mounted on a rotating wheel inside the source head to carry the source from the OFF position to the ON position; (b) the source mounted on a heavy metal drawer plus its ability to slide horizontally through a hole running through the source head, in the ON position the source faces the aperture for the treatment beam and in the OFF position the source moves to its shielded location and a light source mounted on the same drawer occupies the ON position of the source; (c) mercury is allowed to flow into the space immediately below the source to shut off the beam; and (d) the source is fixed in front of the aperture and the beam *can* be turned ON and OFF by a shutter consisting of heavy metal jaws. All of the above mechanisms incorporate a safety feature in which the source is returned automatically to the OFF position in case of a power failure.

Figure (3.3): The cobalt-60 machine that used to irradiate the films in this study.

3.1.4.3 Beam Collimation

A collimator system is designed to vary the size and shape of the beam to meet the individual treatment requirements. The simplest form of a

continuously adjustable diaphragm consists of two pairs of heavy metal blocks. Each pair can be moved independently to obtain a square or a rectangle-shaped field. Some collimators are multivane type, i.e.,multiple blocks to control the size of the beam.

3.1.5 UV-Visible Spectroscopy

UV-visible spectrophotometer Model V-650 UV/VIS/NIR was used to measure the absorption spectra. The instrument is specified by its resolution value of 0.1 nm and wavelength accuracy ± 0.30 nm (at a spectral bandwidth of 0.5 nm) in the UV/Vis region. Single monochromatic, UV/Vis region 1200 lines/mm plane grating, NIR region 300 lines/nm plane grating, Czerny-Turner mount, double beam type.

Figure (3.4): The UV- Visible spectrophotometer used in this study.

3.1.6 Sensitive Balance

Sensitive balance model ABT-220 – 4M was used to measure the weight of PVA and $AgNO_3$ to determine the concentrations (wt%) of PVA and $AgNO_3$ in the PVA/ $AgNO_3$ Films.

Figure (3.5): The sensitive balance used in this study.

3.1.7 Data Logger

Data logger model PRHTemp 2000 was used to measure the temperature, humidity and atmospheric pressure during the synthesis of the PVA/$AgNO_3$ films.

Figure (3.6): The data logger instrument used in this study.

3.1.8 Magnetic Stirrer

Figure (3.7): The magnetic stirrer instrument used in this study.

3.1.9 Micrometer

Micrometer model 99MAA001M was used to measure the thickness of PVA/$AgNO_3$ films.

Figure (3.8): The micrometer Instrument used in this study.

3.1.10 Optical Density and Image J Software

PVA/$AgNO_3$ films with different concentrations were analyzed using a personal computer desktop scanner HP DeskJet2600 and imageJ software on a personal computer workstation 24 hours after irradiation. Images produced were 16 bit RGB color images, the total optical densities of the films were measured and fogs were subtracted to obtain the optical density of each irradiated film. From these results a graph representing the optical density versus applied radiation doses was produced using excel sheet and origin lab software as indicated in the result section. To overcome problems related to scanner homogeneity, the polymer's films were each scanned in identical position at the center of the HP scanner with a control film.

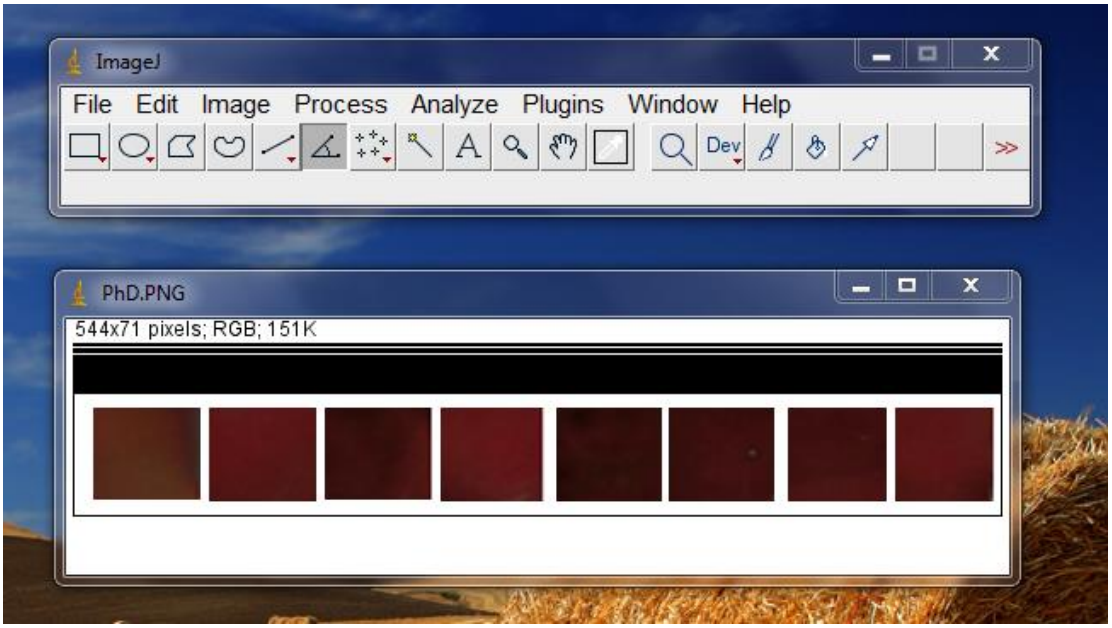

Figure (3.9): The interface of an ImageJ software.

3.1.11 Scanner

HP DeskJet 2600 has been used to scan all polymers films that needed for the optical density in this thesis.

Figure (3.10): The scanner machine used in this study.

3.1.12 Ionization Chamber

PTWFarmer ionization Model N30013 Waterproof was used in radiation dose measurements.

Figure (3.11): The ionization chamber used in this study.

3.1.13 Solid Water Phantom

Solid water phantom 30 cm x 30 cm x 30 cm was used for radiation dose determination.

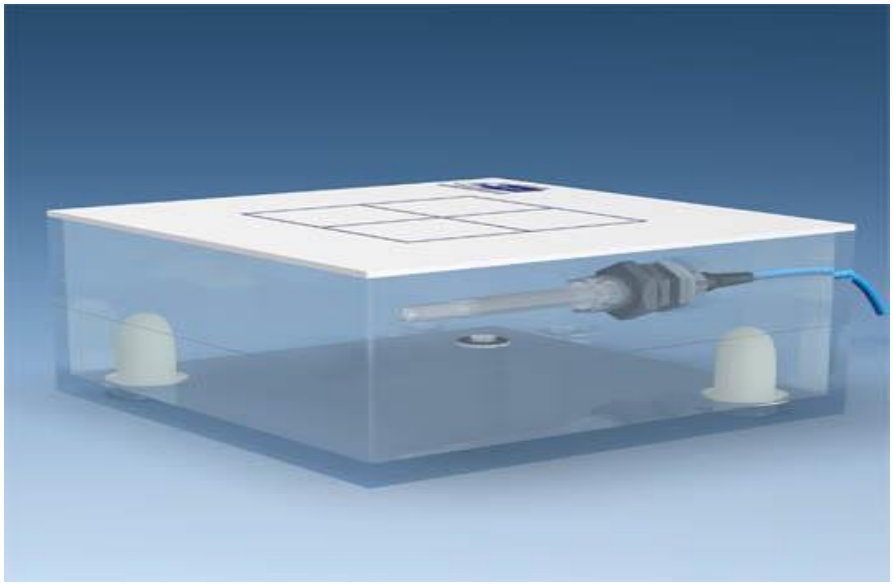

Figure (3.12): The phantom used in this study.

3.1.14 Treatment Planning System (TPS)

Treatment planning system for Radiotherapy PlanW2000 was used for doing plans using Source Axial Distance technique (SAD), with Gantry angle at 0^0, collimator angle 0^0, Source Surface Distance (SSD) 95cm, field size 10x10 cm^2.

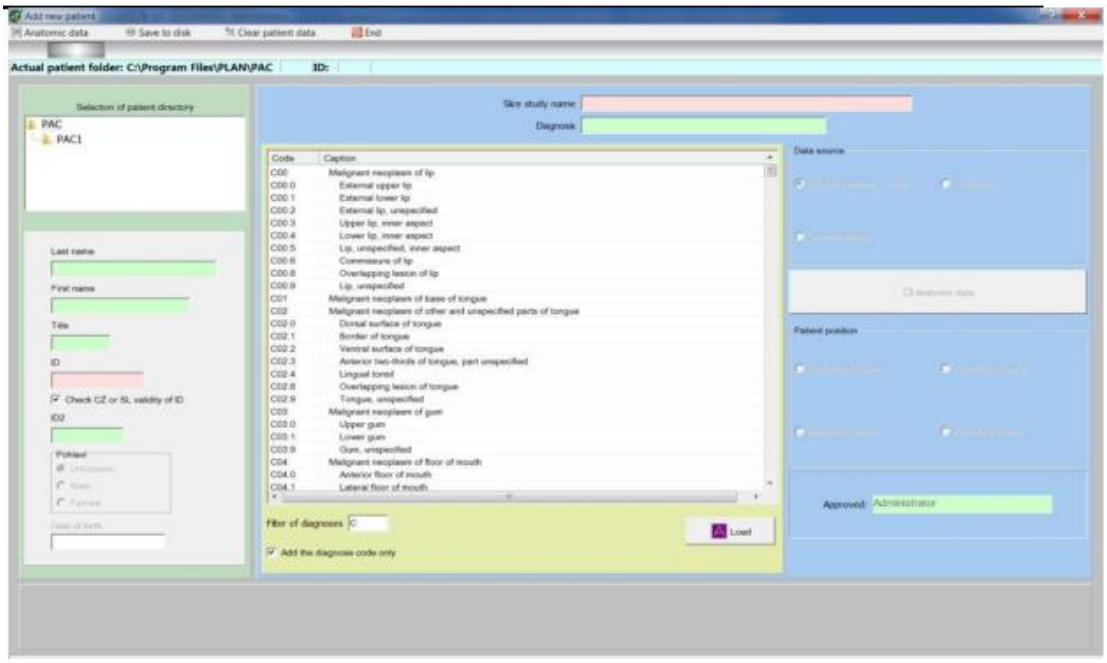

Figure (3.13): The interface of the TPS (PlanW200) used in this study.

3.1.15 TGA and DSC

Simultaneous thermal analysis TGA/DSC apparatus model NETZSCH STA 449 F3 was used in this study. Thermal experiments were carried out on all samples at a heating rate of 10 K/min with nitrogen as a carrier gas at a flow rate of 20 ml/min.

Figure (3.14): The apparatus used for thermal analysis in this study.

3.1.16 Structural Analysis: X-ray Diffraction (XRD)

The XRD pattern and crystalline structure of the prepared samples were determined from X-ray Diffractometer model explorer from GNR analytical instruments group equipped with Cu K_α as radiation source (λ = 1.54Å).

Figure (3.15): The XRD apparatus used for structural analysis in this study.

3.2Methodology

3.2.1 Preparation of PVA/$AgNO_3$ Composite Films

The PVA stock was supplied by TECHNO PHARMCHEM (Mol. wt = 85000 to 124000 g/mol Degree of hydrolysis 86-89%). The PVA/$AgNO_3$ films were made using solvent casting technique with four concentrations of $AgNO_3$ i.e. [C_1 = 5 wt% Ag], [C_2 = 10 wt% Ag], [C_3 = 15 wt% Ag] and [C_4 = 20 wt% Ag] by dissolving each concentration of PVA powder in 100 ml distilled water at room temperature on a beaker. Solutions were magnetically stirred at room temperature for 3 hours then poured in a Petri-dish to form films by casting method in a dark room. Films were left to dry at ambient temperature at least 2 days, the ambient condition was measured using data logger [Temperature = 24.1 ^{0}C, Humidity = 28.5%, atmospheric pressure = 961 mBar]. Films were peeled off the Petri-dish, cut into small films 2x2 cm (suitable for measurements), loaded in sealed dark dental film envelopes. Thicknesses of the films were measured using a micrometer.

Figure (3.16): Some tools used during PVA/$AgNO_3$ synthesis.

Figure (3.17): The dissolution of PVA/$AgNO_3$ in distilled water using magnetic stirrer and a hotplate.

3.2.2 Irradiation of Film Samples

TERABALT Cobalt-60 unit was used for samples irradiation. Different radiation doses which were specify with treatment planning system (TPS) PlanW2000 (0 Gy, 5 Gy and 10 Gy) at Surface Source Distance (SSD) 95cm, field Size (FS) 10 x10 cm^2, Gantry angle 0^0, Collimator angle 0^0. The films were placed in the center of the field size. ^{60}Co γ-rays irradiation facility (TERABALT - radiotherapy cobalt unit type 80 – model SCS, UJP PRAHA, CZECH REPUBLIC) from National Cancer Institute, University of Gazira, Wad-Madani, Sudan was used in this study.

3.2.3 Films Characterization and Data Analysis

All samples of PVA/$AgNO_3$ composites were analyzed using XRF, UV-Vis spectrophotometer, X-ray diffraction analysis (XRD), Differential scanning calorimetry (DSC) and Thermogravimetric analysis (TGA). Graphs were produced and analyzed using Microsoft Excel sheet and Origin Lab software.

3.2.4 Data Storage

Personal computer PC was used for storing all data produced during this study.

Chapter Four: Results

In the following chapter the experimental results of the prepared PVA\$AgNO_3$ composite films and their characterizations after gamma irradiation are presented.

4.1 Color Formation Change

0 Gy 5 Gy 10 Gy

Figure (4.1): The change in PVA/$AgNO_3$ films color intensity due to irradiation with γ-ray doses.

4.2 X-ray Fluorescence (XRF) Measurements

XRF was used to validate the intensity of AgLα characteristic X-ray line dependence on the $AgNO_3$ concentration in the PVA/$AgNO_3$ composite films.

Table (4.1): Shows the intensity of AgLα characteristic X-ray line for PVA/$AgNO_3$ films irradiated with Gamma doses of (0, 5 and 10) Gy.

$AgNO_3$ Concentration	Intensity of AgLα line in (PPT) for non-irradiated (0 Gy) PVA/$AgNO_3$ films.	Intensity of AgLα line in (PPT) for PVA/$AgNO_3$ films irradiated with 5 Gy.	Intensity of AgLα line in (PPT) for PVA/$AgNO_3$ films irradiated with 10 Gy.
5.0 wt %	958.0	952.3	945.0
10 wt %	965.2	958.3	949.1
15 wt %	972.4	966.1	959.8
20 wt %	978.8	972.3	963.4

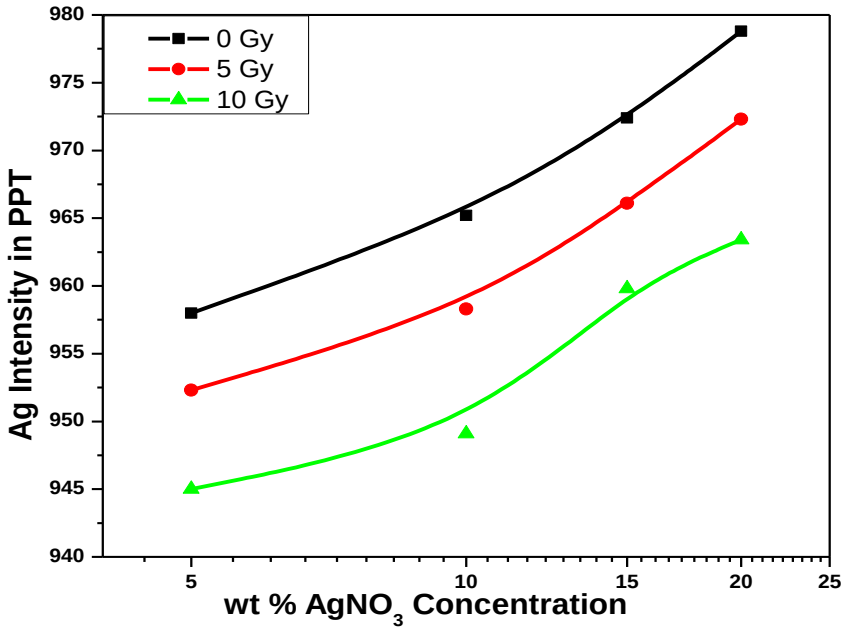

Figure (4.2): Dependence of the intensity in part per thousand (PPT) of AgLα characteristic X-ray line on $AgNO_3$ concentration for non-irradiated and Gamma- irradiated PVA/$AgNO_3$ films.

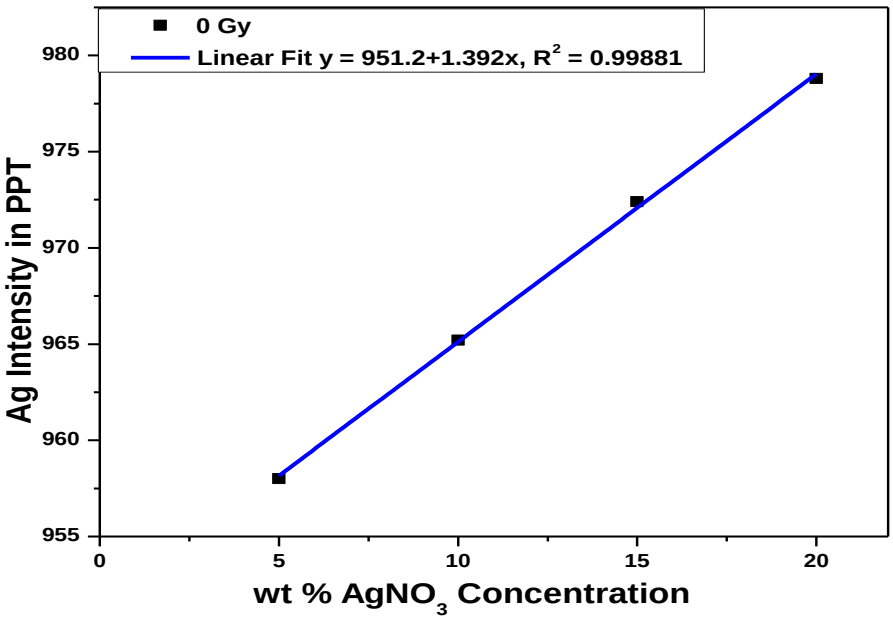

Figure (4.3): Correlation between intensity in part per thousand (PPT) of AgLα characteristic X-ray line and $AgNO_3$ concentration for non-irradiated PVA/$AgNO_3$ films.

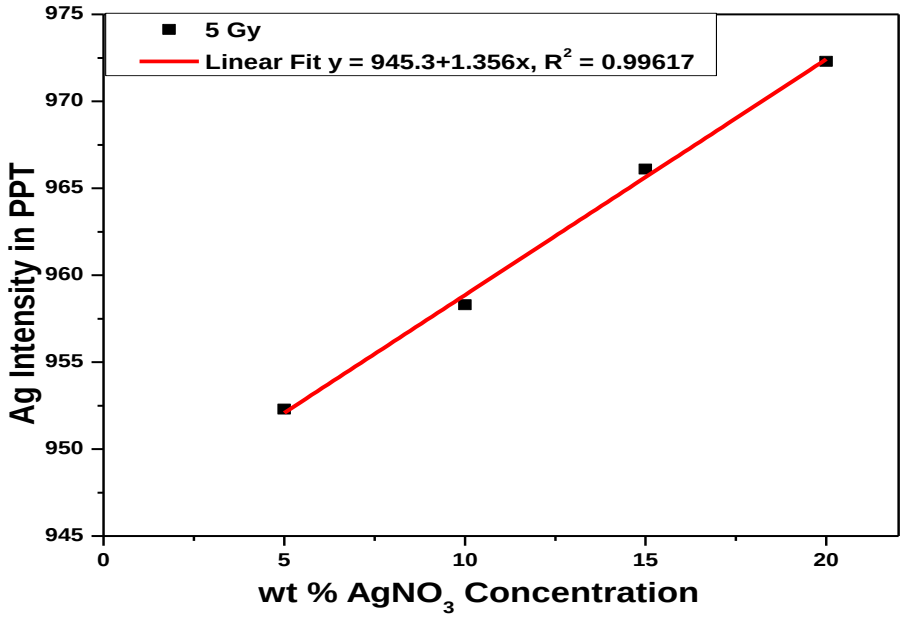

Figure (4.4): Correlation between intensity in part per thousand (PPT) of AgLα characteristic X-ray line and $AgNO_3$ concentration for PVA/$AgNO_3$ films irradiated with 5 Gy.

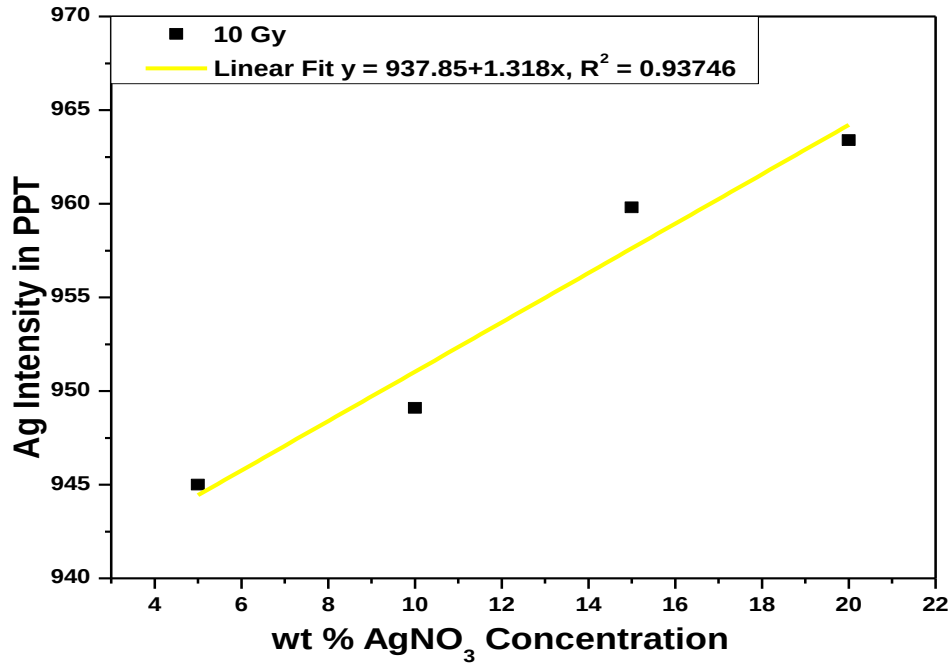

Figure (4.5): Correlation between intensity in part per thousand (PPT) of AgLα characteristic X-ray line and $AgNO_3$ concentration for PVA/$AgNO_3$ films irradiated with 10 Gy.

4.3UV- Visible Spectroscopy Measurements

The absorption spectra in ultraviolet and visible regions (UV-Vis) arise from the electronic transitions in the molecules. The electronic absorption spectra of the non-irradiated and gamma-irradiated PVA/$AgNO_3$ films were measured in the wavelength range of 200-1100 nm; using a non-irradiated PVA/$AgNO_3$ film as reference.

4.3.1 Effects of $AgNO_3$ Addition on the UV-Vis Spectrum of PVA Matrix

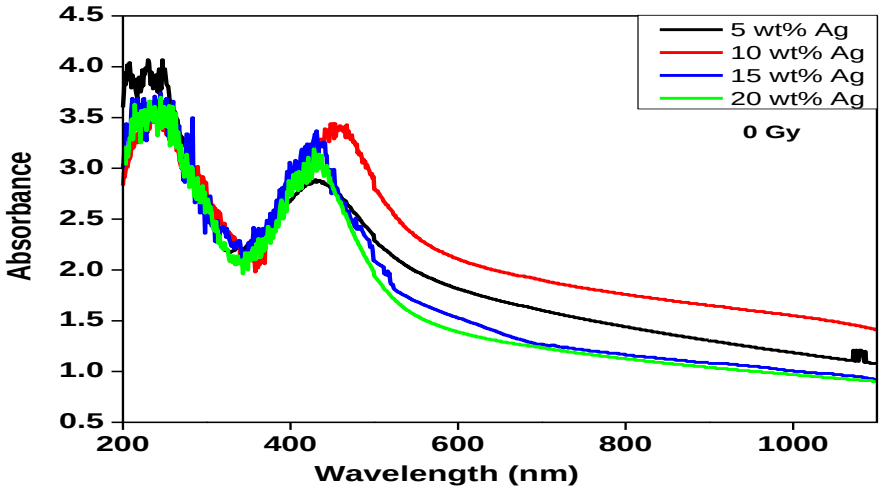

Figure (4.6): UV-visible absorption spectra of PVA/Ag composite films doped with different $AgNO_3$ concentrations non-irradiated (0 Gy).

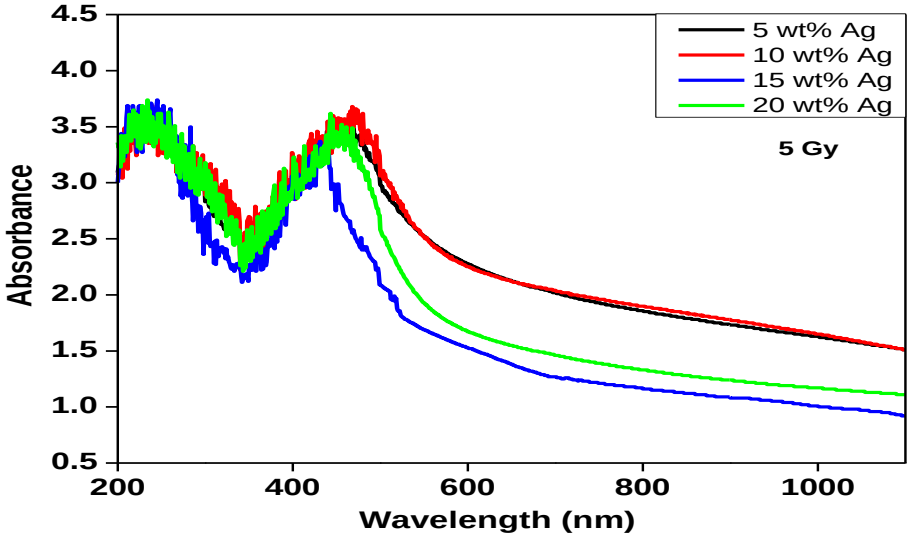

Figure (4.7): UV-visible absorption spectra of PVA/Ag composite films doped with different $AgNO_3$ concentrations, gamma-irradiated at 5 Gy.

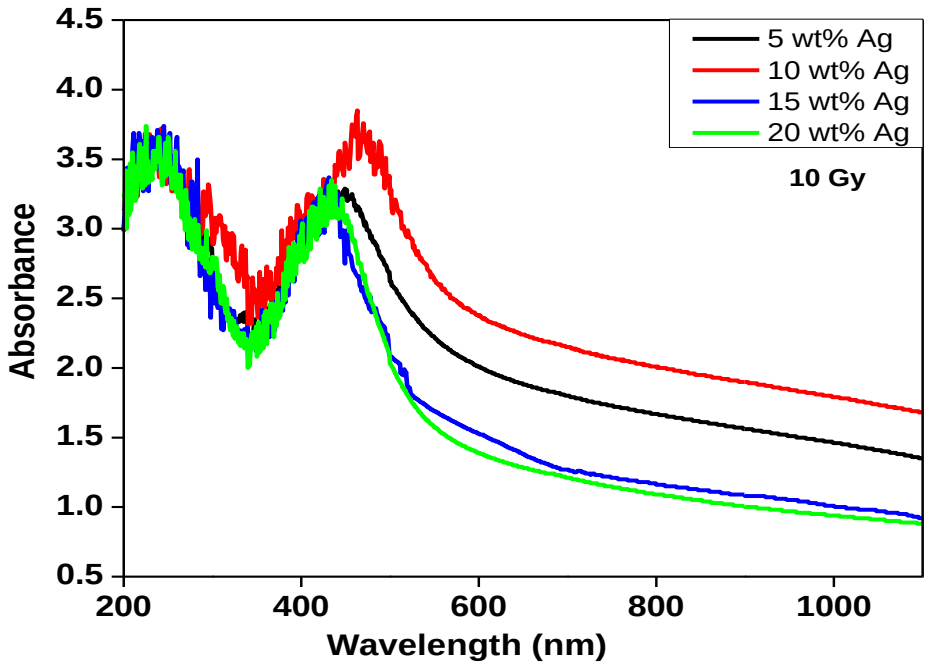

Figure (4.8): UV-visible absorption spectra of PVA/Ag composite films doped with different $AgNO_3$ concentrations, gamma-irradiated at 10 Gy.

4.3.2 Effects of Gamma-Irradiation on the UV-Visible Spectra of PVA/$AgNO_3$

When PVA/$AgNO_3$ films are subjected to γ-irradiation, the optical properties are the net result of the electronic transition of the two materials. **Figures (4.9 through 4.12)** show UV-visible absorption spectra of PVA filled with (5, 10, 15 and 20) wt% of $AgNO_3$ irradiated with different gamma ray doses of (0, 5 and 10) Gy.

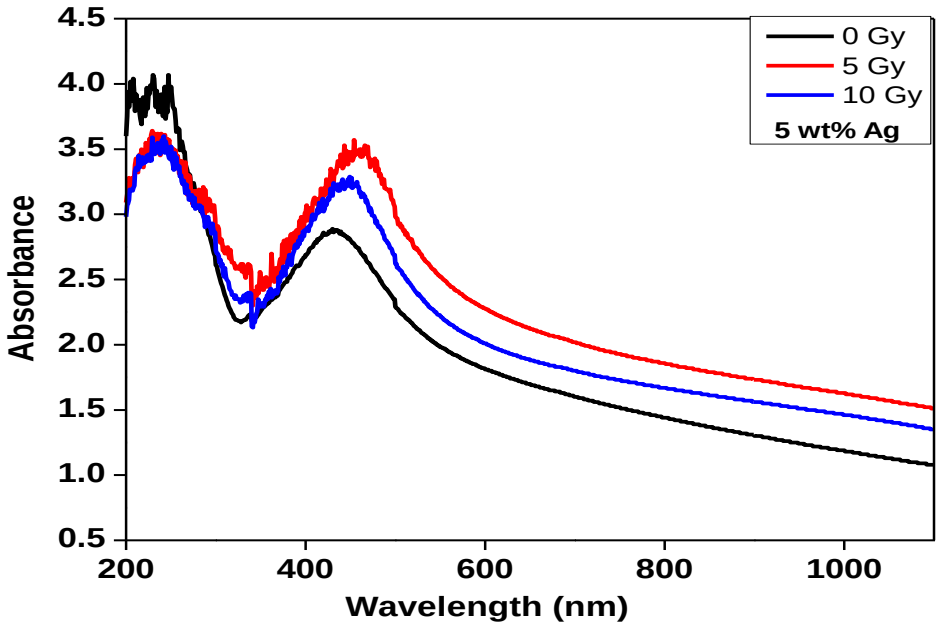

Figure (4.9): UV-Visible absorption spectra of gamma-irradiated PVA/$AgNO_3$ samples with 5.0 wt% Ag.

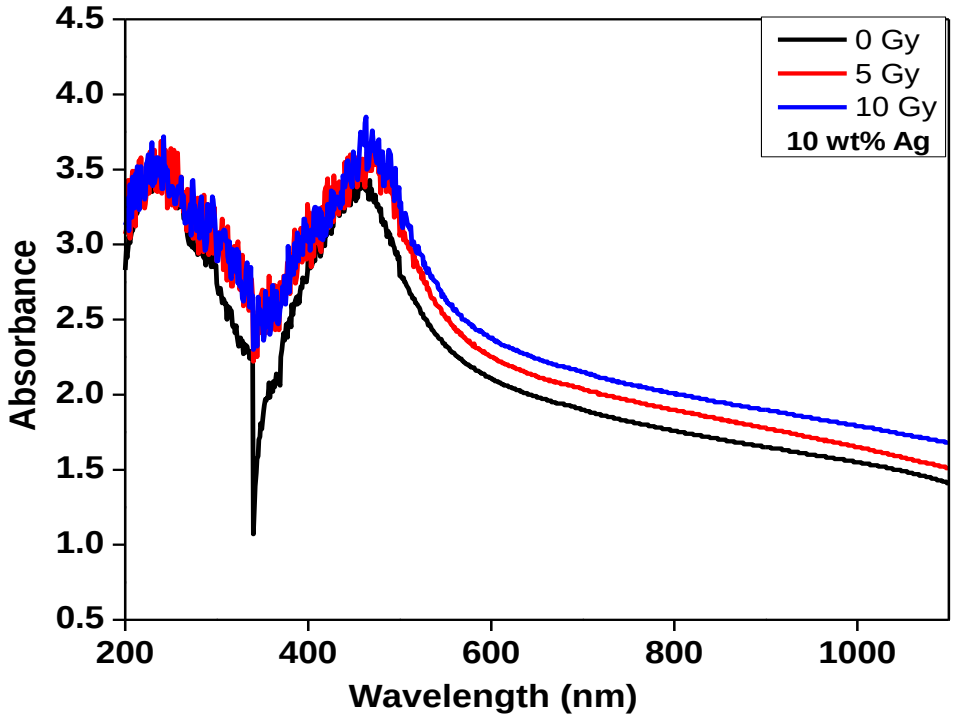

Figure (4.10): UV-Visible absorption spectra of gamma-irradiated PVA/$AgNO_3$ samples with 10 wt% Ag.

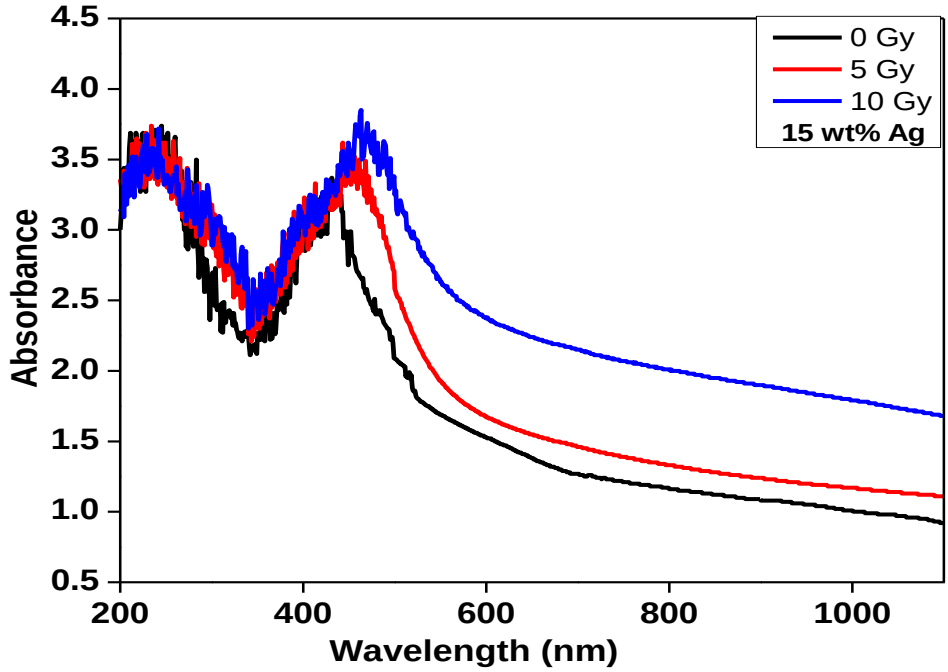

Figure (4.11): UV-Visible absorption spectra of gamma-irradiated PVA/$AgNO_3$ samples with 15 wt% Ag.

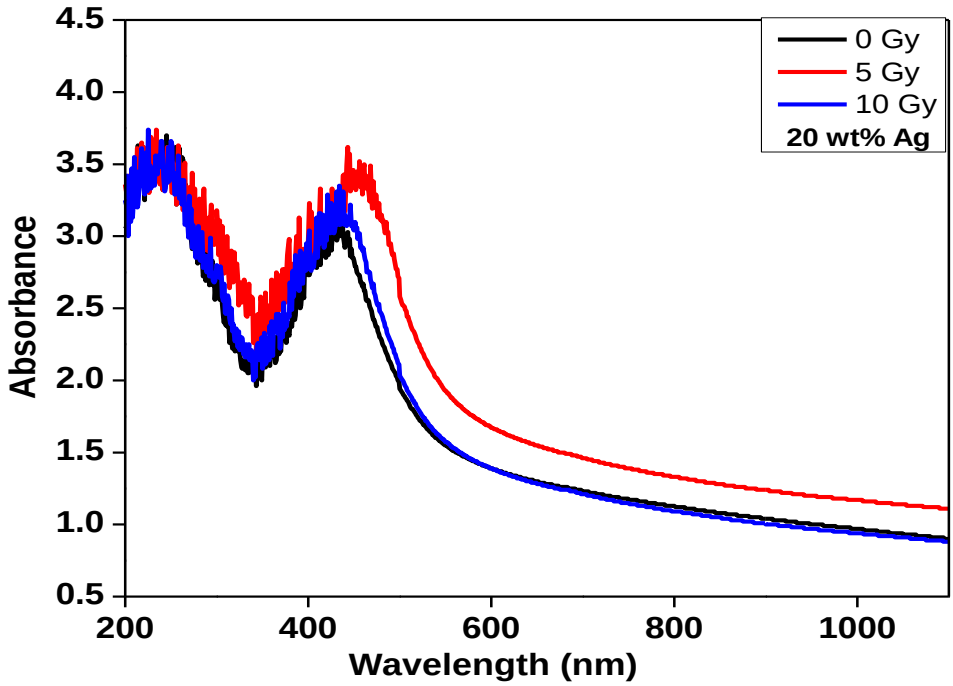

Figure (4.12): UV-Visible absorption spectra of gamma-irradiated PVA/$AgNO_3$ samples with 20 wt% Ag.

4.3.3 Specific Absorbance (A) and Absorption Coefficient (*α*)

Table (4.2): The specific absorbance values for PVA/$AgNO_3$ films with different concentrations of $AgNO_3$ irradiated with γ-radiation doses of (0, 5 and 10) Gy.

$AgNO_3$ Concentration	Specific Absorbance for PVA/$AgNO_3$ films non- irradiated (0 Gy).	Specific Absorbance for PVA/$AgNO_3$ films irradiated with 5 Gy.	Specific Absorbance for PVA/$AgNO_3$ films irradiated with 10 Gy.
5.0 wt %	2.88	3.5	3.25
10 wt %	3.43	3.6	3.74
15 wt %	3.3	3.44	3.73
20 wt %	3.12	3.45	3.26

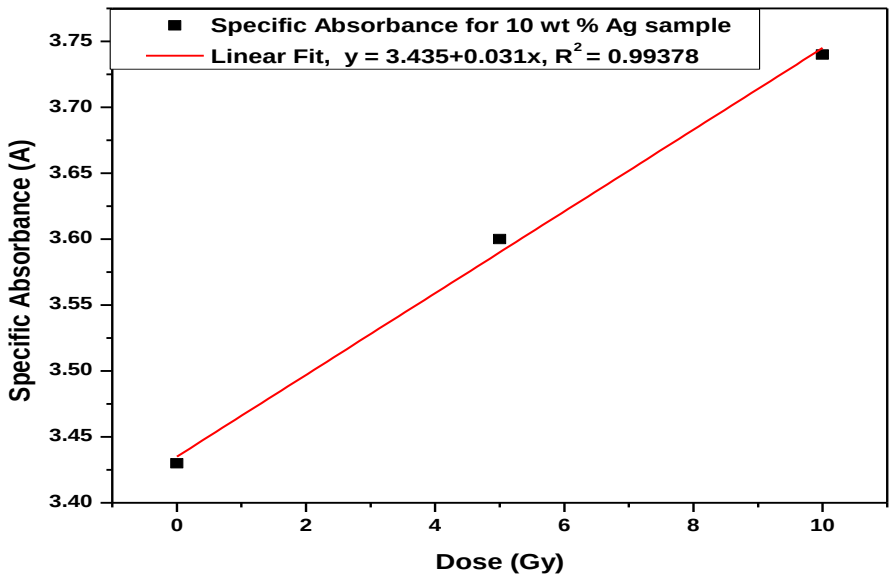

Figure (4.13): Correlation between specific absorbance and radiation dose of gamma-irradiated PVA/$AgNO_3$ sample with 10 wt % Ag as an example.

Table (4.3): The thickness of PVA/$AgNO_3$ films measured using a micrometer. Average thickness = 0.11 mm = 110 μm.

$AgNO_3$ Concentration	Thickness in (mm) for PVA/$AgNO_3$ films non-irradiated (0 Gy).	Thickness in (mm) for PVA/$AgNO_3$ films irradiated with 5 Gy.	Thickness in (mm) for PVA/$AgNO_3$ films irradiated with 10 Gy.
5.0 wt %	0.09	0.12	0.09
10 wt %	0.12	0.10	0.11
15 wt %	0.10	0.11	0.09
20 wt %	0.09	0.09	0.10

Table (4.4): The absorption coefficients values of the PVA/Ag films with different concentration of $AgNO_3$ irradiated with radiation doses of (0, 5 and 10) Gy.

$AgNO_3$ Concentration	Absorption Coefficients for PVA/$AgNO_3$ films non-irradiated (0 Gy).	Absorption Coefficients for PVA/$AgNO_3$ films irradiated with 5 Gy.	Absorption Coefficients for PVA/$AgNO_3$ films irradiated with 10 Gy.
5.0 wt %	0.060	0.0733	0.068
10 wt %	0.0718	0.0754	0.0783
15 wt %	0.069	0.072	0.078
20 wt %	0.0653	0.0722	0.0683

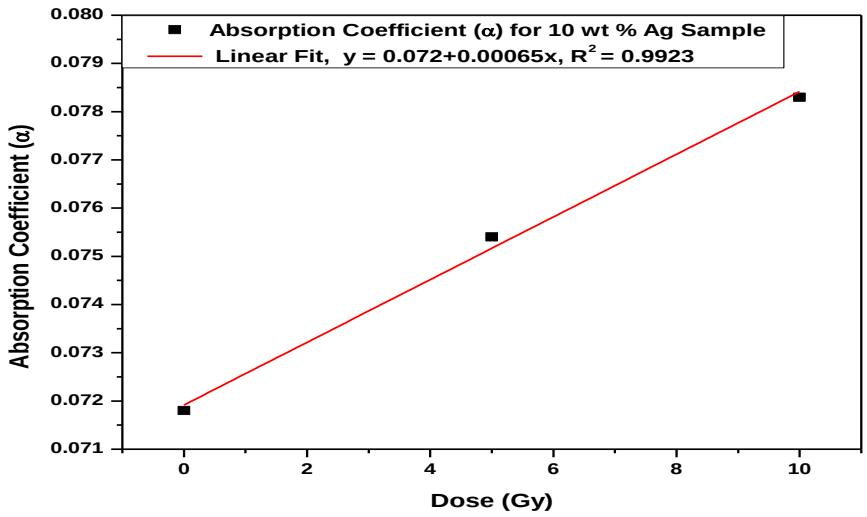

Figure (4.14): Correlation between absorption coefficient and radiation dose of gamma-irradiated PVA/$AgNO_3$ sample with 10 wt % Ag as an example.

4.3.4 Particle Size

Particle size in the composite films was calculated using the equation below

$$D = \frac{2\,hv_f}{FWHM} \qquad (4.1)$$

Where: h is Plank's constant, v_f = 1.39 x10^6 ms^{-1} is Fermi velocity of electron in bulk silver. FWHM is the full width at half maximum of surface Plasmon resonance (SPR) band.

Table (4.5) Dependence of particle size in PVA matrix on gamma-irradiation dose for PVA/$AgNO_3$ samples with different concentrations.

$AgNO_3$ Concentration	Particle Size of PVA/$AgNO_3$ films non-irradiated (0 Gy).	Particle Size of PVA/$AgNO_3$ films irradiated with 5 Gy.	Particle Size of PVA/$AgNO_3$ films irradiated with 10 Gy.
5.0 wt %	8.672	9.58	10.14
10 wt %	11.157	10.241	11.373
15 wt %	11.654	10.337	11.249
20 wt %	11.934	10.456	12.447

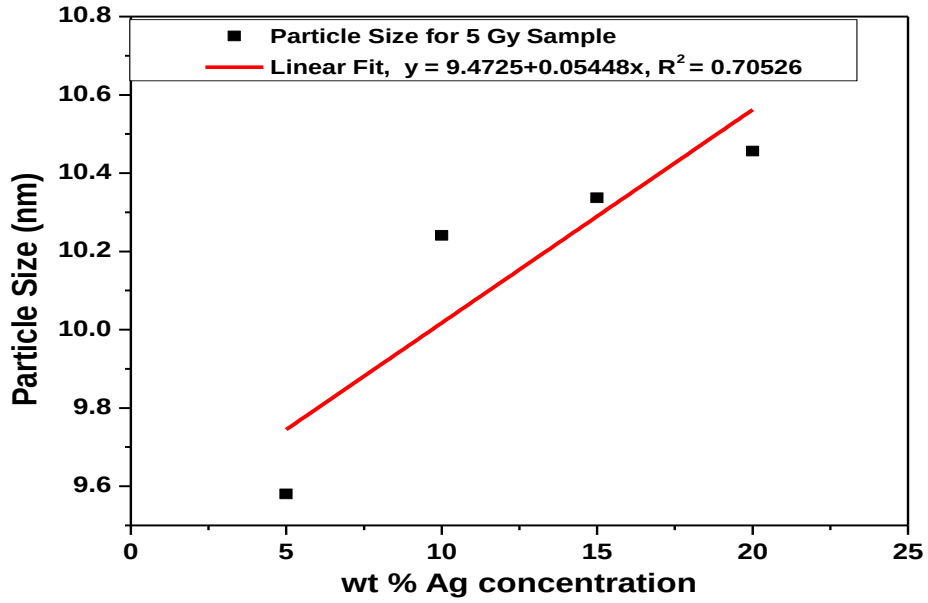

Figure (4.15): Correlation between Ag particle size and $AgNO_3$ concentration for sample irradiated with 5 Gy as an example.

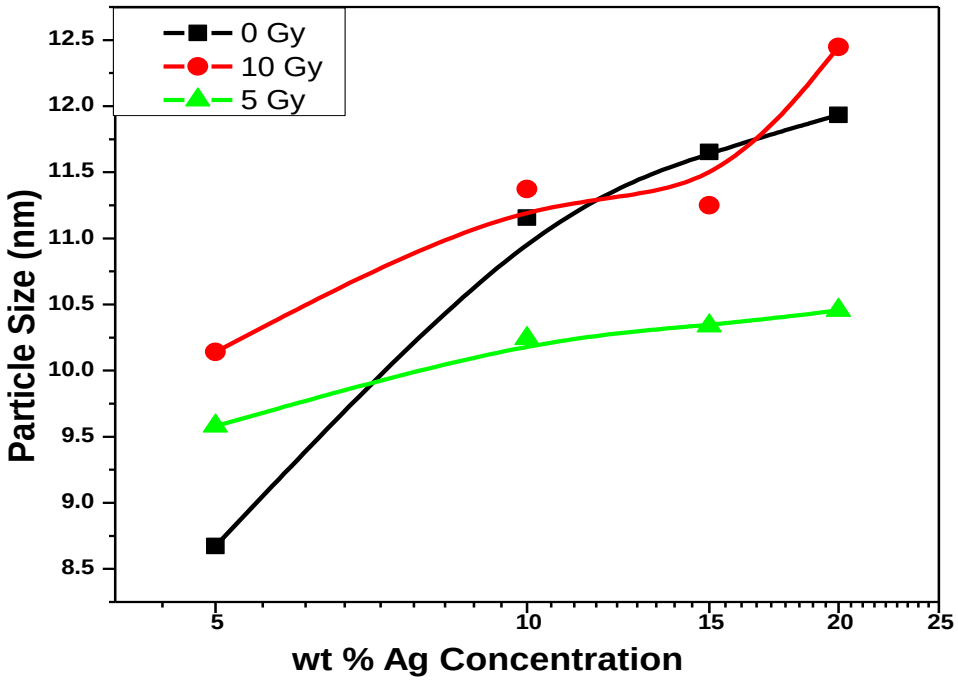

Figure (4.16): Correlation between Ag particle size and $AgNO_3$ concentration for non-irradiated and γ-irradiated samples.

4.3.5 Calculation of the Optical Band Gap of PVA/Ag Nanocomposite

The optical band gap (E_g) has been estimated from absorption coefficient data as a function of wavelength by using Tauc relation.

$$\alpha h\nu = A(h\nu - \mathrm{E_g})^r \qquad (4.2)$$

Where: α is the absorption coefficient, hν is the photon energy, E_g is the optical energy gap, A is a constant known as the disorder parameter also known as band tailing parameter which is nearly independent of the photon energy and r is the parameter measuring the type of transition which take values of 1/2 for direct band gap and 2 for indirect band gap.

It is well known that Ag has a direct band gap semiconductor. The direct band gap value was estimated from the plots of $(\alpha h\nu)^2$ versus hν. The energy gap was calculated by extrapolating of the straight portion in **Figure (4.17)** to hν axis i.e. at α = 0 for 10 wt% of 10 Gy sample, as an example. The calculated values of the band gap are listed in **Table (4.6).**

Table (4.6): The optical band gaps of PVA/Ag nanocomposites prepared with different concentrations and gamma-irradiation doses.

Energy gap (eV)			
Dose (Gy)	Non-irradiated films (0 Gy).	Films irradiated with 5 Gy.	Films irradiated with 10 Gy.
5.0 wt %	3.72	3.36	3.4
10 wt %	3.658	3.17	3.26
15 wt %	3.57	3.16	3.37
20 wt %	3.52	3.19	3.56

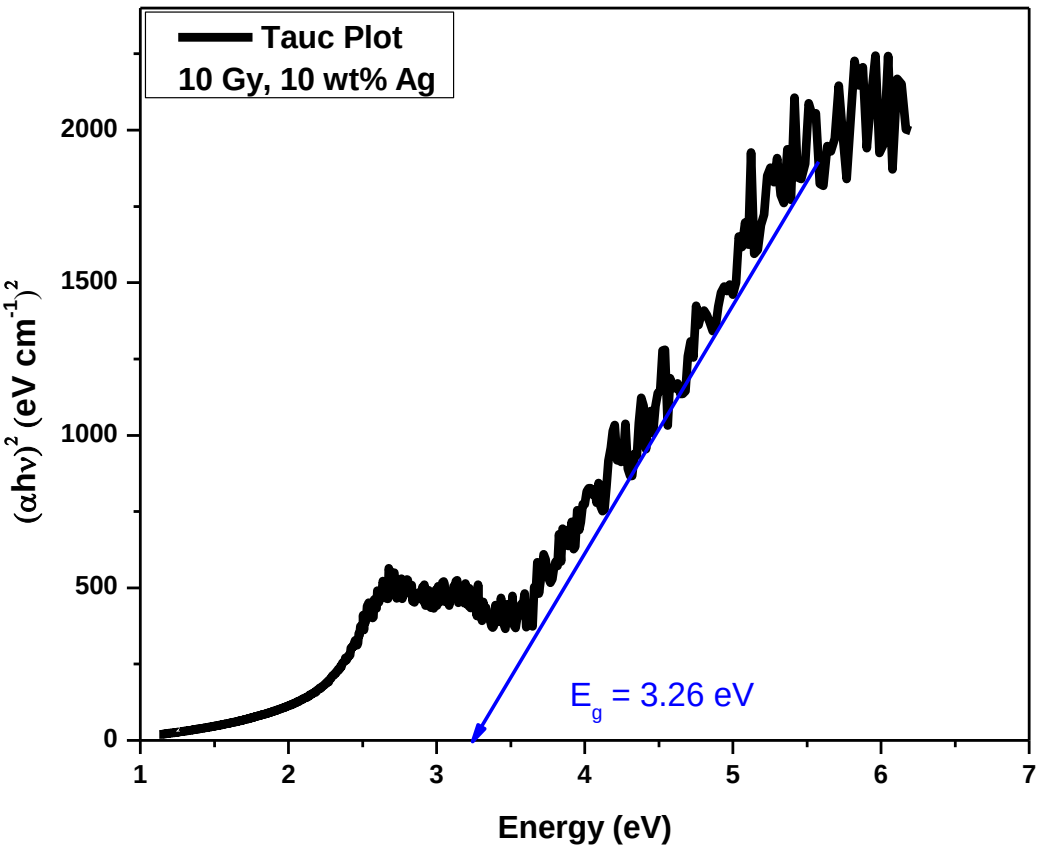

Figure (4.17): Relation between $(\alpha h\nu)^2$ and photon energy ($h\nu$) for PVA/Ag of 10 wt% Ag irradiated with 10 Gy as an example on (E_g) estimation process.

4.3.6 Extinction Coefficient (K)

Also known as the attenuation coefficient was calculated from the absorption coefficient using the equation below:

$$K = \frac{\alpha\lambda}{4\pi} \qquad (4.3)$$

Where: α is the absorption coefficient and λ is the wavelength.

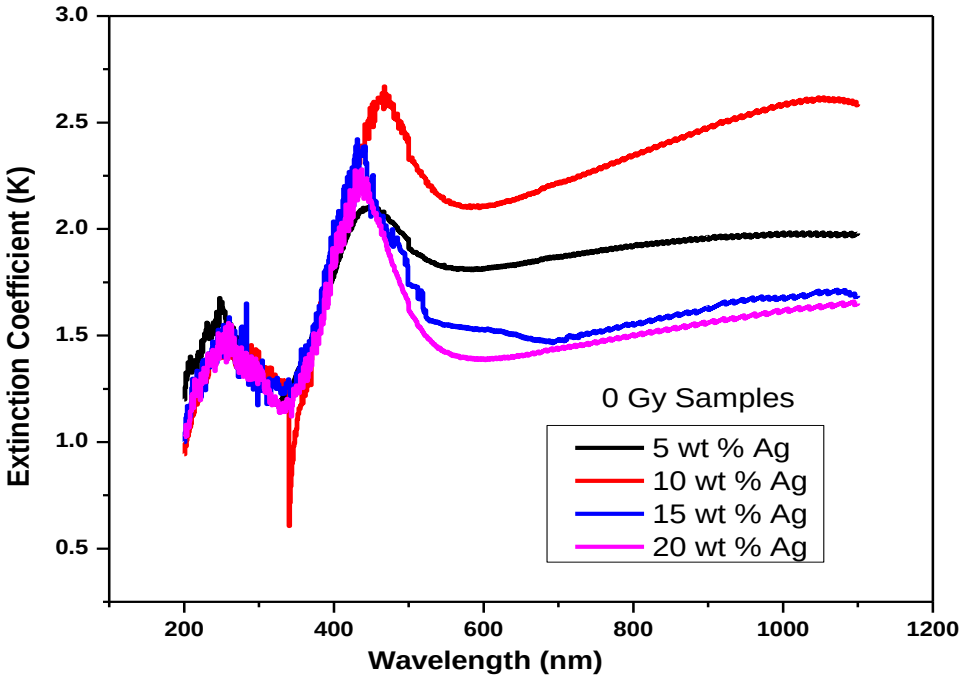

Figure (4.18): Extinction Coefficient of PVA/Ag composite films doped with different $AgNO_3$ concentrations non-irradiated (0 Gy).

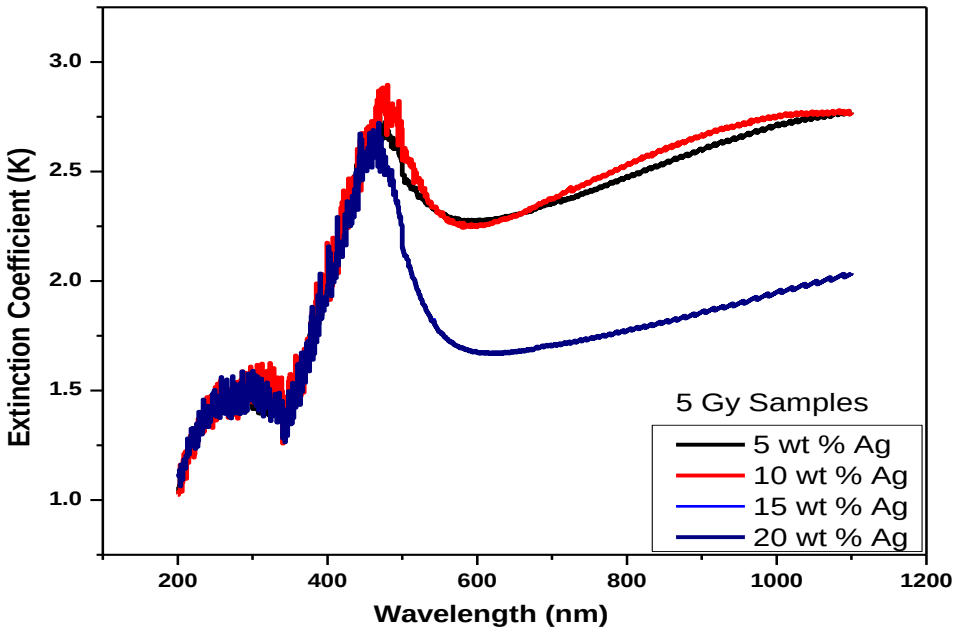

Figure (4.19): Extinction Coefficient of PVA/Ag composite films doped with different $AgNO_3$ concentrations Gamma-irradiated at 5 Gy.

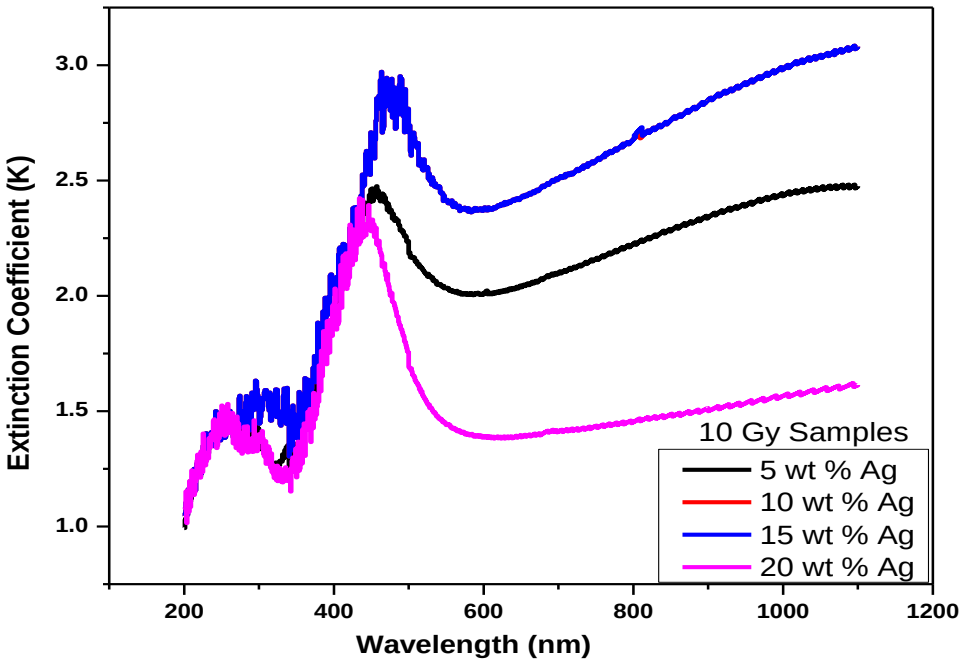

Figure (4.20): Extinction Coefficient of PVA/Ag Composite films doped with different $AgNO_3$ concentrations Gamma-irradiated at 10 Gy.

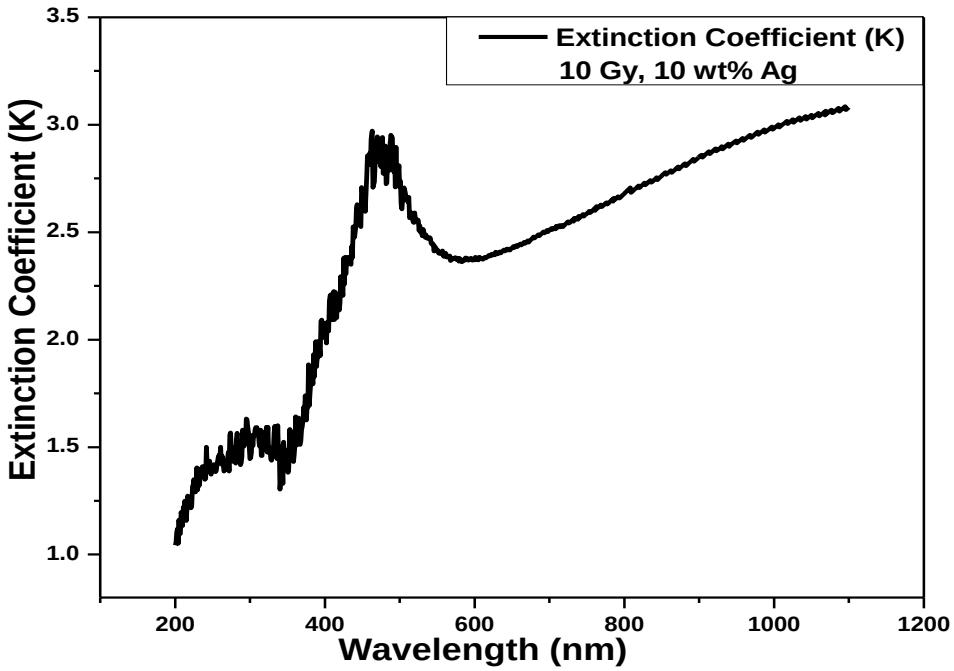

Figure (4.21): The Extinction Coefficient of PVA/Ag composite films doped with 10 wt % Ag concentration Gamma-irradiated at 10 Gy as an example.

4.3.7 Refractive Index (n)

Refractive Index was calculated from the absorbance and transmittance using the equations below:

$$n = \frac{1}{T_s} + \sqrt{\frac{1}{T_s - 1}} \quad (4.4)$$

$$T_s = 10^{(-A)} \times 100 \quad (4.5)$$

Where: T_s is the percentage transmittance and A is the absorbance.

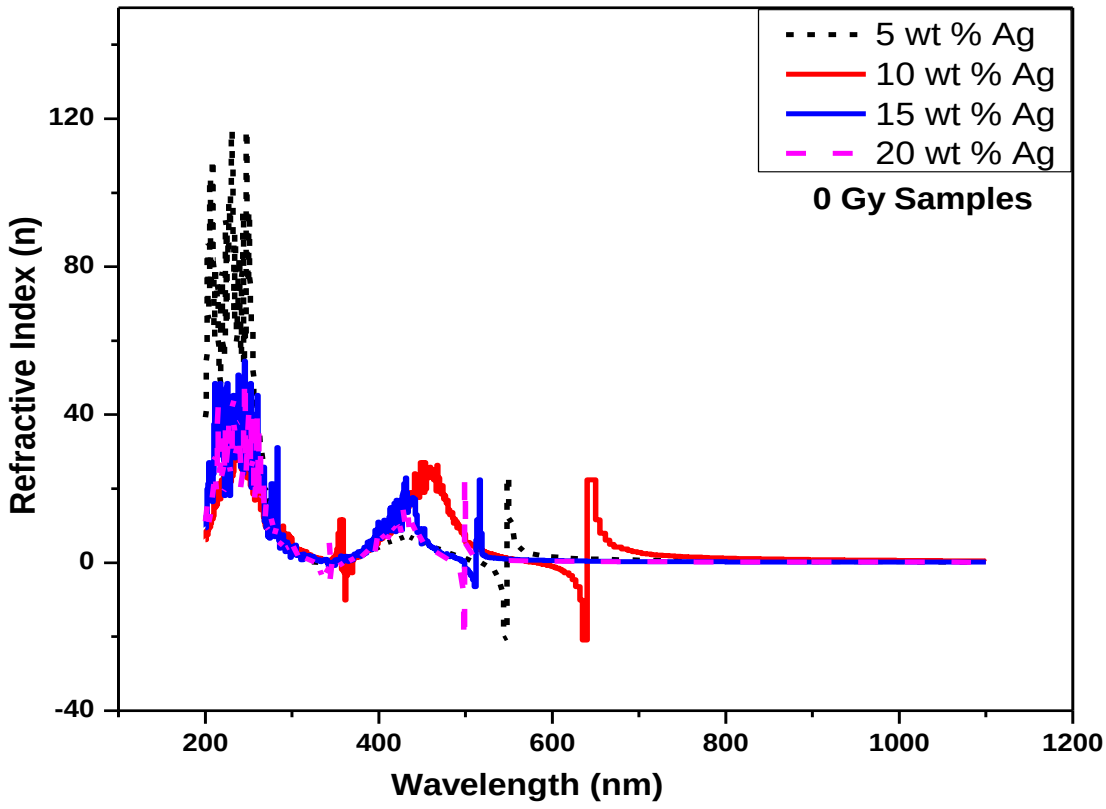

Figure (4.22): Refractive Index of PVA/Ag composite films doped with different $AgNO_3$ concentrations non-irradiated (0 Gy).

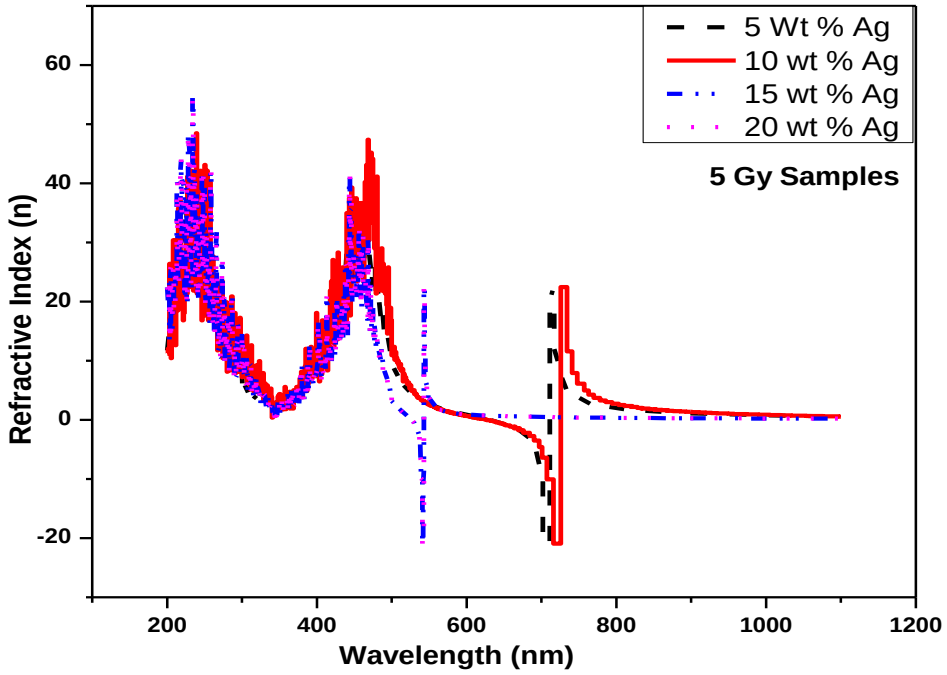

Figure (4.23): Refractive Index of PVA/Ag Composite films doped with different $AgNO_3$ concentrations Gamma-irradiated at 5 Gy.

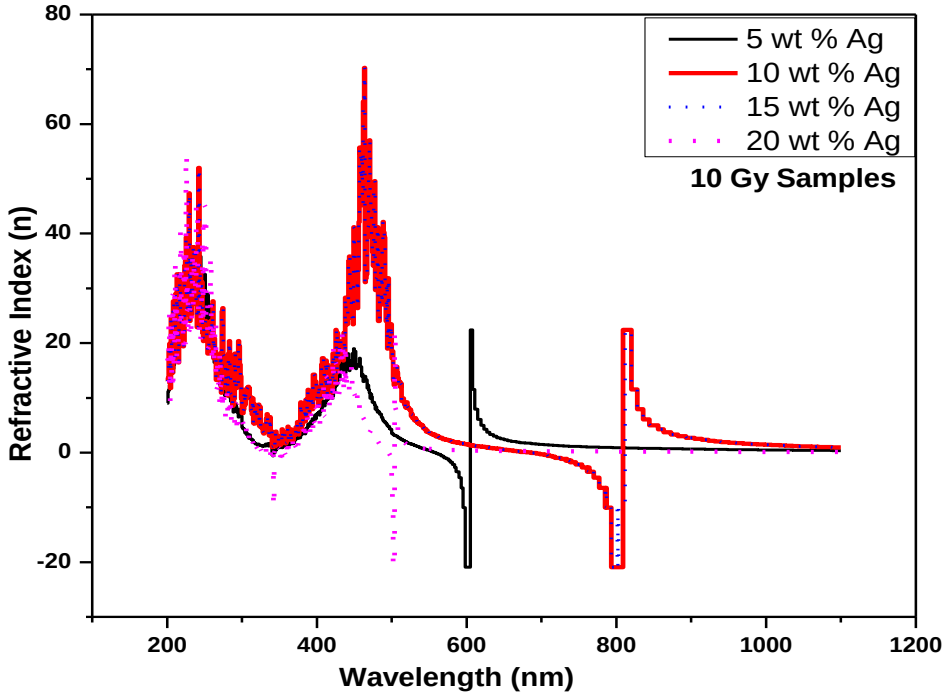

Figure (4.24): Refractive Index of PVA/Ag Composite films doped with different $AgNO_3$ concentrations Gamma-irradiated at 10 Gy.

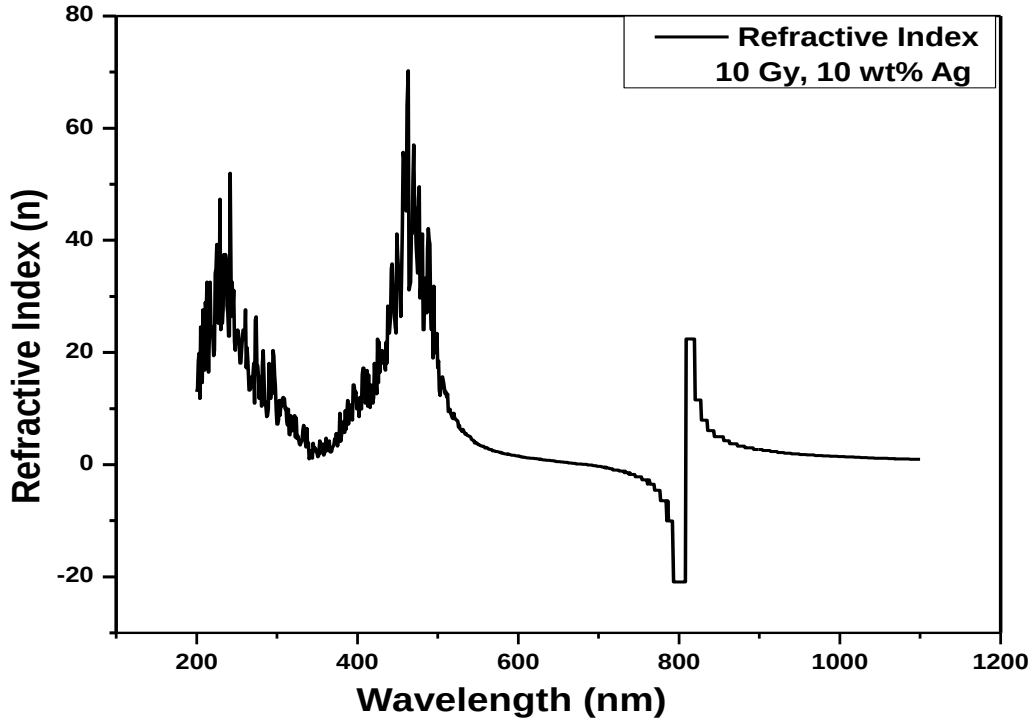

Figure (4.25): Refractive Index of PVA/Ag composite film doped with 10 wt % Ag concentration Gamma-irradiated at 10 Gy as an example.

4.3.8 Optical Conductivity (σ_{opt})

Optical conductivity was calculated from the absorption coefficient using the equations below:

$$\sigma_{opt} = \frac{\alpha n c}{4\pi} \tag{4.6}$$

Where: α is the absorption coefficient, n is the refractive index and c is the speed of light in vacuum.

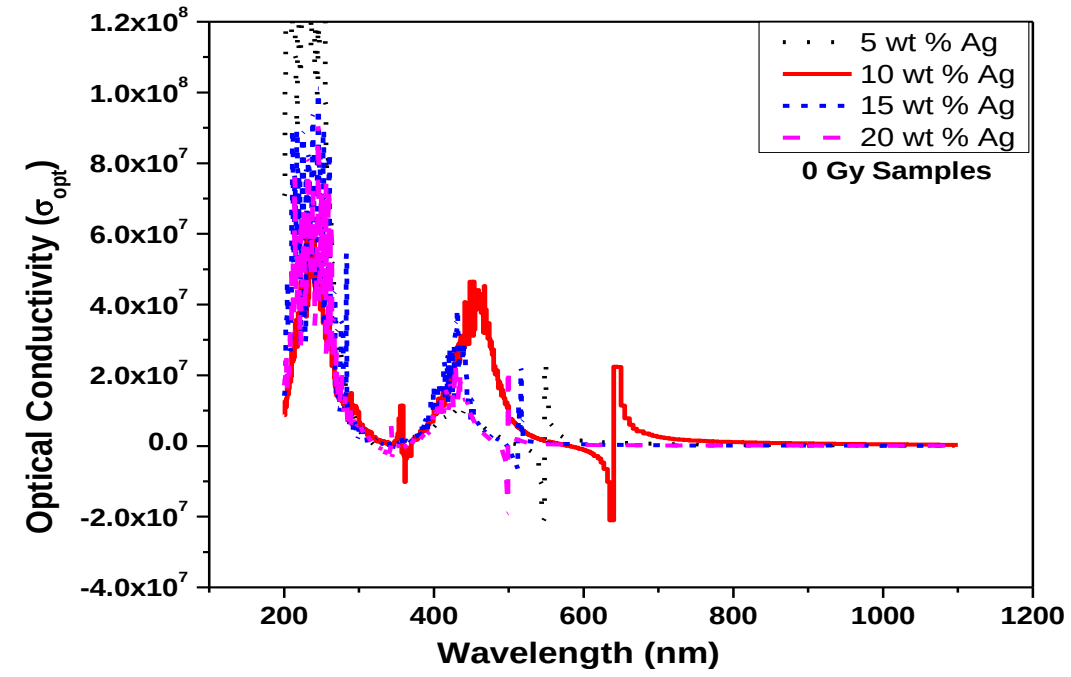

Figure (4.26): Optical conductivity of PVA/Ag composite films doped with different $AgNO_3$ concentrations non-irradiated (0 Gy).

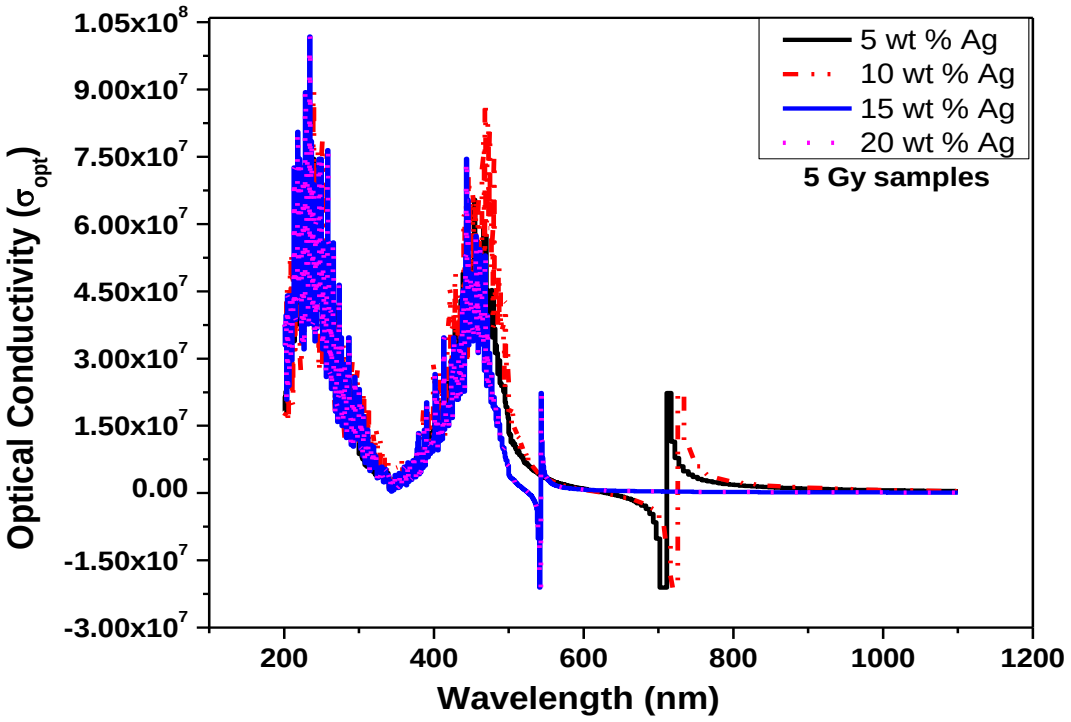

Figure (4.27): Optical conductivity of PVA/Ag composite films doped with different $AgNO_3$ concentrations Gamma-irradiated at 5 Gy.

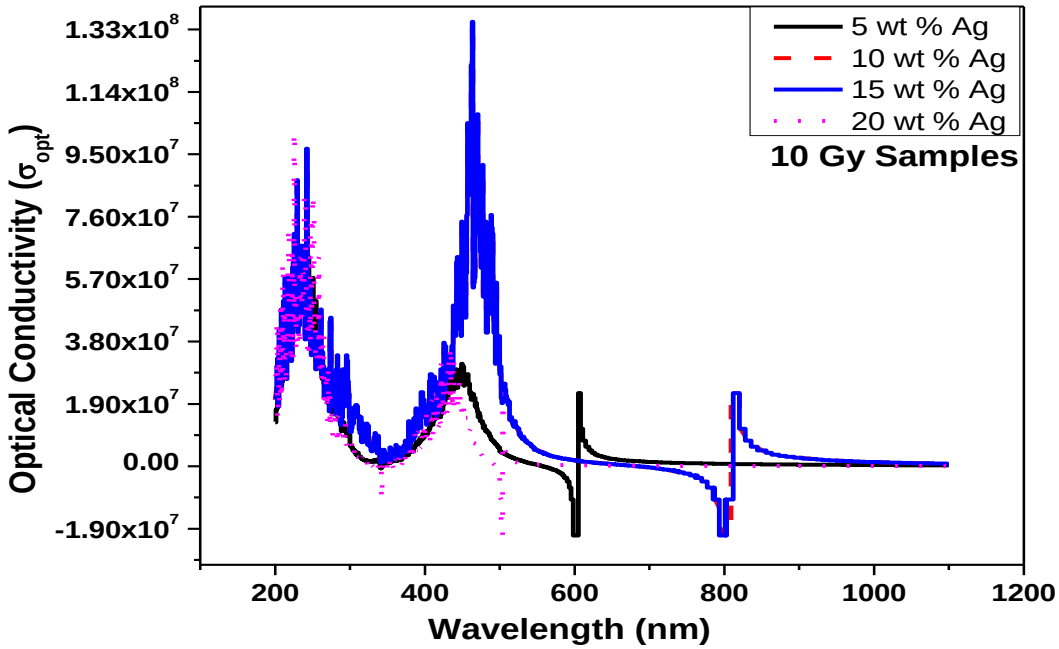

Figure (4.28): Optical conductivity of PVA/Ag composite films doped with different $AgNO_3$ concentrations Gamma-irradiated at 10 Gy

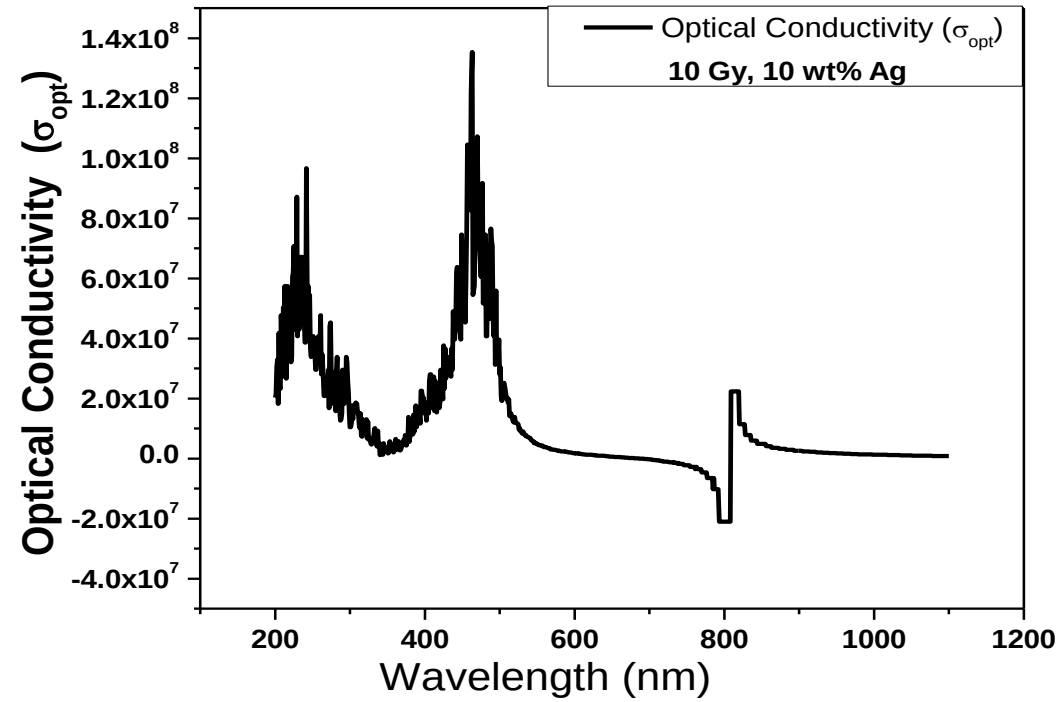

Figure (4.29): Optical conductivity of PVA/Ag composite film doped with 10 wt % Ag concentration Gamma-irradiated at 10 Gy as an example.

4.3.9 Dielectric Constant (ε)

4.3.9.1 Real Part of Dielectric Constant (ε_r)

The real part of dielectric constant was calculated from the refractive index and the extinction coefficient using the equation below:

$$\varepsilon_r = n^2 - K^2 \qquad (4.7)$$

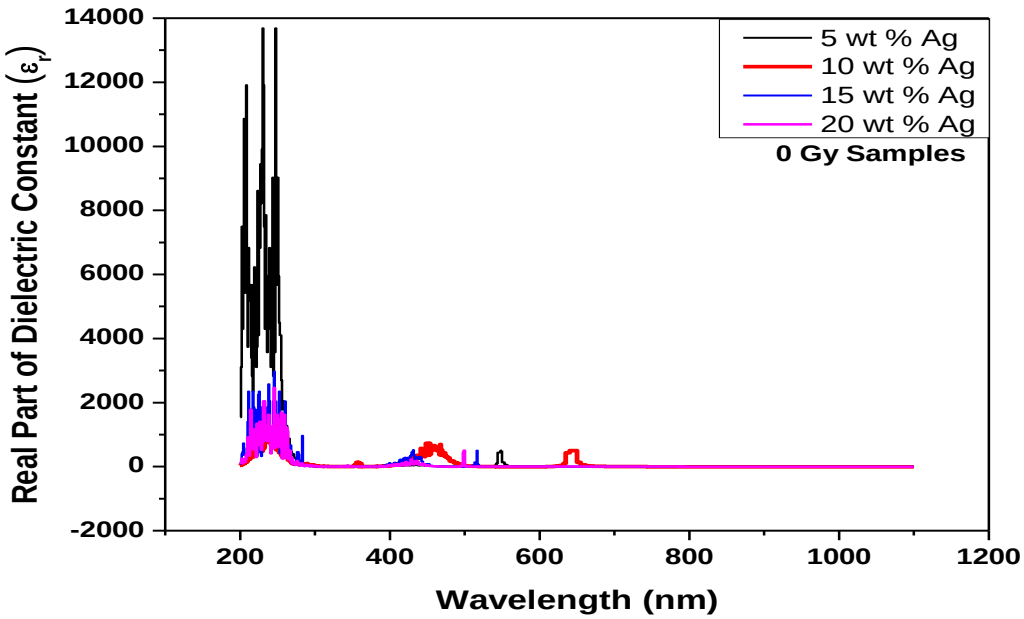

Figure (4.30): Real Part of Dielectric Constant of PVA/Ag composite films doped with different $AgNO_3$ concentrations non-irradiated (0 Gy).

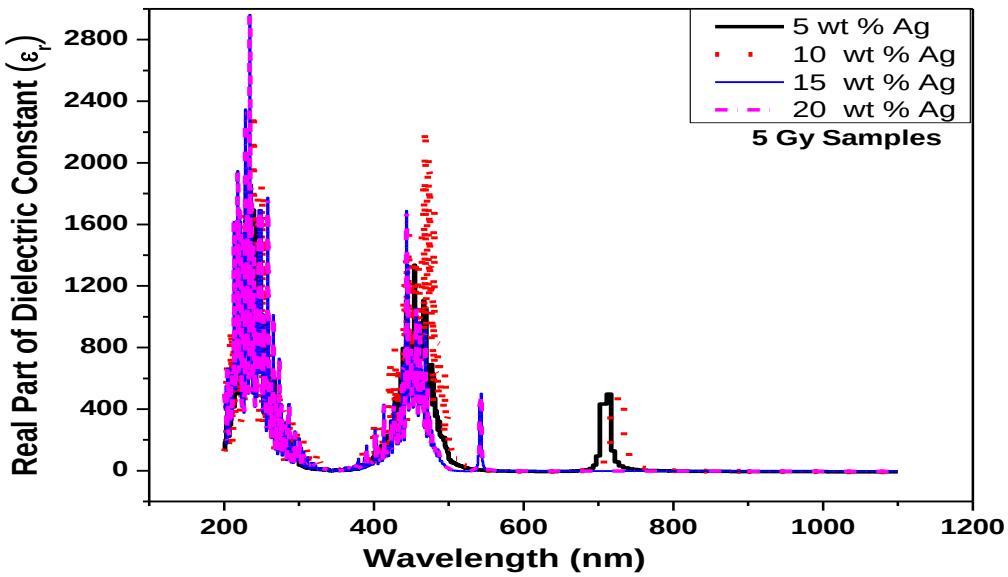

Figure (4.31): Real Part of Dielectric Constant of PVA/Ag composite films doped with different $AgNO_3$ concentrations Gamma-irradiated at 5 Gy.

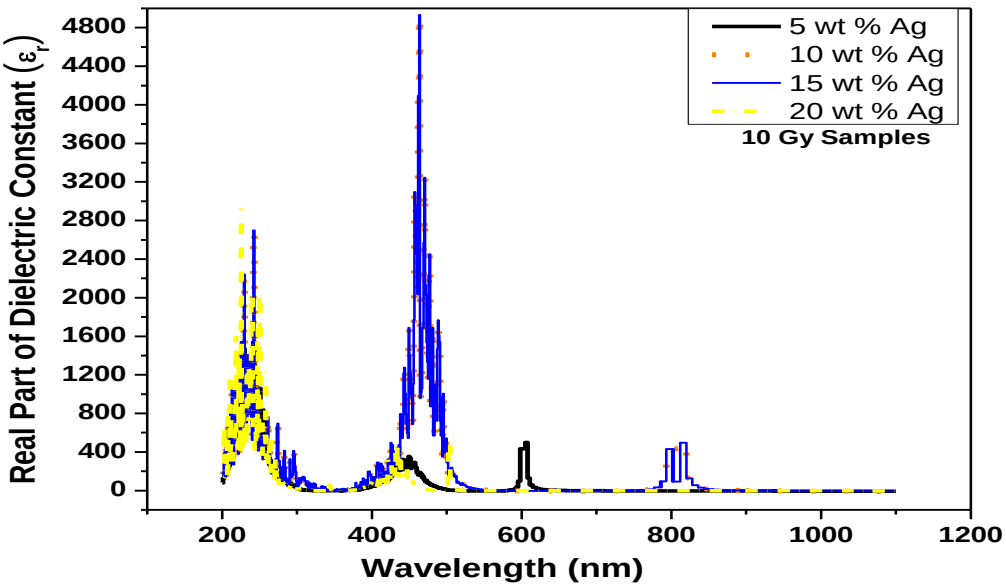

Figure (4.32): Real Part of Dielectric Constant of PVA/Ag composite films doped with different $AgNO_3$ concentrations Gamma-irradiated at 10 Gy.

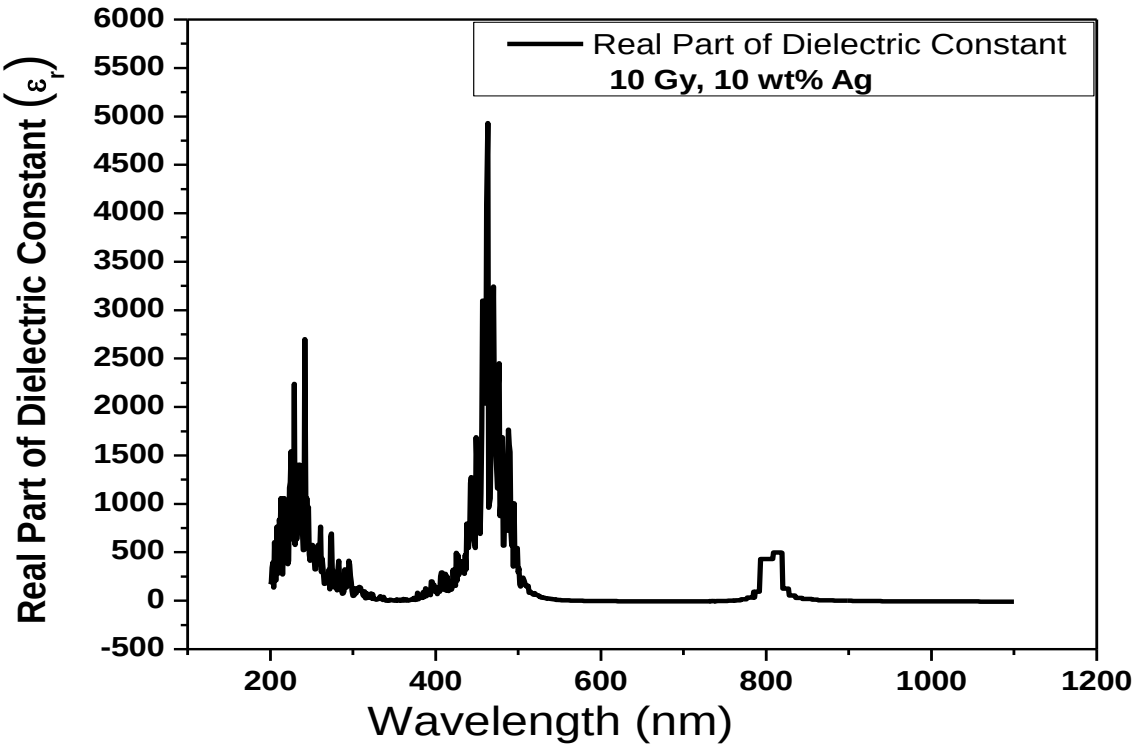

Figure (4.33): Real Part of Dielectric Constant of PVA/Ag composite film doped with 10 wt % Ag concentration Gamma-irradiated at 10 Gy as an example.

4.3.9.2 Imaginary Part of Dielectric Constant (ε_i)

The Imaginary part of dielectric constant was calculated from the refractive index and the extinction coefficient using the equation below:

$$\varepsilon_i = 2nk \qquad (4.8)$$

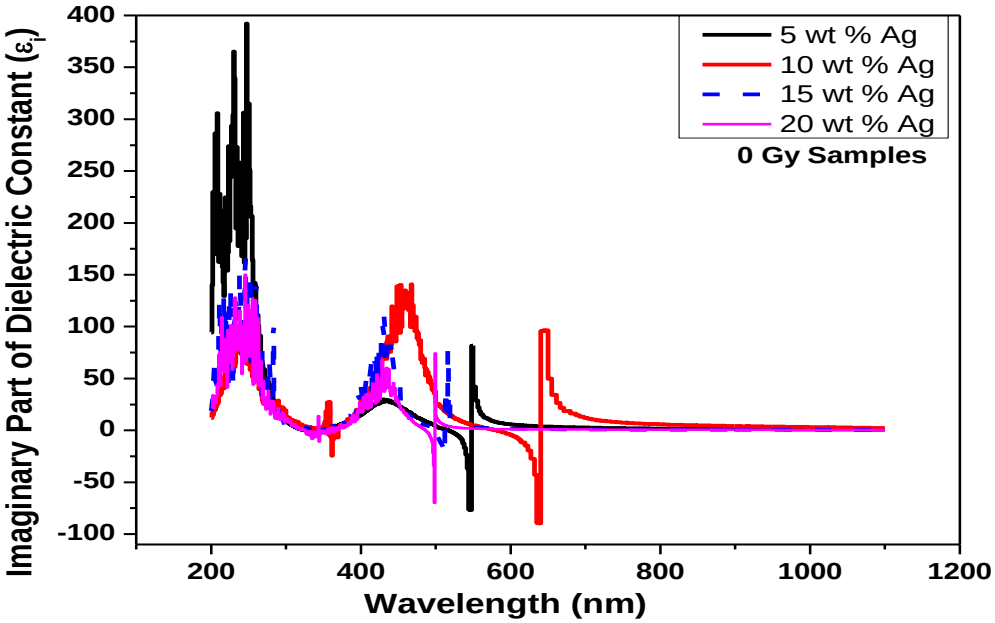

Figure (4.34): Imaginary Part of Dielectric Constant of PVA/Ag composite films doped with different $AgNO_3$ concentrations non-irradiated (0 Gy).

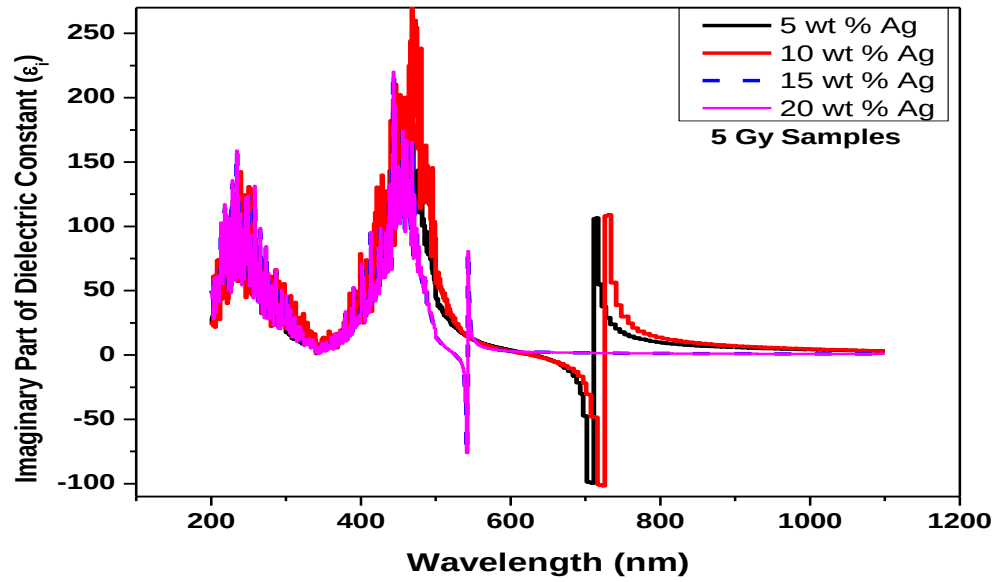

Figure (4.35): Imaginary Part of Dielectric Constant of PVA/Ag composite films doped with different $AgNO_3$ concentrations Gamma-irradiated at 5 Gy.

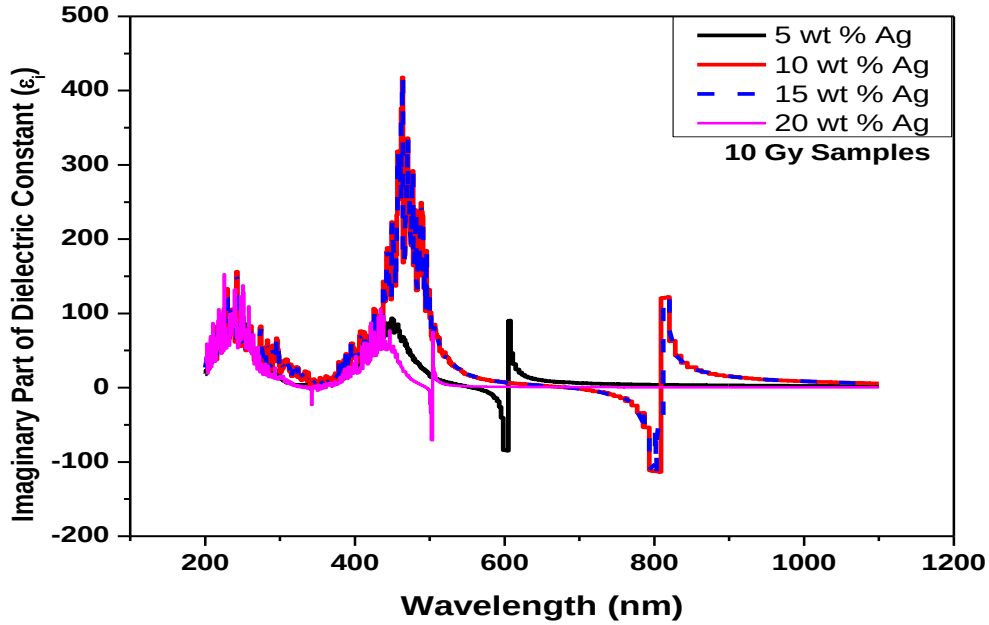

Figure (4.36): Imaginary Part of Dielectric Constant of PVA/Ag composite films doped with different $AgNO_3$ concentrations Gamma-irradiated at 10 Gy.

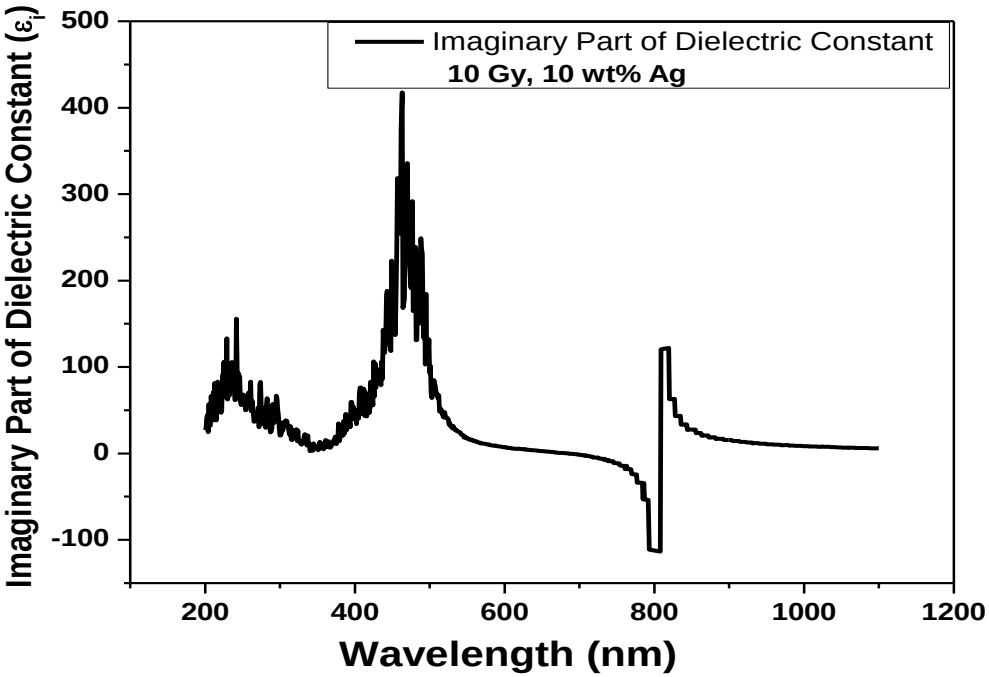

Figure (4.37): Imaginary Part of Dielectric Constant of PVA/Ag composite film doped with 10 wt % Ag concentration Gamma-irradiated at 10 Gy as an example.

4.4 X-ray Diffraction (XRD) Measurements

The crystallography of the produced composite films is characterized by powder x-ray diffraction in the 2θ range of 10^0 to 90^0 using a GNR analytical instruments group apparatus x-ray diffractometer (Explorer model) with Cu Kα radiation (λ = 0.1542 nm).

4.4.1 Effects of $AgNO_3$ Addition on the XRD Diffraction Patterns

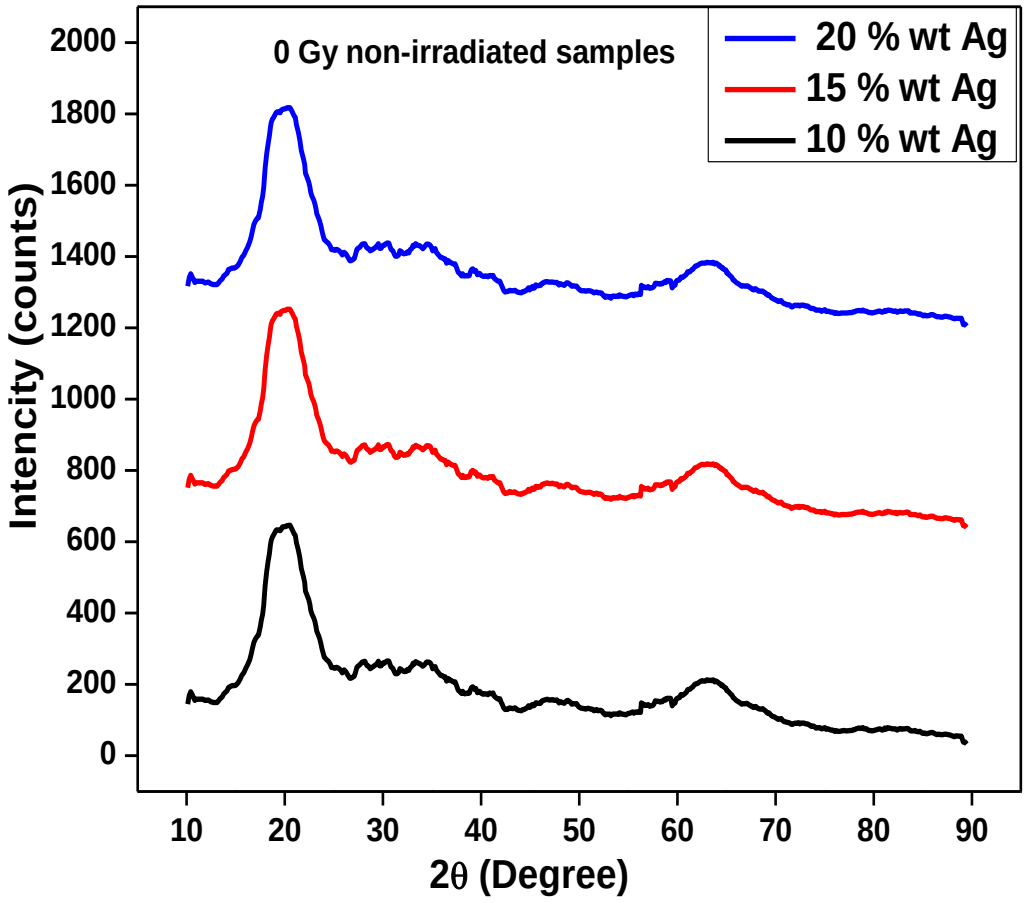

Figure (4.38): Diffraction patterns of PVA/Ag composite films doped with different $AgNO_3$ concentrations non-irradiated (0 Gy).

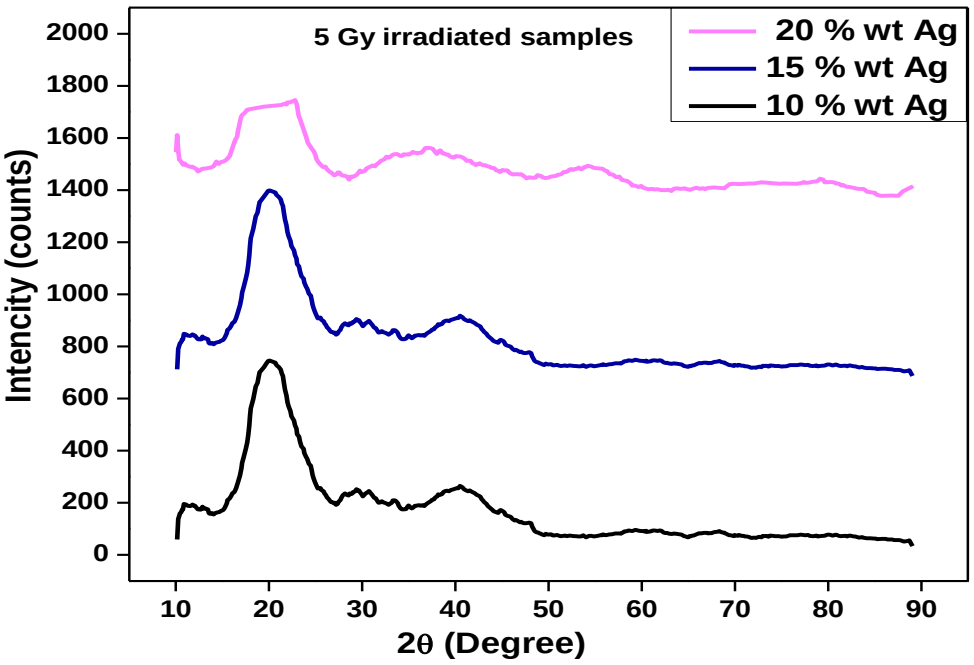

Figure (4.39): Diffraction patterns of PVA/Ag composite films doped with different $AgNO_3$ concentrations irradiated at 5 Gy.

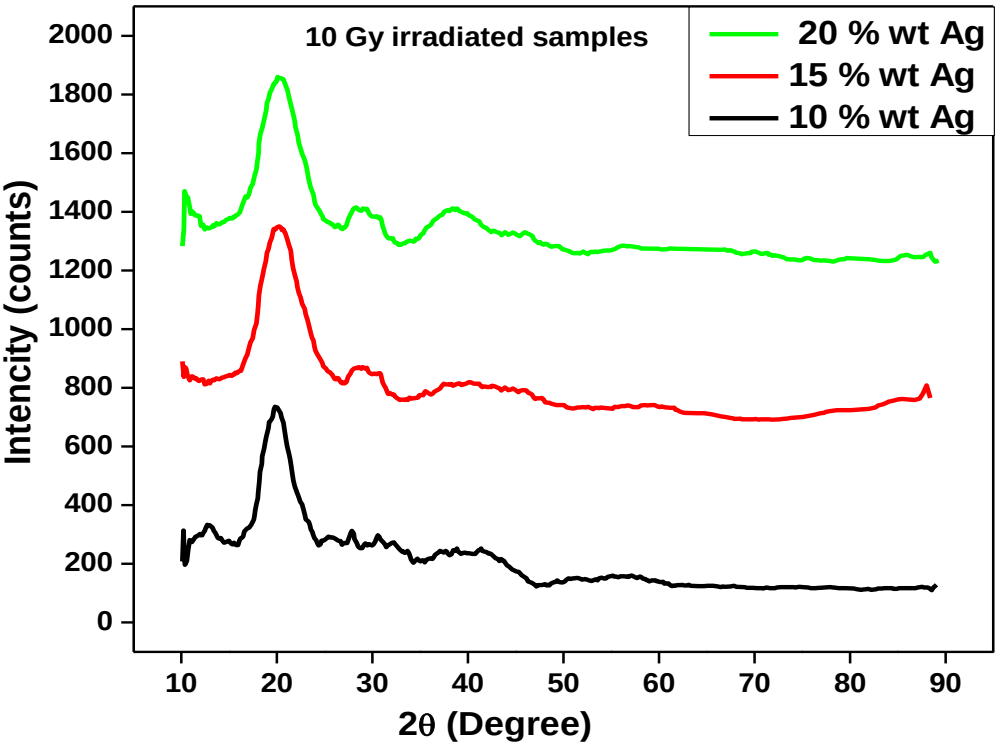

Figure (4.40): Diffraction patterns of PVA/Ag composite films doped with different $AgNO_3$ concentrations irradiated at 10 Gy.

4.4.2 Effects of γ-Irradiation on the XRD Diffraction Patterns

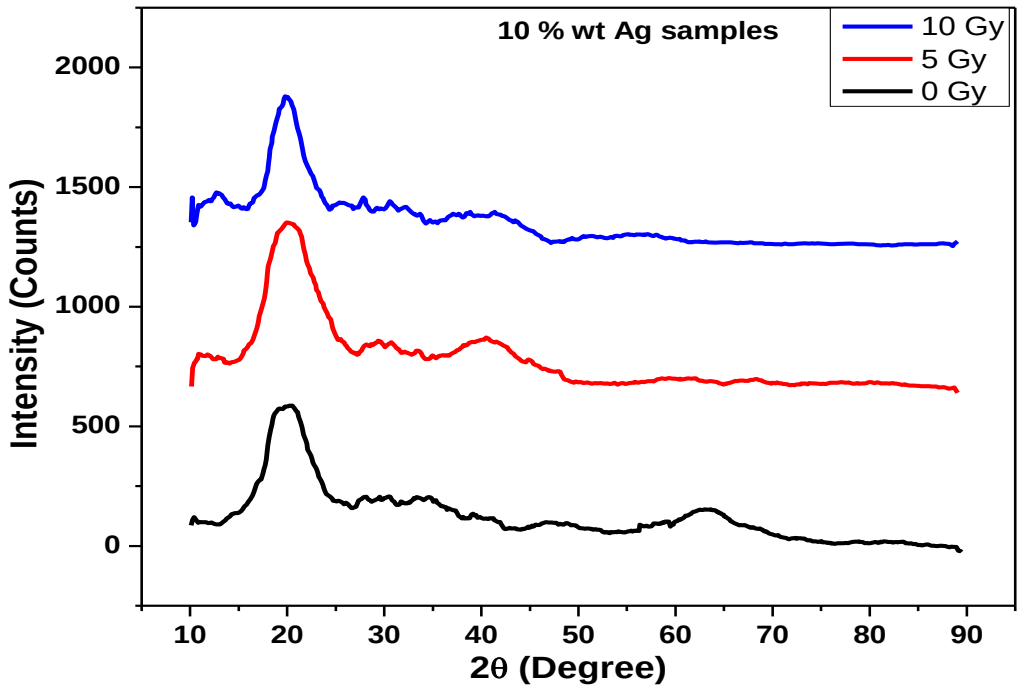

Figure (4.41): Diffraction patterns of non-irradiated and gamma-irradiated PVA/$AgNO_3$ samples with 10 wt% Ag concentration.

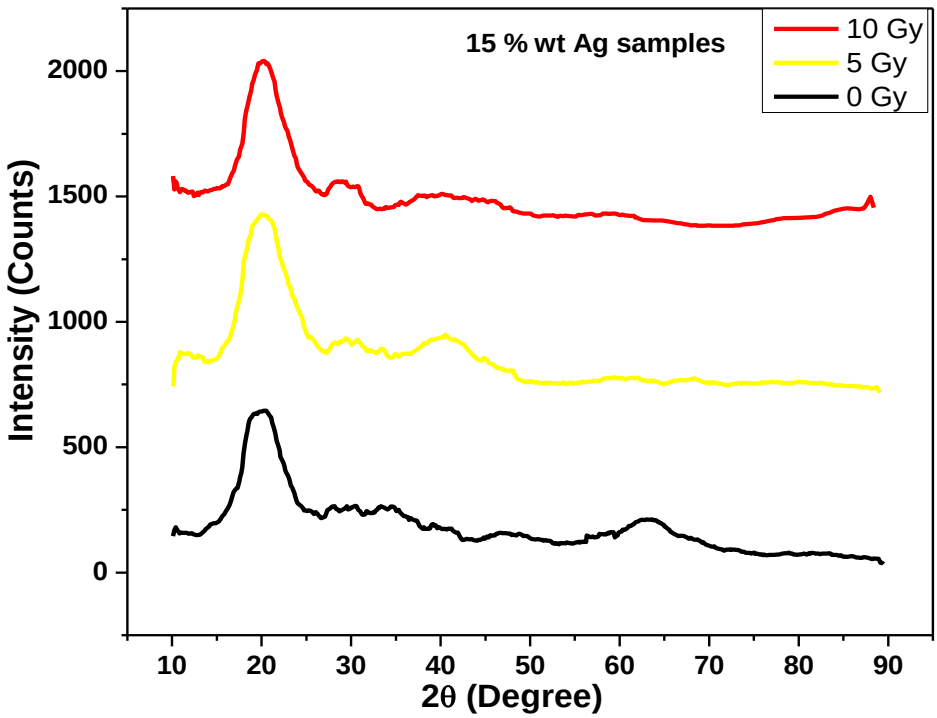

Figure (4.42): Diffraction patterns of non-irradiated and gamma-irradiated PVA/$AgNO_3$ samples with 15 wt% Ag concentration.

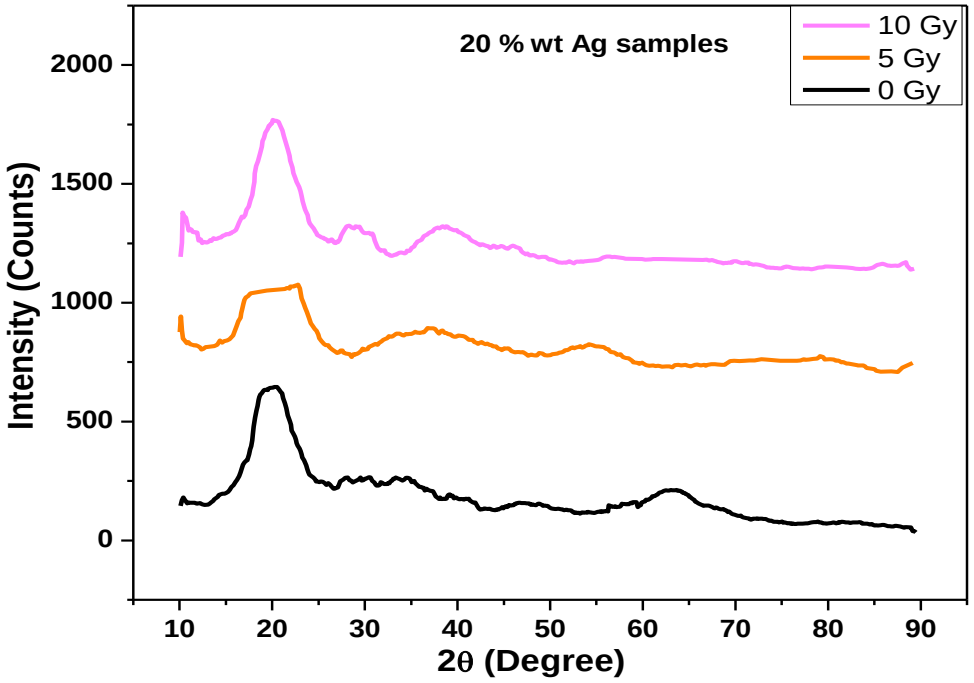

Figure (4.43): Diffraction patterns of non-irradiated and gamma-irradiated PVA/AgNO3 samples with 20 wt% Ag concentration.

4.4.3 Particle Size Estimation Using Scherer Formula

Table (4.7): Particle size in PVA matrix after gamma-irradiation for PVA/$AgNO_3$ samples with different concentrations.

$AgNO_3$ Concentration	Particle Size of PVA/$AgNO_3$ films non-irradiated (0 Gy).	Particle Size of PVA/$AgNO_3$ films irradiated with 5 Gy.	Particle Size of PVA/$AgNO_3$ films irradiated with 10 Gy.
10 wt %	12.117	11.041	13.174
15 wt %	12.65	11.239	13.480
20 wt %	12.977	11.776	13.947

4.4.4 Degree Of Crystallinity (DOC)

Table (4.8): DOC in PVA matrix after gamma-irradiation for $PVA/AgNO_3$ samples with different concentrations.

$AgNO_3$ Concentration	DOC for $PVA/AgNO_3$ films non-irradiated (0 Gy).	DOC for $PVA/AgNO_3$ films irradiated with 5 Gy.	DOC for $PVA/AgNO_3$ films irradiated with 10 Gy.
10 wt %	21.75 %	15.03 %	13.43 %
15 wt %	15.30 %	12.10 %	11.77 %
20 wt %	13.70 %	10.69 %	10.35 %

4.4.5 Interplaner Distance (d)

Table (4.9): Distances in PVA matrix after gamma-irradiation for $PVA/AgNO_3$ samples with different concentrations.

$AgNO_3$ Concentration	For $PVA/AgNO_3$ films non-irradiated (0 Gy).	For $PVA/AgNO_3$ films irradiated with 5 Gy.	For $PVA/AgNO_3$ films irradiated with 10 Gy.
10 wt %	4.5132	4.563	4.507
15 wt %	4.521	4.565	4.512
20 wt %	4.605	4.569	4.542

4.5 Thermogravimetric Analysis (TGA) Measurements

In the present study the $PVA/AgNO_3$ films with different concentrations of $AgNO_3$ (i.e. 10 and 20) wt% were prepared by casting method and the reduction of Ag^+ ions in $PVA/AgNO_3$ films was done via gamma irradiation with different doses i.e. (0, 5,and 10) Gy.

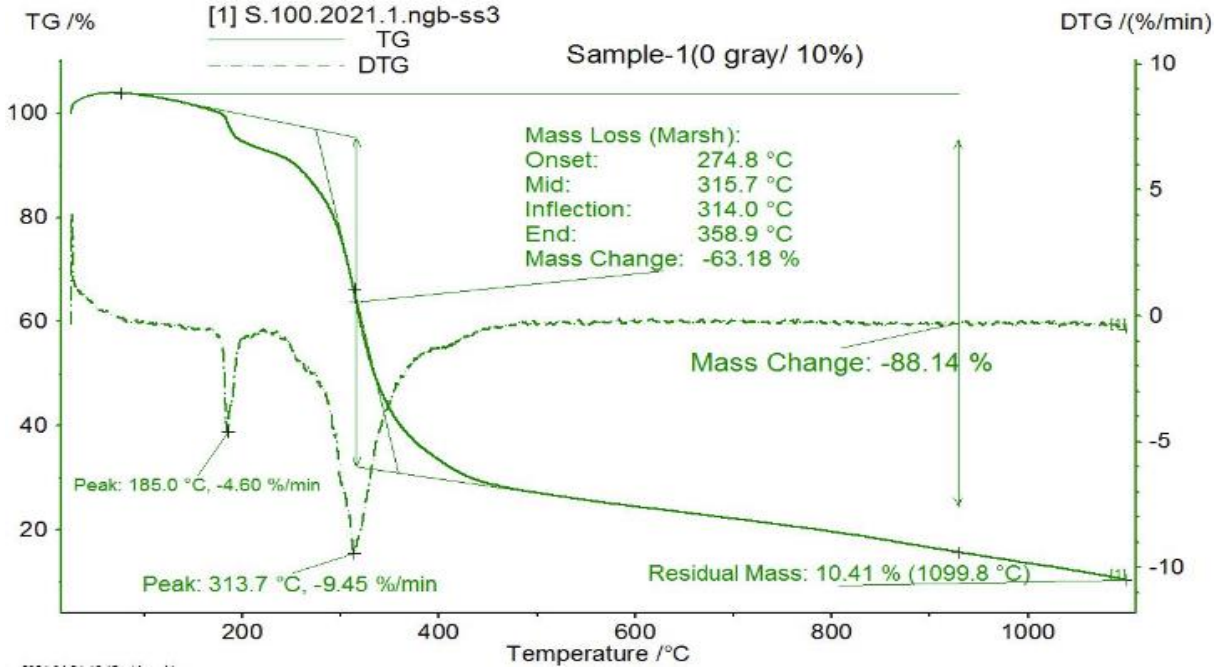

Figure (4.44): TGA and DTGA Thermograms measured in the temperature range from room temperature up to 1000 ^{0}C at a heating rate of 10 ^{0}C min^{-1} for the 10 wt% $AgNO_3$ non-irradiated PVA/$AgNO_3$ composite.

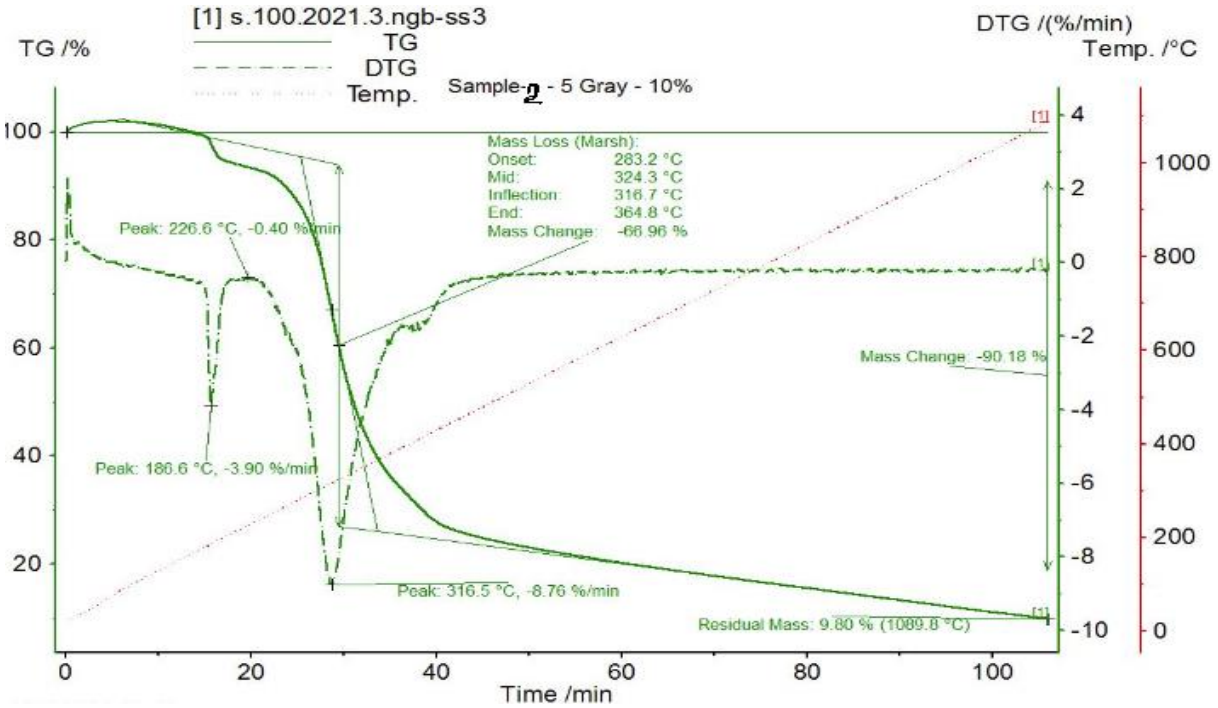

Figure (4.45): TGA and DTGA Thermograms measured in the temperature range from room temperature up to 1000 ^{0}C at a heating rate of 10 ^{0}C min^{-1} for the 10 wt% $AgNO_3$, 5 Gy irradiated PVA/$AgNO_3$ composite.

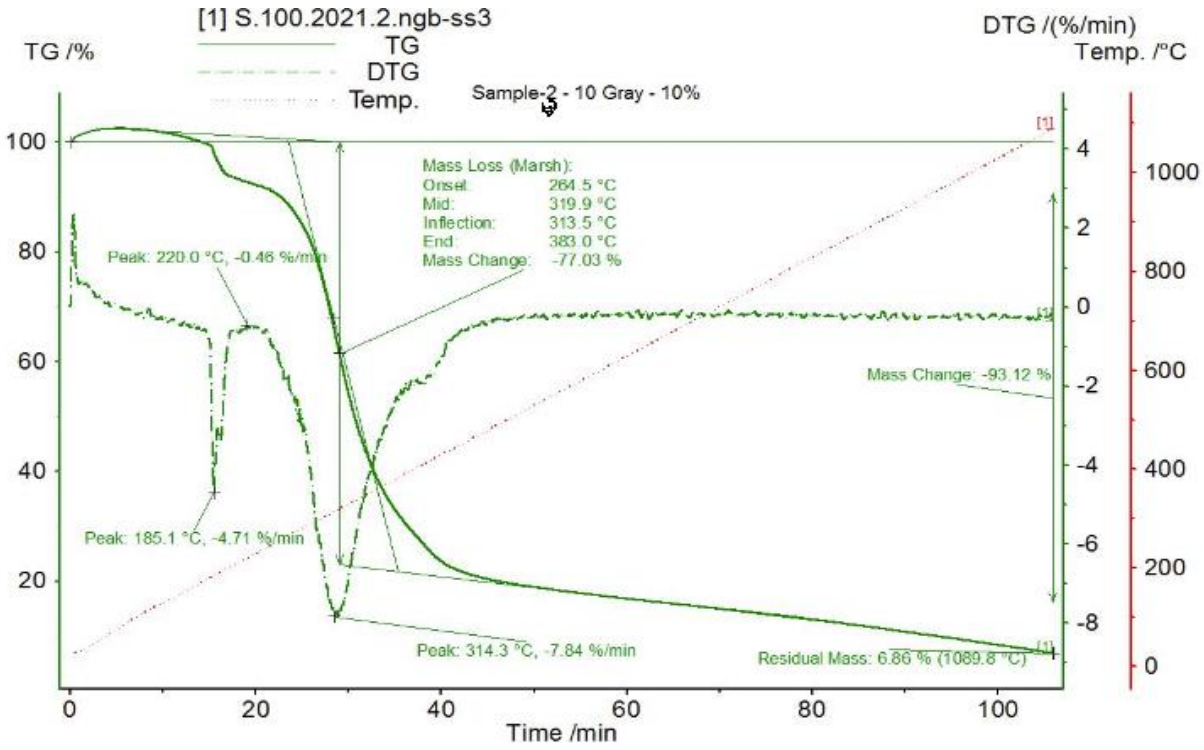

Figure (4.46): TGA and DTGA Thermograms measured in the temperature range from room temperature up to 1000 ^{0}C at a heating rate of 10 ^{0}C min^{-1} for the 10 wt% $AgNO_3$, 10 Gy irradiated PVA/$AgNO_3$ composite.

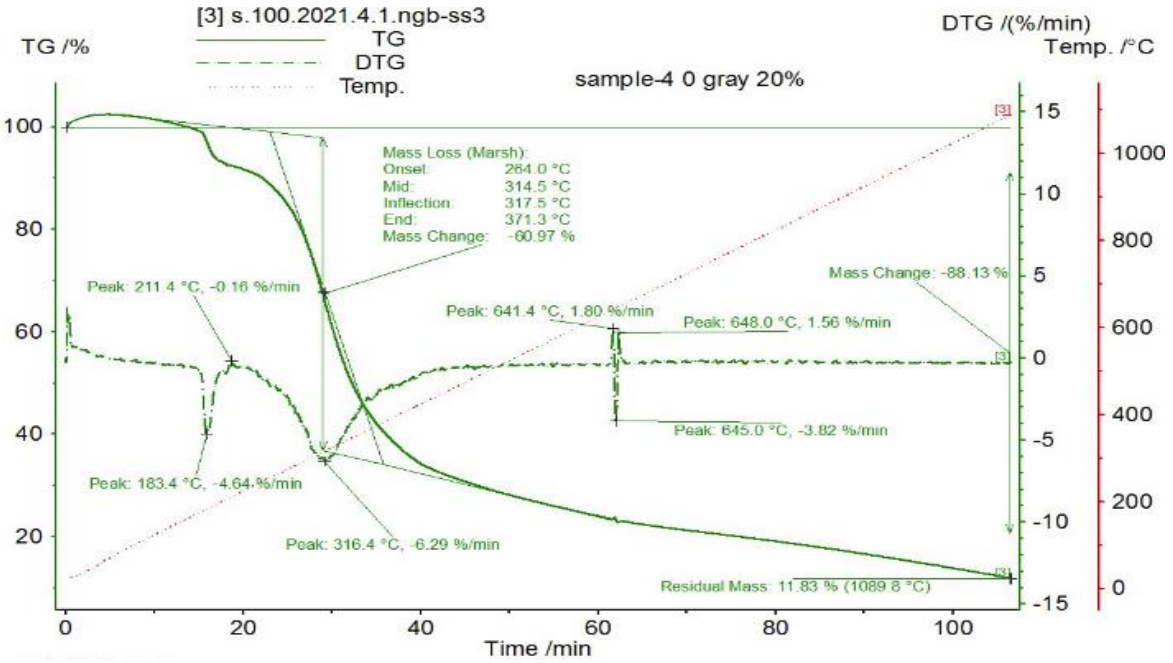

Figure (4.47): TGA and DTGA Thermograms measured in the temperature range from room temperature up to 1000 ^{0}C at a heating rate of 10 ^{0}C min^{-1} for the 20 wt% $AgNO_3$ non-irradiated PVA/$AgNO_3$ composite.

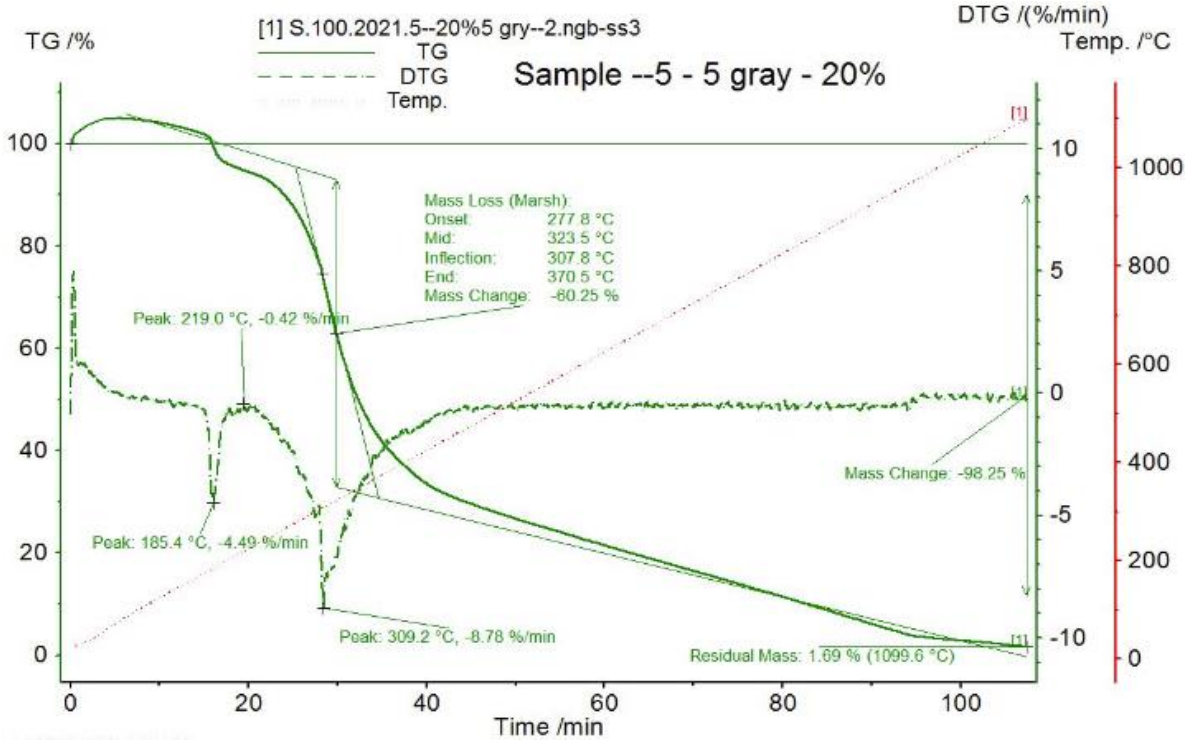

Figure (4.48): TGA and DTGA Thermograms measured in the temperature range from room temperature up to 1000 ^{0}C at a heating rate of 10 ^{0}C min^{-1} for the 20 wt% $AgNO_3$, 5 Gy irradiated PVA/$AgNO_3$ composite.

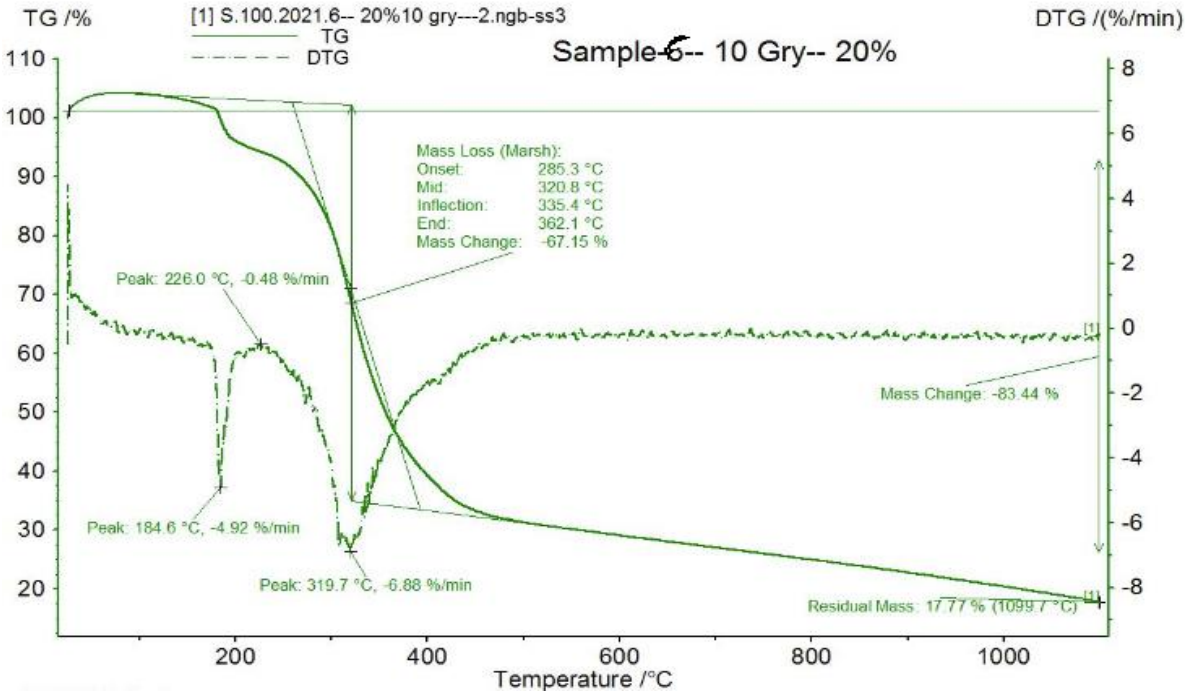

Figure (4.49): TGA and DTGA Thermograms measured in the temperature range from room temperature up to 1000 ^{0}C at a heating rate of 10 ^{0}C min^{-1} for the 20 wt% $AgNO_3$, 10 Gy irradiated PVA/$AgNO_3$ composite.

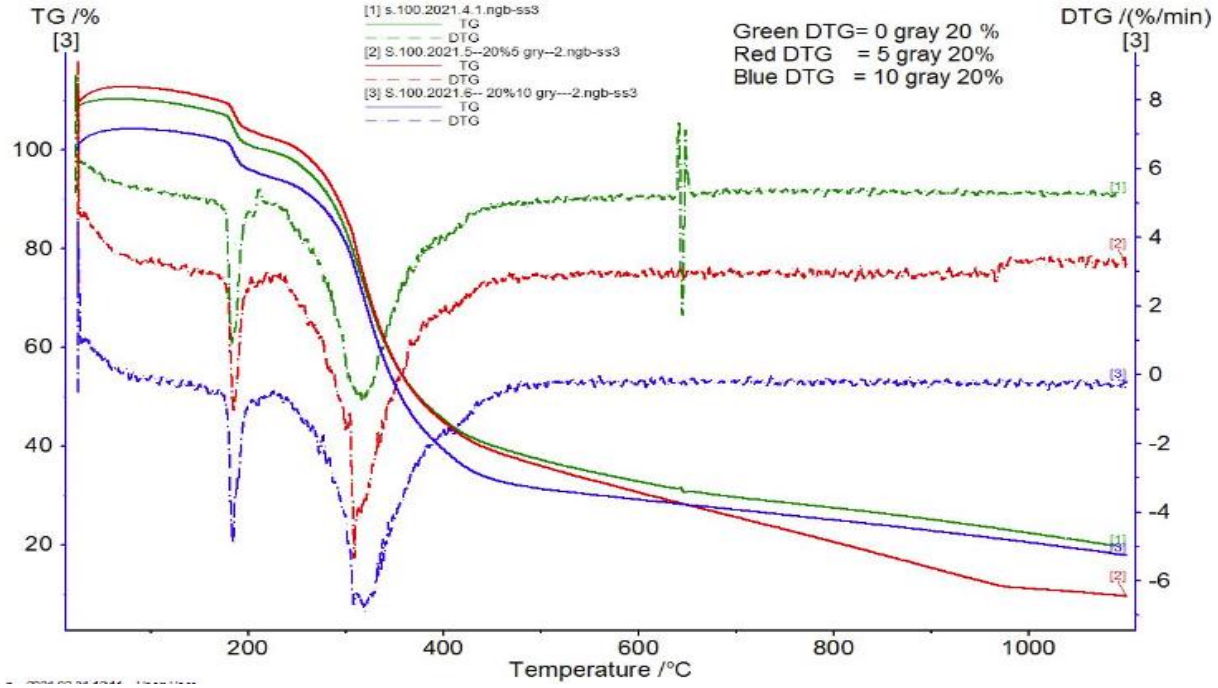

Figure (4.50): Combined TGA and DTG Thermograms measured in the temperature range from room temperature up to 1000 ^{0}C at a heating rate of 10 ^{0}C min^{-1} for the 20 wt% $AgNO_3$, non-irradiated, 5 Gy and 10 Gy irradiated PVA/$AgNO_3$ composites.

4.6 Differential Scanning Calorimetry (DSC) Measurement

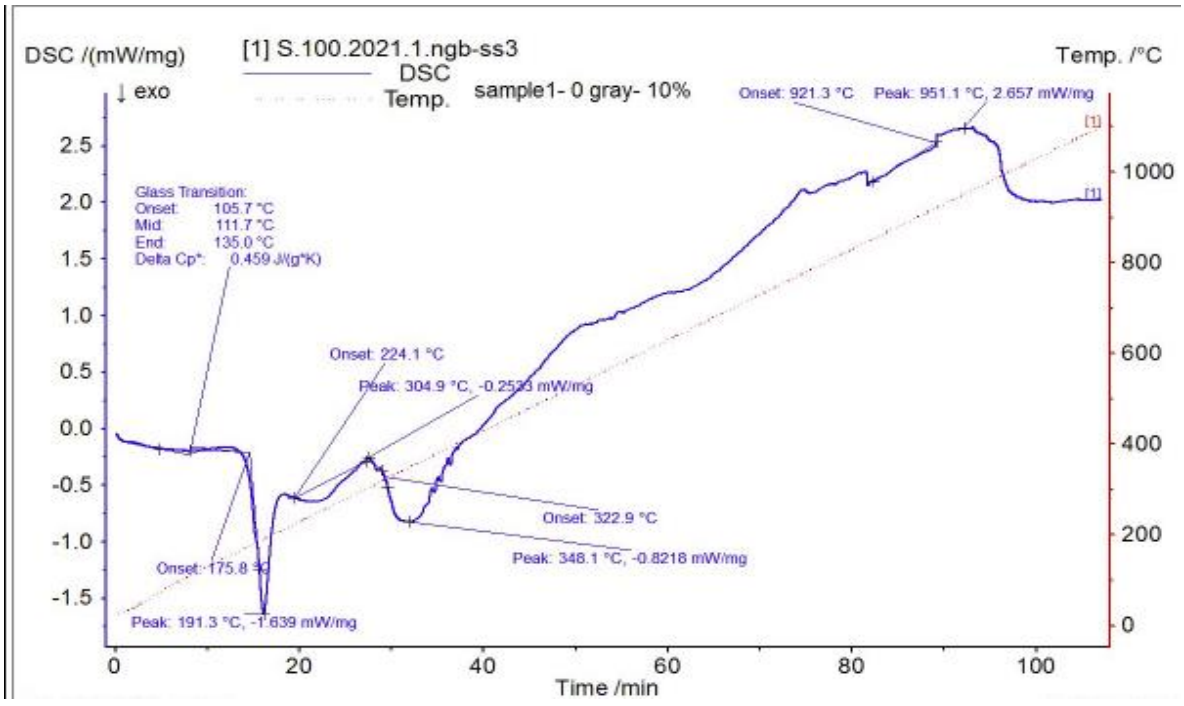

Figure (4.51): DSC Thermograms of the 10 wt% $AgNO_3$, non-irradiated PVA/$AgNO_3$ composite.

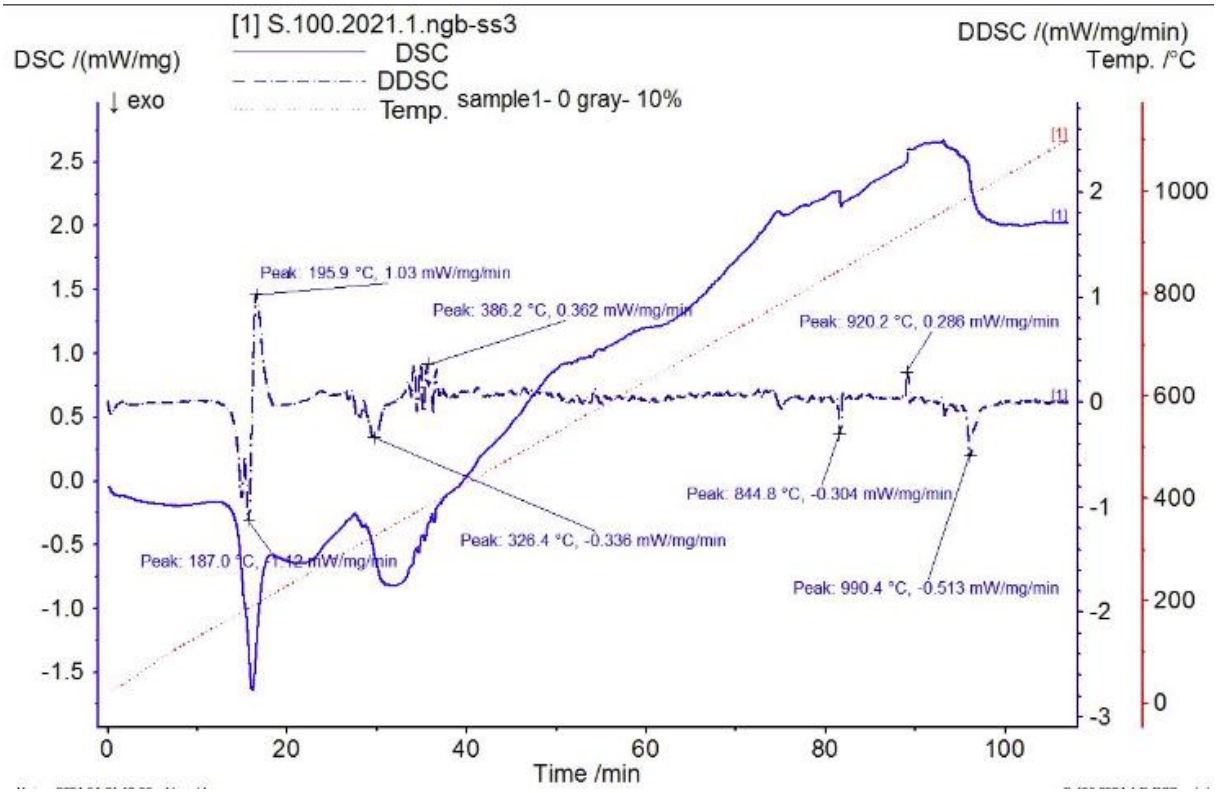

Figure (4.52): Combined DSC/DDSC Thermograms of the 10 wt% $AgNO_3$, non-irradiated PVA/$AgNO_3$ composites.

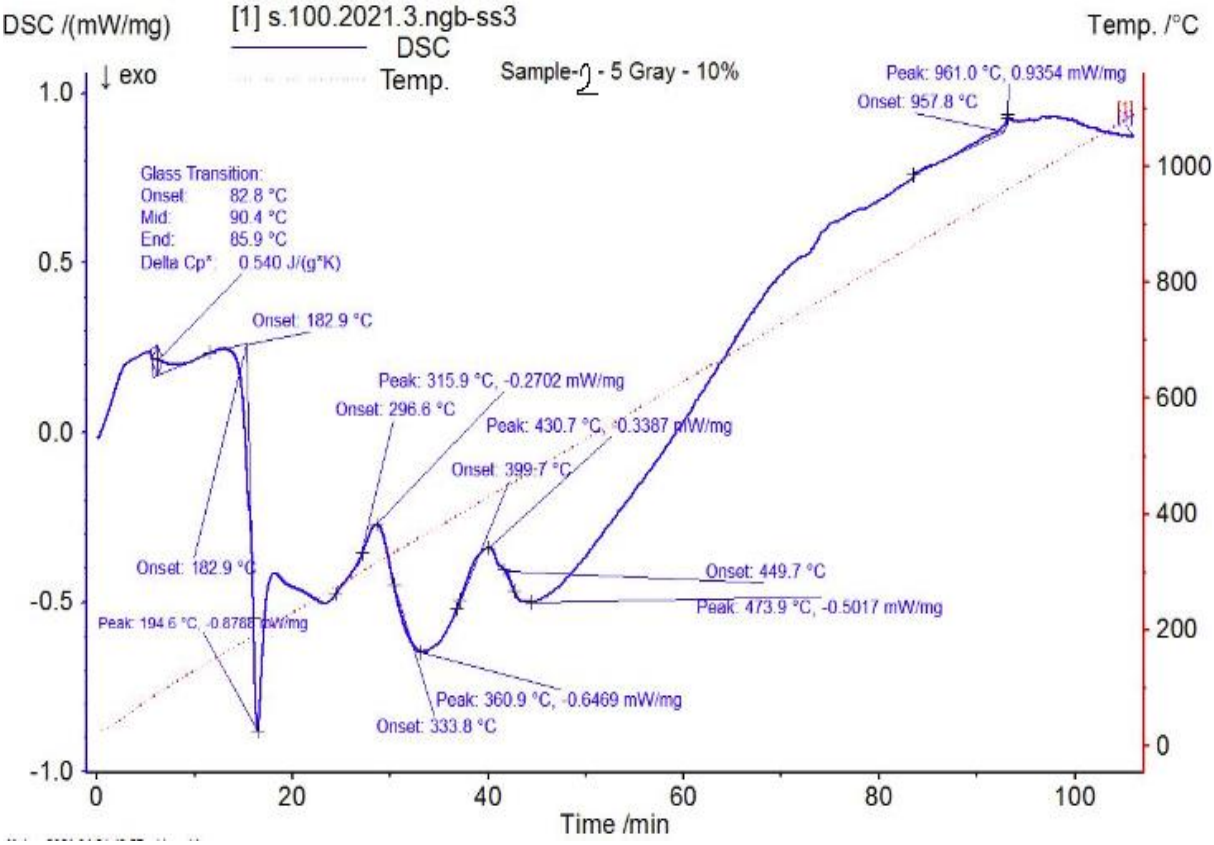

Figure (4.53): DSC Thermograms of the 10 wt% $AgNO_3$, 5 Gy irradiated PVA/$AgNO_3$ composite.

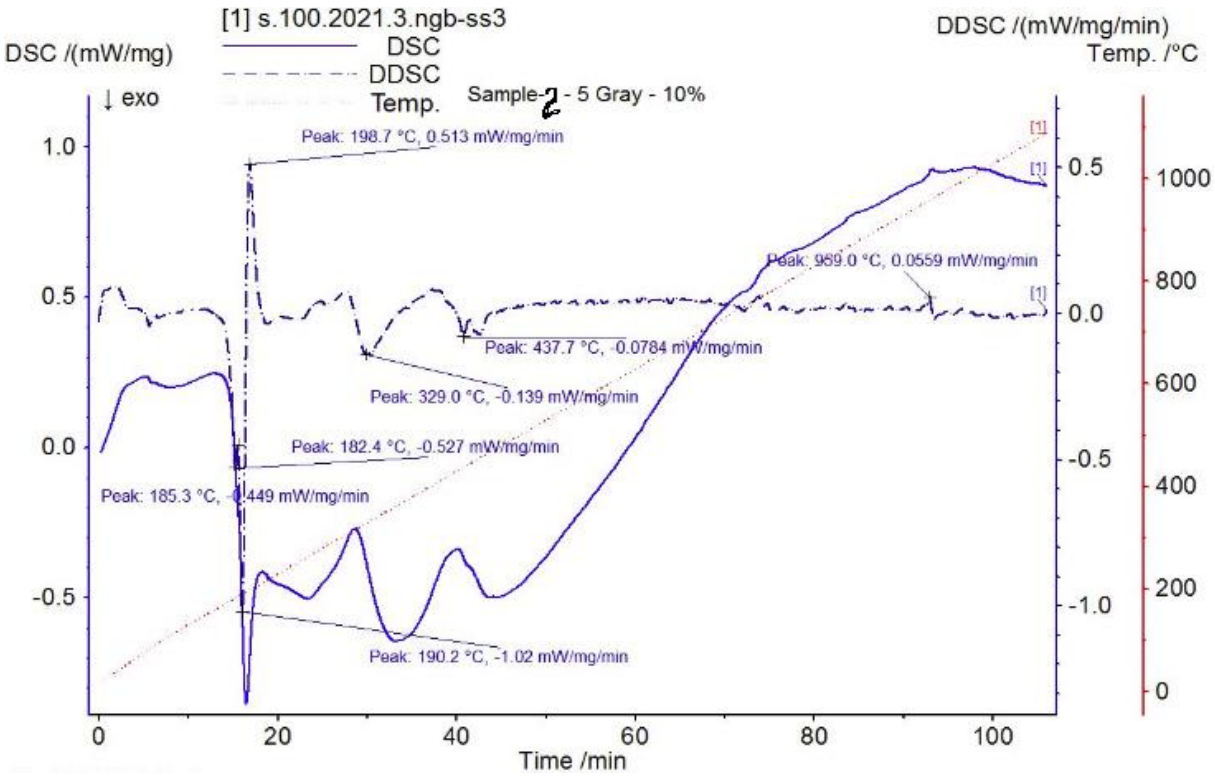

Figure (4.54): Combined DSC/DDSC Thermograms of the 10 wt% $AgNO_3$, 5 Gy irradiated PVA/$AgNO_3$ composites.

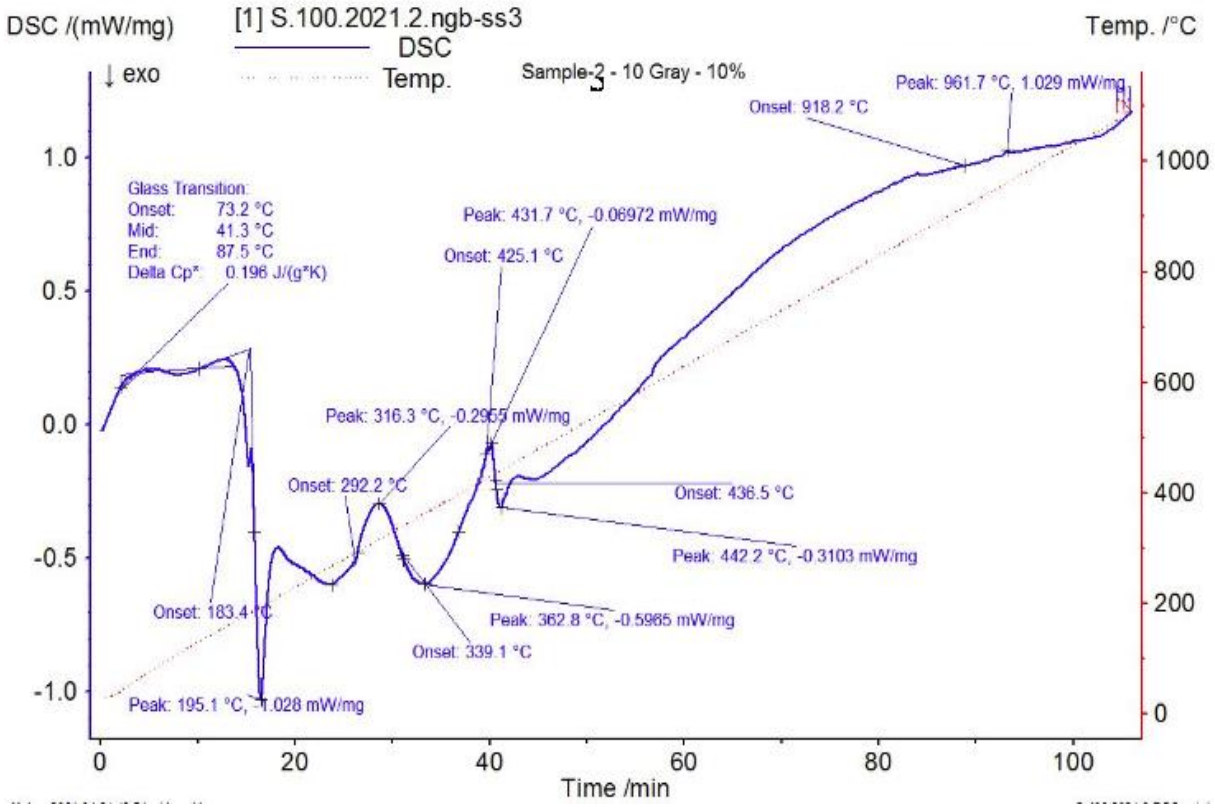

Figure (4.55): DSC Thermograms of the 10 wt% $AgNO_3$, 10 Gy irradiated PVA/$AgNO_3$ composite.

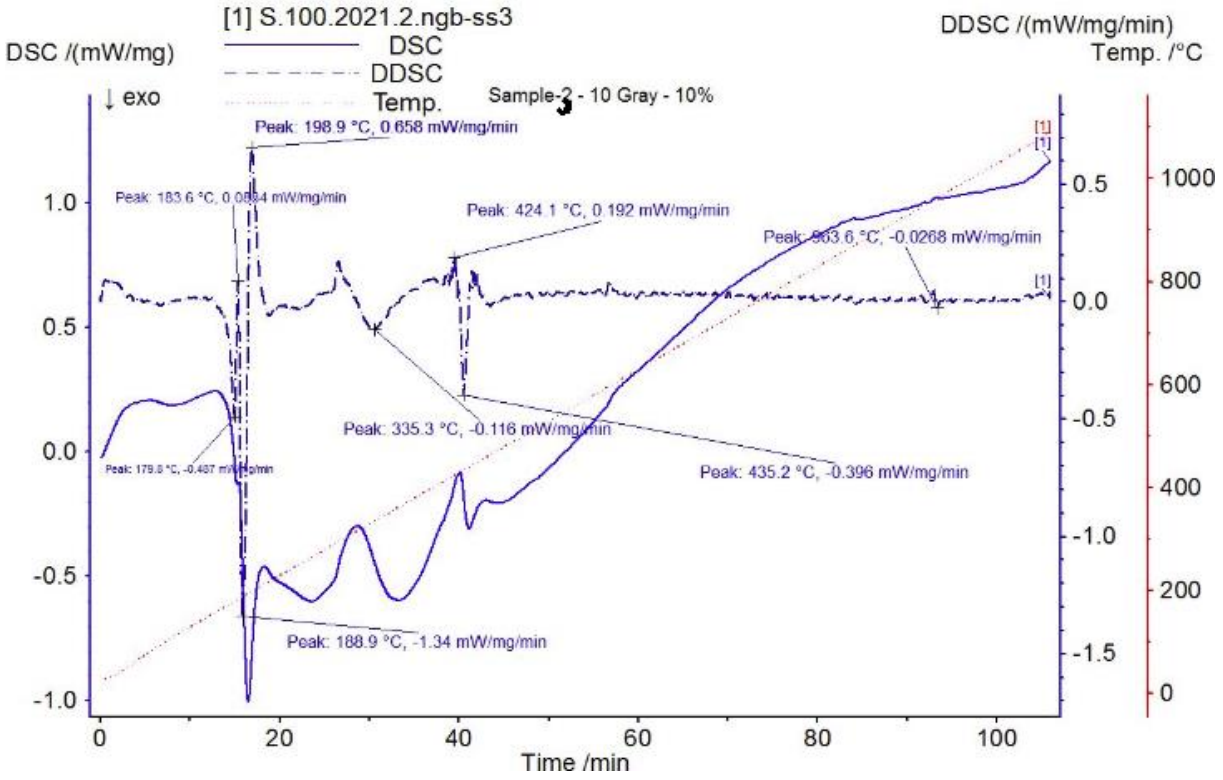

Figure (4.56): Combined DSC/DDSC Thermograms of the 10 wt% $AgNO_3$, 10 Gy irradiated PVA/$AgNO_3$ composites.

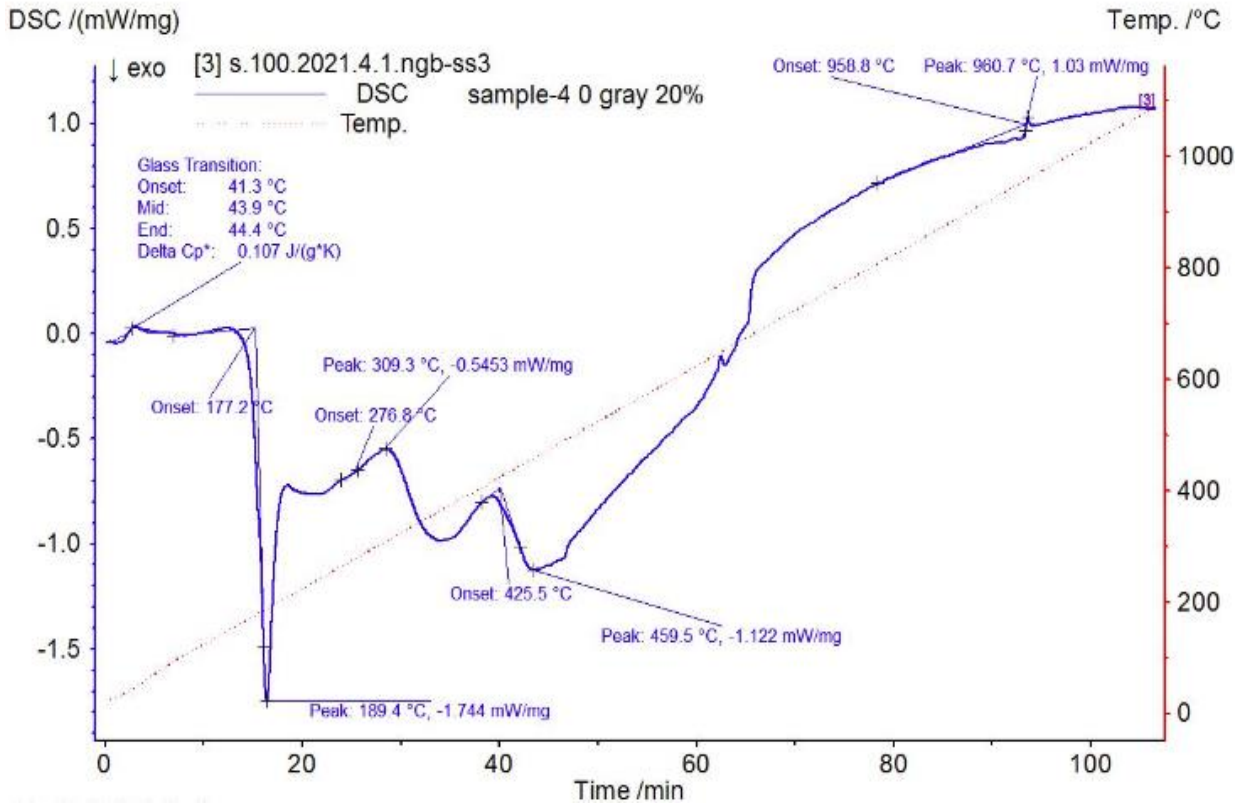

Figure (4.57): DSC Thermograms of the 20 wt% $AgNO_3$, non- irradiated PVA/$AgNO_3$ composite.

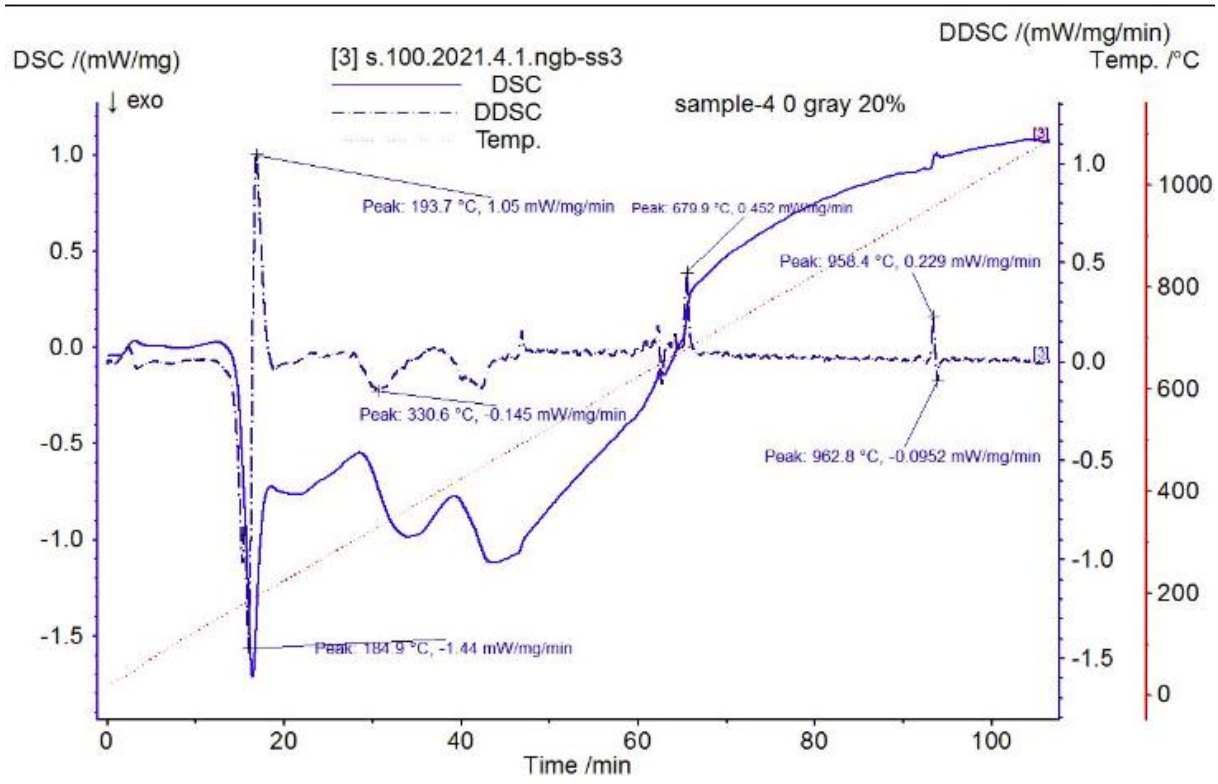

Figure (4.58): Combined DSC/DDSC Thermograms of the 20 wt% $AgNO_3$, non- irradiated PVA/$AgNO_3$ composites.

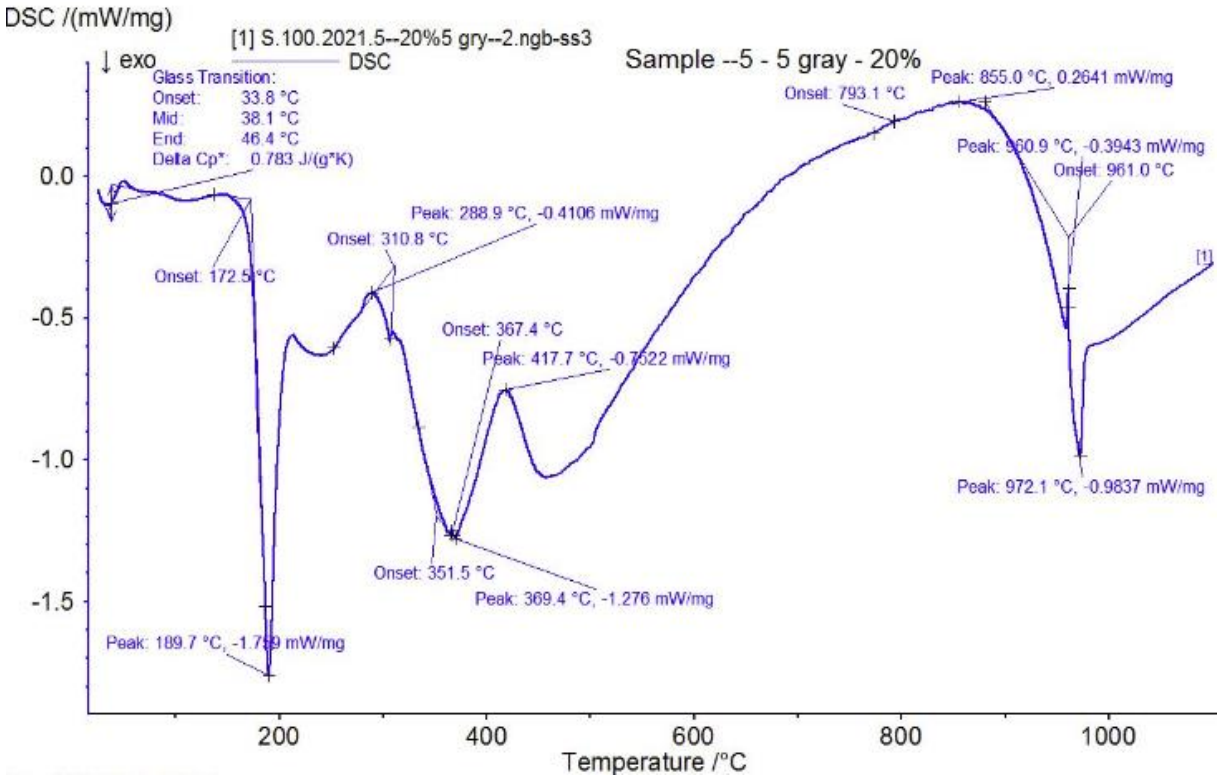

Figure (4.59): DSC Thermograms of the 20 wt% $AgNO_3$, 5 Gy, irradiated PVA/$AgNO_3$ composite.

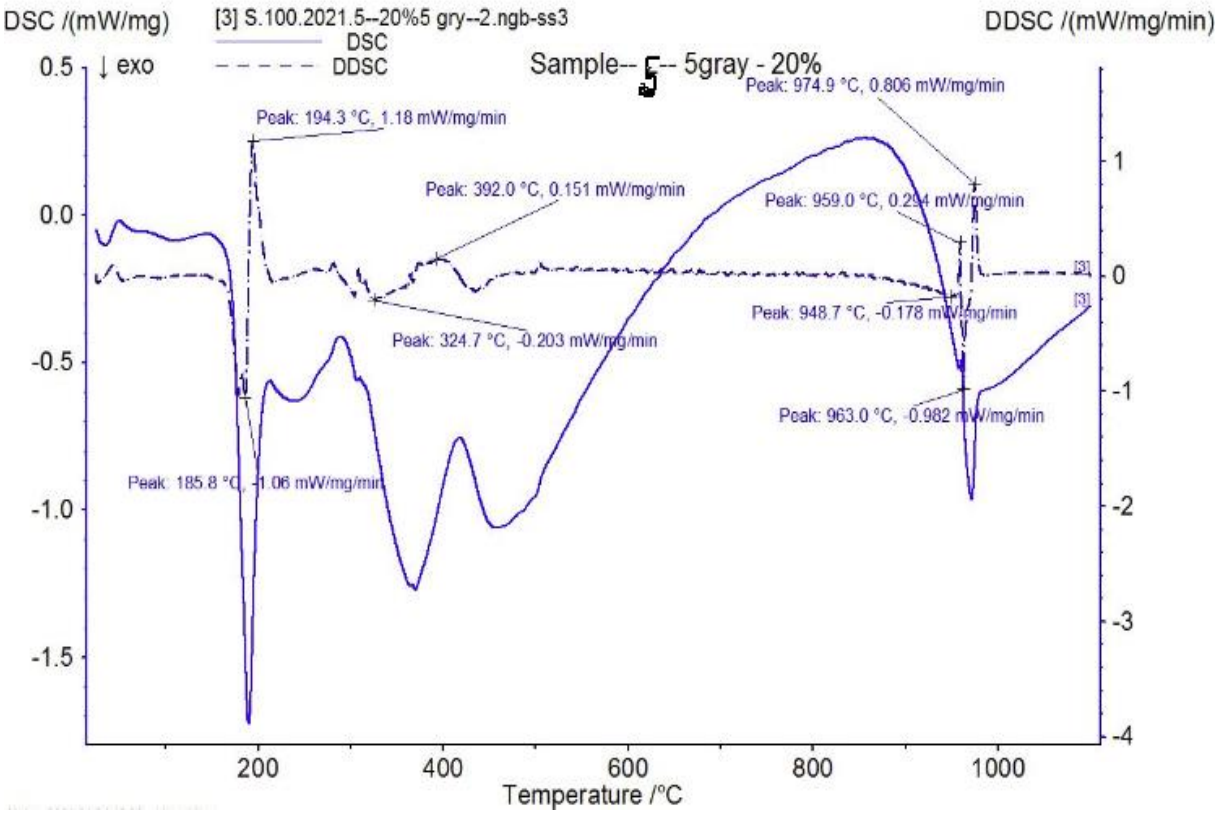

Figure (4.60): Combined DSC/DDSC Thermograms of the 20 wt% $AgNO_3$, 5 Gy, irradiated PVA/$AgNO_3$ composites.

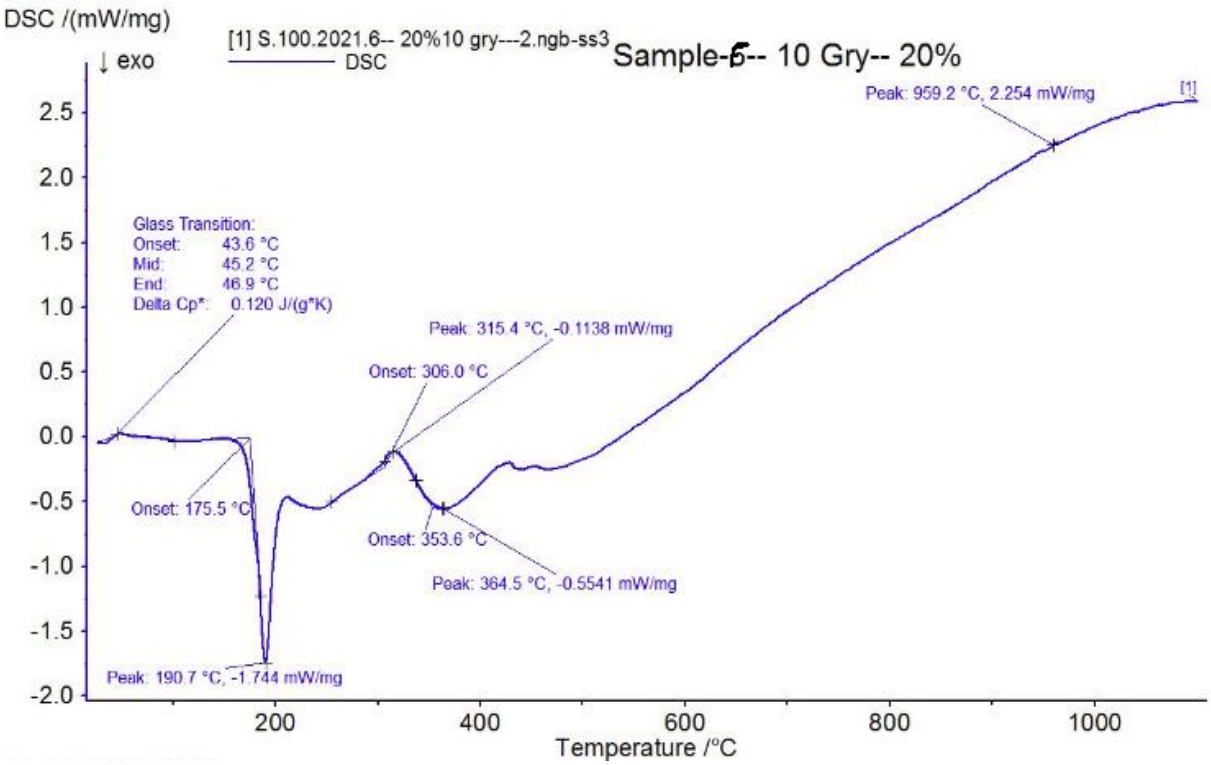

Figure (4.61): DSC Thermograms of the 20 wt% $AgNO_3$, 10 Gy, irradiated PVA/$AgNO_3$ composite.

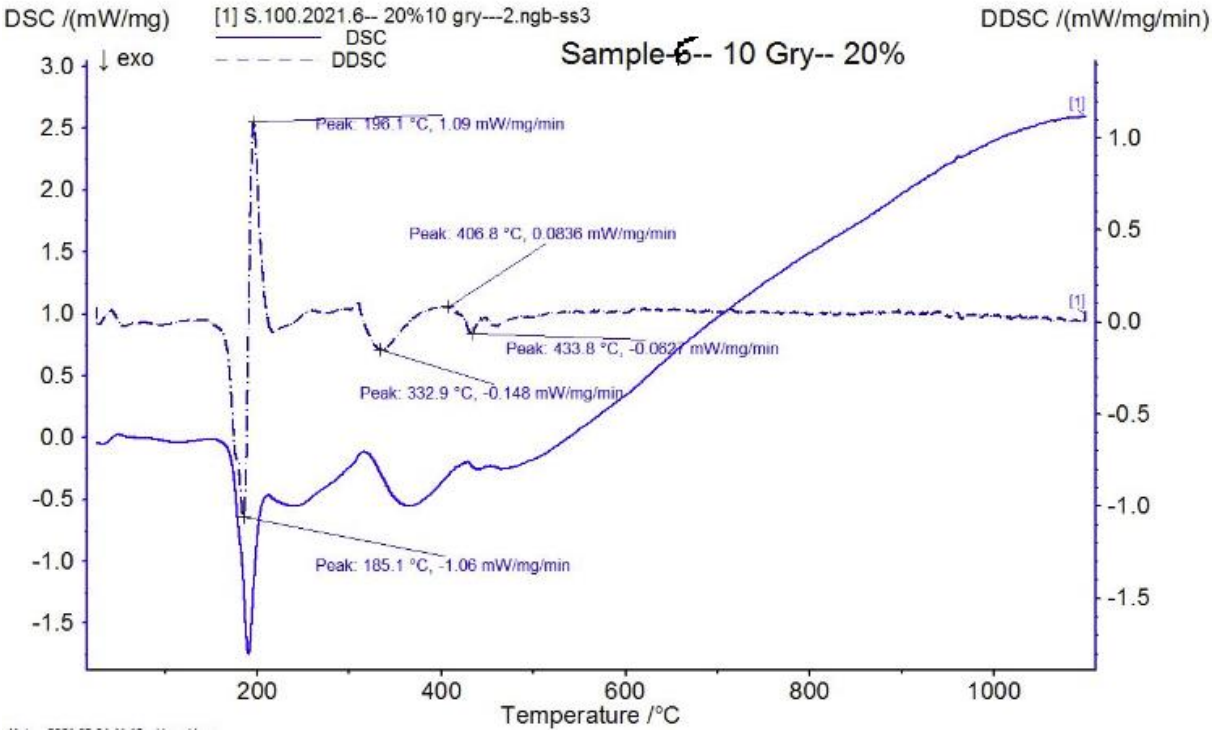

Figure (4.62): Combined DSC/DDSC Thermograms of the 20 wt% $AgNO_3$, 10 Gy, irradiated PVA/$AgNO_3$ composites.

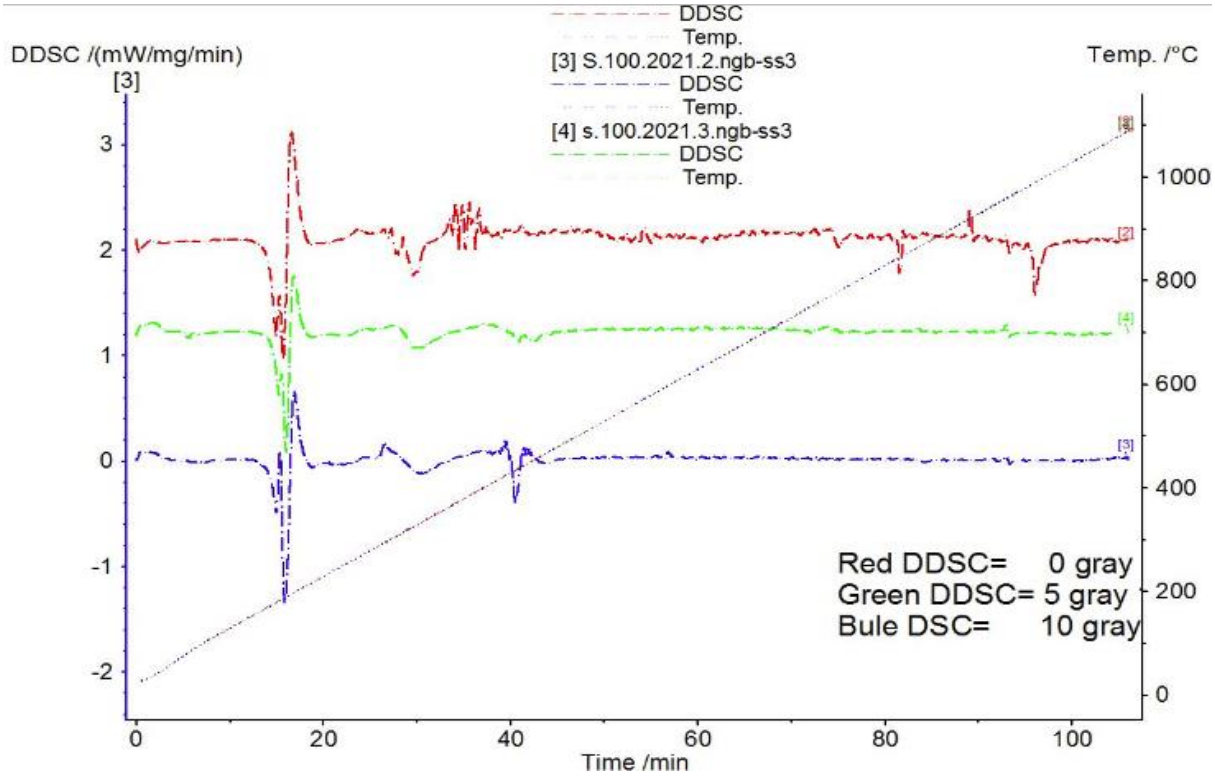

Figure (4.63): DDSC Thermograms of the 10 wt% $AgNO_3$ for the non-irradiated, 5 Gy and 10 Gy irradiated PVA/$AgNO_3$ composites.

Table (4.10) TGA characteristics of the composite films as function of irradiation dose.

Concentrations	Samples	Stages	T_{Onset} (^{0}C)	T_{Peak} (^{0}C)	M residue %
10 wt% $AgNO_3$	PVA/$AgNO_3$ (0 Gy)	I	165.7	185.0	
		II	274.8	313.7	10.41
20 wt% $AgNO_3$	PVA/$AgNO_3$ (o Gy)	I	174.8	183.4	
		II	264.0	316.4	11.83
10 wt% $AgNO_3$	PVA/$AgNO_3$ (5 Gy)	I	171.6	186.6	
		I I	283.2	316.5	9.80
20 wt% $AgNO_3$	PVA/$AgNO_3$ (5 Gy)	I	177	185.4	
		I I	277.8	309.2	1.69
10 wt% $AgNO_3$	PVA/$AgNO_3$ (10 Gy)	I	169.5	185.1	
		I I	264.5	314.3	6.86
20 wt% $AgNO_3$	PVA/$AgNO_3$ (10 Gy)	I	179.4	184.6	
		I I	285.3	319.7	17.77

Table (4.11) DSC characteristics of the composite films as function of irradiation dose.

Concentrations	Samples	Glass transition T_g (^{0}C)	Specific heat [J/(g*K)]	Melting point T_m (^{0}C)
10 wt% $AgNO_3$	PVA/$AgNO_3$ (0 Gy)	105.7	0.459	304.9
20 wt% $AgNO_3$	PVA/$AgNO_3$ (0 Gy)	41.3	0.107	309.3
10 wt% $AgNO_3$	PVA/$AgNO_3$ (5 Gy)	82.8	0.540	315.9
20 wt% $AgNO_3$	PVA/$AgNO_3$ (5 Gy)	33.8	0.783	288.9
10 wt% $AgNO_3$	PVA/$AgNO_3$ (10 Gy)	73.2	0.196	316.3
20 wt% $AgNO_3$	PVA/$AgNO_3$ (10 Gy)	43.6	0.120	315.4

Chapter Five
Discussion, Conclusion and Recommendations

5.1 Discussion

According to **table (4.1)** and **figure (4.2)**, the XRF analysis shows that the concentration of Ag increases upon increasing gamma ray dose from 0 to 5, then to 10 Gy. This may be attributed to the fact that increasing gamma ray dose may increase ionization of Ag atoms to become positive ions, which causes them to repel each other. Thus increasing the atomic spacing and nano size, this in turn decreases Ag concentration.

The UV spectral analysis for Ag in **tables (4.2, 4)** and **figures (4.13, 14),** indicates that the specific absorbance and the absorbance coefficient increase upon increasing gamma ray dose from 0 to 5, then to 10 Gy. This may be related to the fact that increasing exposure increases the ionization of Ag which in turn increases the applied local electric field. According to Stark effect, this causes the bottom of the conduction band E_c to be shifted by an amount of ΔE_c depending on the orientation of the local electric field, as shown in the equation below:

$$E_c{}' = E_c \pm \Delta E_c \qquad (5\text{-}1)$$

Similar effect applies to the top of the valence band, where

$$E_v{}' = E_v \pm \Delta E_v \qquad (5\text{-}2)$$

The new energy gap can be written as:

$$E_g{}' = E_c{}' - E_v{}' = E_g \pm (\Delta E_c - E_v) = E_g \pm \Delta E_g \qquad (5\text{-}3)$$

From that we can write:

$$E_g{}' = E_g - \Delta E_g \qquad (5\text{-}4)$$

When one takes the minus sign, the new energy gap becomes narrower. Thus, upon increasing exposure dose the energy gap becomes narrower

forcing increasing number of electrons to absorb more photons in order to reach the conduction band. This in turn causes absorbance to increase.

Table (4.5) and **figure (4.15)** show that the particle size increases upon increasing gamma ray dose. This may again be attributed to the fact that the increase of Ag ionization concentration upon the increment of radiation dose leads to an increase of repulsive force in the system which in turns increases atomic spacing thus increases the nano particle size. **Table (4.6)** shows that the band gap decreases generally when gamma ray dose was applied, the ionization causes energy splitting which causes the energy gap to decrease as shown by **equation (5-4)**. The increase of energy gap can be explained by **equation (5-3)**, where the orientation of the local electric field sometimes increases the energy.

It is also very interesting to note that **table (4-11)** shows that upon increasing the radiation dose the melting point increases. This may be related to the fact that increasing radiation dose leads to an increment in the nano size thus the thermal energy gained by each particle distributes itself on a larger volume, which causes the melting process for larger particles to require higher temperature. According to **table (4.11),** a raise in melting temperature can be observed. This raise in the melting temperature upon increasing gamma ray dose may be related to the ionization of the Ag atoms. The melting process needs the vibration amplitude to be larger so as to force atoms to be separated from each other during the melting process. In the case of no ionization, the amplitude can be easily increased by a proper amount of thermal energy. However, the ionization of the Ag atoms produces repulsive force for the vibrating atoms or molecules by the surrounding medium. This makes atoms have smaller amplitude of vibration for a given temperature compared to the case when no repulsion exists. Thus extra thermal

energy must be applied to overcome the repulsion and to increase the amplitude so as to cause melting.

Another explanation of changes in the optical, electrical and thermal properties upon applying gamma doses can also be based on Ag deionization, where the exposure of different types and large number of atoms to gamma rays make them loose electrons and form large huge number of positive ions that repel each other. Later on, some of these electrons are captured by Ag positive ions to be transformed to neutral atoms.

In the present study the PVA/Ag nanocomposite with different contents of inorganic phase were prepared by reduction of Ag^{+} ions in PVA solution using gamma irradiation with different doses. The Ag particle size was found to be around 12.0 nm based on the UV-Vis spectroscopy and XRD measurements. Also, the structural studies of the synthesized PVA/Ag nanocomposites have been carried out through XRD studies. Further, the dependence of the optical and thermal properties of PVA on the concentration of the embedded Ag particles was reported. As well, the effects of γ- irradiation have been studied applying UV-Vis spectroscopy, TGA and DSC techniques.

The observed color change was due to reduction of Ag^{+} ions by the formed reducing species such as hydrated electron, hydrogen atom radical (H^{0}) and hydroxyl radical (OH^{0}). UV-Vis spectra of PVA/Ag films recorded show absorption band peaking at the wavelengths around 230 and 450 nm which are related to criteria of the pure PVA and PVA/Ag respectively. According to literature, the band at 450 nm could be attributed to chelate formation of Ag+ coordinated with the hydroxyl group of PVA (Zidan, 1999) or to silver particle formation (Porel et al., 2005). The absorption bands increased following the radiation dose

increment. This enhancement in absorption is found to be in agreement with the color change of PVA samples.

The changes in the optical band gap value of the PVA films have been studied using UV-Vis spectroscopy. The value of optical band gap has been found to be reducing; this decrease in optical band gap can be correlated to the formation of the charge transfer complexes within the polymer network on dispersing Ag particles in it. In addition, γ-irradiation of PVA/Ag samples lead to the formation of Ag nanoparticles, and chain scission and/or cross-linking in the polymer and consequently improved optical and electrical properties. These lower values of the band gap in case of PVA/Ag nanocomposite than that of Ag bulk may be ascribed to the strong quantum confinement in the nanocomposites; it may also be attributed to the creation of electronic disorder which becomes prominent with increasing γ-ray doses; in other terms, due to the photo-degradation of dyed polymer and the formation of defects and clusters in the material as confirmed by the XRD results.

The spontaneous formation of silver nanoparticles can be attributed to the direct redo between PVA and Ag^{+} because there is no other reducing agent in the studied system. Moreover, the increased intensity as well as the red shift of the SPR band may be attributed to considerable increase in the amount of reduced silver and growth of silver nanoparticles as revealed by the UV-Vis results. Moreover, it was also observed from the XRD results that the addition of $AgNO_3$ has no effect on the crystal type of the film; which means that it has been uniformly distributed inside the host polymer (PVA). Also, it is clear that no peaks were observed corresponding to the $AgNO_3$ or other impurities indicating the purity extent of the reduced Ag NPs.

The change in the refractive index values of the irradiated samples observed from the UV-Vis results can be attributed to varying electronic structure and crystallinity induced by gamma irradiation depending upon whether degradation or cross-linking process is predominant. Also the increase in the refractive index of the prepared films with irradiation may be due to ionization or atomic displacements that resulted from gamma ray collision with the samples, which may change the internal structure in the polymer films; this degradation process was confirmed by both XRD and TGA measurements.

XRD results show that with the increase in the applied dose, peaks intensity tends to slightly decrease, broaden and shift to lower angles reflecting the fact that the polymer matrix suffers from some kind of structural rearrangement due to irradiation treatments as confirmed by the TGA and DSC results. Moreover, particle size slightly increased with increasing $AgNO_3$ concentration and the combined effect of γ-irradiation dose resulted in increasing particle size as well. These results are in good agreement with those obtained from UV-visible absorption measurements.

TGA results revealed the existence of initial scission and the chemical crosslinking in the samples. The DTG shows that the thermal degradation runs in two main stages based on the rate of thermal decomposition peaks which indicates a different degradation pathway according to the $AgNO_3$ concentration and irradiation dose. At the first stage, the temperature is below 180 ^{0}C due to the moisture evaporation, vaporization of physically absorbed solvent, the second stage with more rapid weight loss is attributed to the degradation reaction by either of the side chain decomposition or the random chain scission in the polymer backbone, this second weight loss at higher temperature indicates a structural

decomposition of the polymer in nitrogen atmosphere and was confirmed by the DSC observations as well as in the XRD results.

DSC results show endothermic peaks lesser than 200 °C which can be attributed to make out moisture in the polymer which is consistent with the TGA result. The chemical process associated with the exothermic peaks on the DSC thermograms may be related to crystallization or crosslinking reactions as revealed by the XRD results.

The glass transition temperature values of composite films of PVA/$AgNO_3$ shift to lower temperatures with increasing radiation dose and $AgNO_3$ concentration reflecting that there is some interaction between the components i.e. $AgNO_3$ and PVA which gives the more stable stage of the material. We observe that increasing the radiation dose leads to a random breaking of bonds, thus degradation predominates, in other terms, chain scission started to dominate over crosslinking lowering thermal stability. These results can be explained as follow, the addition of $AgNO_3$ molecules to the PVA polymer causes the consumption of the $AgNO_3$ stabilizer into the PVA chains, displacing some of the structural defects for the sample. Thus, the thermal stability increases. But excess concentrations may lead to a detachment of the stabilizer that is previously incorporated into the polymeric chains due to steric hindrance as confirmed from the XRD and TGA results. When samples were heated up to the melting stage, extra energy was required by its components to vibrate and broke up the bonds out of the rigid/crystal arrangement. In general, melting stage can be observed through the present of an endothermic peak in DSC thermograms.

Recently, studies on organic-inorganic hybrid materials have attracted much attention in view of their combination of various features of organic materials with those of inorganic materials. In particular, PVA/Ag nanocomposites are promising materials. PVA is a potential

material having a very high dielectric strength, good charge storage capacity and dopants dependent electrical and optical properties (Alan, 2002 and Chiang et al., 1977). Since Ag^+ is a fast conducting ion in different number of crystalline and amorphous materials, its incorporation within any polymeric system may be expected to enhance its electrical and optical performance. In the present study PVA/$AgNO_3$ films with different concentrations of $AgNO_3$ (i.e. 5, 10, 15 and 20) wt% were prepared by casting method and the reduction of Ag^+ ions in PVA/$AgNO_3$ films was done via gamma irradiation with different doses (i.e. 0, 5, and 10) Gy. The induced structural changes in PVA after the formation of embedded Ag nanoparticles and subsequently through gamma irradiation were revealed through X-ray diffraction (XRD), while the observed changes in their optical behavior were studied using UV-Vis spectroscopy. Also the study focused on the thermal behavior of PVA/Ag nanocomposite films with varying the concentration of the doped silver nanoparticles as well as with the applied gamma-irradiation doses.

Figure (4.1) shows the PVA/$AgNO_3$ films undergoing color change after irradiation with gamma-ray doses of (0, 5 and 10) Gy. The color intensity increased with increasing radiation doses indicating that the color change is largely dependent on the proportion of the red and yellow color components, the color changed from gray at 0 Gy (non-irradiated films) to a combination of light yellow, golden, brown and dark brown colors following increasing intensity with increasing radiation doses. Such color change was due to reduction of Ag^+ ions by the formed reducing species such as hydrated electron, hydrogen atom radical (H^o) and hydroxyl radical (OH^o). Similar results were reported previously in the literature by (Omer M. et al, 2011), (Muhammad Attique. et al., 2014), (Susilawati et al., 2009), (ShaheenAkhtar et al., 2013) and (Iskandar et al., 2013).

X-ray Fluorescence (XRF) analysis was performed to validate that the intensity of AgLα characteristic X-ray line depends on the $AgNO_3$ concentration in the PVA/$AgNO_3$ films. **Table (4.1)** summarizes the intensities obtained for AgLα characteristic X-ray line for PVA/$AgNO_3$ films irradiated with gamma doses of (0, 5 and 10) Gy whereas **figure (4.2)** graphically represent the dependence of the intensity in part per thousand (PPT) of AgLα characteristic X-ray line on $AgNO_3$ concentration for non-irradiated and gamma-irradiated PVA/$AgNO_3$ films; a strong linear correlation is observed. Moreover, **figure (4.3)** reveals the strong dependence of intensity of AgLα characteristic X-ray line on Ag concentration for non-irradiated (0 Gy) PVA/$AgNO_3$ films with correlation coefficient $\boldsymbol{R^2 = 0.99881}$ and the correlation equation $\boldsymbol{y = 1.392x + 951.2}$. **Figure (4.4)** reveals strong dependence of the intensity of AgLα characteristic X-ray line on Ag concentration for PVA/$AgNO_3$ films irradiated with 5 Gy with correlation coefficient $\boldsymbol{R^2 = 0.99617}$ and the correlation equation $\boldsymbol{y = 1.356x + 945.3}$. **Figure (4.5)** shows strong dependence of the intensity of AgLα characteristic X-ray line on Ag concentration for PVA/$AgNO_3$ films irradiated with 10 Gy with correlation coefficient $\boldsymbol{R^2 = 0.93746}$ and the correlation equation $\boldsymbol{y = 1.318x + 937.85}$.

UV absorption is mainly due to electron (or anion) transitions from the top of the valence band to the bottom of the conduction band. The absorption spectra produced two absorption bands in the visible region. These visible bands correspond to the excitation of outer electrons, which provide information on the electronic transitions of the molecules in the samples, they are attributed to the π-π* transitions and to the presence of ions in the polymer. In this study, the electronic absorption spectra of the investigated samples have been recorded in the region from 200 to 1100 nm for non-irradiated and γ−irradiated PVA samples. UV-Vis spectra of

PVA/$AgNO_3$ films recorded show absorption band peaking at the wavelengths around 230 and 450 nm which are related to criteria of the pure PVA and PVA/$AgNO_3$ respectively. According to literature, the band at 450 nm could be attributed to chelate formation of Ag^+ coordinated with the hydroxyl group of PVA (Zidan, 1999) or to silver particle formation (Porel et al., 2005). The absorption bands increased following the radiation dose increment, such phenomenon has been reported by (Mohammed et al., 2014) and (Ramnani et al., 2007). In one hand, it is well known that pure PVA films are transparent and contains only single bonds; therefore it would be expected to absorb radiation only in the far UV region (120–200) nm. On the other hand, the physical properties of PVA are dependent on its preparation technique whether from the fully hydrolysis or partial hydrolysis of poly vinyl acetate (C.C. De Merlis & D.R. Schoneker, 2003 and Eman Kamal, 2013). Thus the absorption band at 230 nm may be assigned to $\pi \rightarrow \pi^*$ transition. This transition is related to the carbonyl groups (C═O) associated with ethylene unsaturation (C=C) of the type –$(CH=CH)_2CO$-. The existence of carbonyl functionalities is probably due to residual acetate groups remaining after the manufacture of PVA from hydrolysis of polyvinyl acetate or oxidation during manufacturing and processing (C.C. De Merlis and D.R. Schoneker, 2003).

Figure (4.6) shows UV-Vis spectra of the non-irradiated PVA/$AgNO_3$ films prepared with various concentrations (i.e. 5, 10, 15 and 20 wt %) of $AgNO_3$, films have absorption peaks at (432, 455, 434, 435) nm respectively, it can be seeing that with increasing the concentration of $AgNO_3$, very weak and broad absorption shoulder appeared around 400 nm. The absorbance of this band is gradually increased in intensity with increasing the concentration of $AgNO_3$. In addition, the absorption band gets narrower and shifts continuously to longer wavelengths. Similar

results were reported by (Omer M. et al., 2011), (Muhammad Attique et al., 2014), (Susilawati et al., 2009), (Abdo Mohd Meftah et al., 2014) and (ShaheenAkhtar et al., 2013). **Figure (4.7)** shows UV-Vis spectra of the 5 Gy gamma-irradiated PVA/$AgNO_3$ films prepared with various concentrations (i.e. 5, 10, 15 and 20 wt %) of $AgNO_3$, films have absorption peaks at (455, 465, 458, 456) nm respectively, it can be seeing that with increasing the concentration of the $AgNO_3$, very weak and broad absorption shoulder appeared around 400 nm. The absorbance of this band is gradually increased in intensity with increasing the concentration of $AgNO_3$. In addition, the absorption band gets narrower and shifts continuously to longer wavelengths. **Figure (4.8)** shows UV-Vis spectra of the 10 Gy irradiated PVA/$AgNO_3$ films prepared with various concentrations (i.e. 5, 10, 15 and 20 wt %) of $AgNO_3$, films have absorption peaks at (450, 466, 455, 456) nm respectively, it can be seeing that with increasing the concentration of the $AgNO_3$, very weak and broad absorption shoulder appeared around 400 nm. The absorbance of this band is gradually increased in intensity with increasing the concentration of $AgNO_3$. In addition, the absorption band gets narrower and shifts continuously to longer wavelengths.

Figures (4.9), (4.10), (4.11) and (4.12) show UV-Visible absorption spectra of γ-irradiated PVA/$AgNO_3$ samples with (5.0, 10, 15 and 20) wt % Ag respectively. We observe that with increasing $AgNO_3$ content; a strong increase in the absorbance in the ultraviolet and visible regions; i.e., in the spectral range (200-600) nm, the absorption coefficient of the samples also increased with increasing of irradiation dose. The dramatic enhancement in absorption is found to be in agreement with the color change of PVA samples. Furthermore, the peaks got narrower and sharper and also increased in intensity with increasing irradiation dose. **Tables (4.2) and (4.4)** show the specific absorbance and the absorption

coefficient respectively; which were measured from the absorption spectrum of all PVA/$AgNO_3$ films. We can deduce that both specific absorbance and absorption coefficient linearly increase with increasing radiation dose and $AgNO_3$ concentration. **Figure (4.13)** shows the correlation between specific absorbance and radiation dose for γ-irradiated PVA/$AgNO_3$ sample with 10 wt % Ag as an example, it shows a strong linear correlation with $\boldsymbol{R^2 = 0.99378}$ and the correlation equation $\boldsymbol{y = 0.031x+3.435}$. **Figure (4.14)** shows the correlation between absorption coefficient and radiation dose for γ-irradiated PVA/$AgNO_3$ sample with 10 wt % Ag as an example, it shows a strong linear correlation with $\boldsymbol{R^2 = 0.9923}$ and the correlation equation $\boldsymbol{y = 0.00065x+0.072}$.

Nanosized noble metals are well-known for their surface Plasmon resonance (SPR) properties which originate from collective oscillations of the conduction electrons confined to metallic nanoparticles. Excitation of the localized surface Plasmon causes strong light scattering by the electric field at a wavelength where resonance occurs; this phenomenon results in appearance of strong surface Plasmon absorbance (SPR) bands. The optical absorption spectrum of metal nanoparticles is dominated by the SPR which exhibits a shift towards the red end or blue end depending upon the particle size, shape, state of aggregation and the surrounding dielectric medium (A. Ravindran et al., 2010). For silver nanoparticles, λ_{max} values were reported in the visible range 400–500 nm (N. Mohri et al., 1995). In this study the Plasmon band of the Ag nanoparticles was noted around 430–466 nm. Hence, the appearance of this very weak band may be related to the formation of small quantity of reduced silver nanoparticles. The spontaneous formation of silver nanoparticles can be attributed to the direct redo between PVA and Ag^+ because there is no other reducing agent in the studied system. Moreover, the increased

intensity as well as the red shift of the SPR band may be attributed to considerable increase in the amount of reduced silver and growth of silver nanoparticles (Eman Kamal, 2013). In particular, silver nitrate is soluble in PVA to such an extent that a complete dissolution is observed at the first step of the reaction; in the next step, the OH^0 groups of PVA molecule anchor the Ag^+ ion at the cluster surface which efficiently reduces the precursor metal ions Ag^+ to Ag nanoparticles, while the polymeric chain protects the cluster from fusion with the next silver molecule. The final size of silver clusters stabilized by the polymer is of few tens of nanometers and the sole presents the very weak and broad classical surface absorption band at 450 nm which means that PVA is a weak reducing agent for silver salt.

Table (4.5) shows the dependence of particle size of Ag nanoparticles in PVA matrix on γ-irradiation dose for PVA/$AgNO_3$ samples with different concentrations, while **figure (4.16)** represents the correlation between Ag particle size and $AgNO_3$ concentration for the non-irradiated and gamma-irradiated samples. It is observed that particle size slightly increases as a function of the $AgNO_3$ concentration. However, an additional increase of $AgNO_3$ dopants concentration leads to segregation of the dopants in the host matrix; these molecular aggregates impede the Ag nanoparticles resulting in a decrease in their sizes. **Figure (4.15)** shows the correlation between Ag particle size and $AgNO_3$ concentration for samples irradiated with 5 Gy as an example, it shows a positive linear correlation with $\boldsymbol{R^2 = 0.70526}$ and the correlation equation $\boldsymbol{y = 0.05448x+9.4725}$.

Table (4.6) lists optical band gaps of PVA/Ag nanocomposites prepared with different $AgNO_3$ concentrations and γ-irradiated with various doses. From this table it can be observed that the values of the band gap in case of PVA/Ag nanocomposite are lower than that of Ag bulk. This is may be ascribed to the strong quantum confinement in the nanocomposites; it

may also be attributed to the creation of electronic disorder which becomes prominent with increasing γ-ray doses; in other terms, due to the photo-degradation of dyed polymer and the formation of defects and clusters in the material (E.M. Antar, 2014). **Figure (4.17)** shows the relation between $(\alpha h\nu)^2$ and photon energy ($h\nu$) for PVA/Ag films of 10 wt% Ag irradiated with 10 Gy as an example on energy gap (E_g) estimation process.

Figures (4.18), (4.19) and (4.20) show the extinction coefficient of PVA/Ag composite films doped with different $AgNO_3$ concentrations gamma-irradiated with doses of (0, 5 and 10) Gy respectively. It can be observed that the values of the extinction coefficient linearly increase with increasing $AgNO_3$ concentration; same thing happens with the increment of radiation dose. Moreover, the peaks get narrower and shift continuously to longer wavelengths.

Figures (4.22), (4.23), and (4.24) show the refractive index of PVA/$AgNO_3$ composite films doped with different $AgNO_3$ concentrations γ-irradiated with doses of (0, 5 and 10) Gy respectively. It can be observed that the refractive index linearly decreases with increasing $AgNO_3$ concentration but tends to increase again at higher concentrations. Refractive index increases with the increment of radiation dose but again tends to decrease at higher doses. Moreover, the peaks get narrower and shift continuously to longer wavelengths. The change in the refractive index values of the irradiated samples can be attributed to varying electronic structure and crystallinity induced by gamma-irradiation depending upon whether degradation or cross-linking process is predominant. Also the increase in the refractive index of the prepared films with irradiation may be due to ionization or atomic displacements

that resulted from gamma ray collision with the samples, which may change the internal structure in the polymer films (Eman kamal, 2013).

Figures (4.26), (4.27) and (4.28) show optical conductivity of PVA/$AgNO_3$ composed films doped with different $AgNO_3$ concentrations gamma-irradiated with doses of (0, 5 and 10) Gy respectively. It can be observed that the value of the optical conductivity linearly increases with increasing $AgNO_3$ concentration, similar thing happens with the increment of radiation dose. Moreover, the peaks get narrower and shift continuously to longer wavelengths. In both cases, the value of optical conductivity which is highly linked to the dielectric constant degrades at higher dopants concentration and higher doses.

The dielectric constant also known as relative permittivity is a measure of the amount of electric potential energy, in the form of induced polarization that is stored in a given volume of material under the action of an electric field. It can be expressed as the ratio of the dielectric permittivity of the material to that of a vacuum or dry air. Practically, it is determined as the ratio of the capacity of a capacitor with a desired material as the dielectric between the plates to that with dry air. This polarization originates from a number of sources including electronic (electron cloud displaced relative to nucleus), atomic (relative displacement of charged ions), dipolar (alignment of dipoles in electric field), space charge (movement of charge carriers trapped by interfaces in heterogeneous systems) and ionic (movement of ionic charges).

Figures (4.30), (4.31) and (4.32) show the real part of dielectric constant of PVA/Ag composed films doped with different $AgNO_3$ concentrations gamma-irradiated with doses of (0, 5 and 10) Gy respectively. It can be observed that its value linearly increases with increasing $AgNO_3$ concentration, same thing happens with the increment of radiation dose. Moreover, the peaks get narrower and shift continuously to longer

wavelengths. **Figures (4.34), (4.35) and (4.36)** show the imaginary part of dielectric constant of PVA/Ag composed films doped with different $AgNO_3$ concentrations gamma-irradiated with doses of (0, 5 and 10) Gy respectively. It can be observed that its values linearly increase with increasing $AgNO_3$ concentrations, same thing happens with the increment of radiation dose. Moreover, the peaks get narrower and shift continuously to longer wavelengths. The high values of dielectric constant are very crucial in electric applications and for capacitance applications of small sizes as it gives possibilities of new devices with minimized dimensions. The dielectric constant is affected by temperature and current frequency (E. Alfredo Campo, 2008).

XRD is the most common bulk analysis technique used to identify the crystalline phase present and crystal particle sizes. XRD analysis has been routinely used for crystalline phase identification based on diffraction peak position and pattern and the measurement of the average crystalline sizes and lattice parameters. It can also supply information about deformation of a crystalline sample in other terms the strain of a crystal lattice which will result in a change in the inter-atomic distances (Eman Kamal, 2013; Alireza Kharazmi et al., 2013 and P.K. Mochahari et al., 2015).

In this study, X-ray diffraction technique has been used to investigate and characterize the structure of the prepared samples. It indicates that PVA/$AgNO_3$ samples have in large an amorphous feature, shown in **figures (4.38 through 4.43)**. It is important to note that there are two halos cited at 19.66^0 and 40.5^0 characteristic of PVA. The first one has a clear crystalline peak at a diffraction angle 2θ = 20.04^0 which corresponds to a (101) spacing, this main peak centered at 19.66^0 corresponds to the PVA crystalline phase with the accepted monoclinic unit cell with a = 7.81, b = 2.52, c = 5.51 Å and β = 91.42^0; one unit cell

comprises two monomer units of vinyl alcohol (CH2CHOH**)** (Alireza Kharazmi et al., 2013 and P.K. Mochahari et al., 2015)**.** The second halo has a low intensity and broad shape which corresponds to noncrystalline zones within the crystalline polymeric matrix. Moreover, there are several very low intense peaks in these figures which are assigned to the Ag nanoparticles; their low intensities are due to the very low concentration of Ag NPs compared with amount of PVA.

It is obvious from the XRD pattern that the diffraction peak at 2θ = 19.66^0 revealed a clear crystalline peak of maximum intensity implying the more organized distribution of the $AgNO_3$ in the polymeric matrix. It was observed that the addition of $AgNO_3$ has no effect on the crystal type of the film; which means that it has been uniformly distributed inside the host polymer. Also, it is clear that no peaks were observed corresponding to the $AgNO_3$ or other impurities indicating the purity extent of the reduced Ag NPs. On the other hand, no significant effect of gamma irradiation noticed on either the intensity of the diffraction peak or on its full width at half maximum (FWHM); but with the increase in the applied dose, peaks intensity tends to slightly decrease, broaden and shift to lower angles reflecting the fact that the polymer matrix suffers from some kind of structural rearrangement due to irradiation treatments (S. Lotfy and Y.H.A. Fawzy, 2014).

The average crystallite size (D) of the non-irradiated and γ-irradiated films is calculated from the Scherer's formula and listed in **Table (4.7).** From the table, we observe that particle size slightly increased with increasing $AgNO_3$ concentration and the combined effect of γ-irradiation dose results in increasing particle size as well. These results are in good agreement with those obtained from UV-visible absorption measurements. The semicrystalline nature of PVA is attributed to the

strong intermolecular interaction among PVA chains through hydrogen bonding. The addition of $AgNO_3$ to PVA matrix leads to a decrease in the intermolecular interaction between chains and thus to a decrease in the degree of crystallinity (DOC) as shown in **Table (4.8)**, this in turns means more amorphous crystal and increasing in intera-atomic distances (d) as shown in **Table (4.9).**

Thermogravimetric Analysis (TGA) was performed to confirm the existence of initial scission that occurs and/or the possible chemical crosslinking in the prepared samples. Thermographs obtained from room temperature up to 1000 ^{0}C, heating rate 10 ^{0}C/min in a nitrogen flow of 20 ml/min for the non-irradiated and γ-irradiated PVA/$AgNO_3$ samples are given in **figures (4.44 through 4.50)**. There are three major stages of weight losses for the composites regardless of the experimental environments. The first weight loss at the lower temperature near 180 °C results from moisture evaporation, the loss is small between 7-14%. The second weight loss at higher temperature indicates a structural decomposition of the polymer composite in N_2 atmosphere which is probably attributed to large–scale thermal degradation of polymer chains that started to degrade near at 200 °C and partially degrade up to 450 °C (M. S. N. Salleh. et al, 2017). In the third stage at higher temperature, a sharp and considerable weight loss is observed, which is attributed to the vaporization and elimination of volatile products (A. NimrodhAnanthet al., 2011). There was decomposed residuals powder left in the sample pan for composite material. A clear distinction between the different stages of the degradation process is evidenced in the DTG curves.

Figures (4.44) and (4.47) show the combined TGA/DTGA behavior of the non-irradiated (10 and 20) wt% of $AgNO_3$ composite films respectively; when heated in nitrogen is divided into three main stages

based on the rate of thermal decomposition peaks. At the first stage, the temperature is below 180 ^{0}C due to the moisture evaporation, vaporization of physically absorbed solvent, at a maximum loss rate of -4.6 % per min and -4.54 % per min with DTG peaks of 185 ^{0}C and 183.4 ^{0}C respectively. In the second stage, more rapid weight loss is observed at a maximum rate of -9.45 % per min and -6.29 % per min with DTG peaks of 313.7 ^{0}C and 316.4 ^{0}C respectively. The marked loss of weight in the second stage is attributed to the degradation reaction by either of the side chain decomposition or the random chain scission in the backbone of the polymer, this second weight loss at higher temperature indicates a structural decomposition of the polymer in nitrogen atmosphere and was confirmed by the XRD and DSC measurements (Mónica Cobos et al., 2020). In the third stage more weight loss was observed at higher temperature. Thermal stability values observed and residue mass left behind at 1000 ^{0}C were 10.41 and 11.83 % respectively. The onset temperature of thermal decomposition, the temperature where the decomposition process starts, values observed were 274.8 and 264.0 ^{0}C respectively. The largest weight loss, greatest rate of change on the weight loss curve, also known as the inflection point values observed were 314.0, and 317.5 ^{0}C respectively. We can see the enhancement in the stability of the composite polymer with increasing silver concentration.

Figures (4.45) and (4.48) show the combined TGA/DTGA behavior of the 5 Gy irradiated (10 and 20) wt% $AgNO_3$ composite films respectively; when heated in nitrogen is divided into three main stages based on the rate of thermal decomposition peaks. At the first stage, the temperature is below 180 ^{0}C due to the moisture evaporation, vaporization of physically absorbed solvent, at a maximum loss rate of -3.9 % per min and -4.49 % per min with DTG peaks of 186.6 ^{0}C and

185.4 ^{0}C respectively. In the second stage, more rapid weight loss is observed at a maximum rate of -8.76 % per min and -8.78 % per min with DTG peaks of 316.5 ^{0}C and 309.2 ^{0}C respectively. In the third stage more weight loss was observed at higher temperature. Thermal stability values observed and residue mass left behind at 1000 ^{0}C were 9.80 and 1.69 % respectively. The onset temperature of thermal decomposition values observed were 283.2 and 277.8 ^{0}C respectively. The inflection points values observed were 316.7, and 307.8 ^{0}C respectively. We can see the enhancement in the stability of the composite polymer with increasing silver concentration and radiation dose.

Figures (4.46) and (4.49) show the TGA/DTGA behavior of the 10 Gy irradiated (10 and 20) wt% $AgNO_3$ composite films respectively; when heated in nitrogen is divided into three main stages based on the rate of thermal decomposition peaks. At the first stage, the temperature is below 180 ^{0}C due to the moisture evaporation, vaporization of physically absorbed solvent, at a maximum loss rate of -4.71 % per min and -4.92 % per min with DTG peaks of 185.1 ^{0}C and 184.6 ^{0}C respectively. In the second stage, more rapid weight loss is observed at a maximum rate of -7.84 % per min and -6.88 % per min with DTG peaks of 314.3 ^{0}C and 319.7 ^{0}C respectively. In the third stage more weight loss was observed at higher temperature. Thermal stability values observed and residue mass left behind at 1000 ^{0}C were 6.86 and 17.77 % respectively. The onset temperature of thermal decomposition values observed were 264.5 and 285.3 ^{0}C respectively. The inflection points values observed were 313.5, and 335.4 ^{0}C respectively. We can see the enhancement in the stability of the composite polymer with increasing silver concentration and radiation dose.

A summary of the important thermogravimetric characteristics obtained from the thermograms are listed in **Table (4.10).** It's evident that non-

irradiated (10 and 20) wt% $AgNO_3$ composite films are thermally stable up to 274.8 ^{0}C and 264.0 ^{0}C respectively. While the irradiation enhances the thermal stability in the low doses around 10 Gy, it falls beyond at higher doses above 100 Gy (M. Streckova et al., 2017). In the dose range around 10 Gy, the free radicals formed due to chain scission are chemically active and can be used in some chemical reactions that lead to the crosslinking mechanism. As the dose increases, chain scission started to dominate over crosslinking lowering thermal stability (M. S. N. Salleh. et al, 2017). This leads to a random breaking of bonds, thus degradation predominates which leads to a rapid decomposition of the polymer composed and auto self-combustion process accompanied by evolution of volatile by-product as confirmed by the DSC measurements.

Moreover, thermal analysis of PVA/$AgNO_3$ composites with different $AgNO_3$ concentrations showed that with the incorporation of $AgNO_3$ into the blends the onset degradation temperature was shifted to higher temperature than pure PVA. As shown in **Table (4.10)** with high $AgNO_3$ concentration (at 20 wt%) in the composite, the degradation temperature noted its highest value. On the same time, the composition of carbonaceous and char residue for 20 wt% $AgNO_3$ were higher than that of 10 wt% $AgNO_3$. In general, PVA/$AgNO_3$ samples show a decomposition pattern similar to that shown by neat PVA. The DTG curves, however, revealed that the intensity of the peak at around 319 ^{0}C increases with respect to that of the peak at around 313 ^{0}C as the content of the $AgNO_3$ increased, and the second peak shifts to a higher temperature. Therefore, the addition of $AgNO_3$ improves the thermal stability of PVA. This can be due to the high thermal stability of the filler acting as a retardant agent for PVA decomposition (Mónica Cobos et al., 2020). Char residue at 1000 ^{0}C is higher for composites than for neat PVA. The higher the filler content, the higher the residue.

Differential Scanning Calorimetry (DSC) can be used to determine the thermal transition temperatures glass transition, melting and decomposition temperatures as well as the specific heat and heat capacity. However, it measures only the total heat flow and the sum of all thermal transitions in the sample (E.M. Antar, 2014). **Figures (4.51) and (4.52)** respectively show the DSC and DDSC curves of the non-irradiated 10 wt% $AgNO_3$ composite films, there appear an endothermic peak lesser than 200 ^{0}C which can be attributed to make out moisture in the polymer composite (Qing Liu, et al., 2018) which is consistent with the TGA result. The chemical processes associated with the exothermic peaks may be related to crystallization or crosslinking reactions. TGA information is further supported by the DSC measurements. Onset glass transition temperature (Tg) and specific heat recorded were 105 ^{0}C and 0.459 J/(g*K) respectively.

Figures (4.57) and (4.58) respectively show the DSC and DDSC curves of the non-irradiated 20 wt% $AgNO_3$ composite films, there appear an endothermic peak lesser than 200 ^{0}C which can be attributed to make out moisture in the polymer composite which is consistent with the TGA result. Onset glass transition temperature (Tg) and specific heat recorded were 105 ^{0}C and 0.459 J/(g*K) respectively. **Figures (4.53) and (4.54)** respectively show the DSC and DDSC curves of the 5 Gy irradiated 10 wt% $AgNO_3$ composite films, it shows an endothermic peak lesser than 200 ^{0}C which can be attributed to make out moisture in the polymer composite which is consistent with the TGA result. Onset glass transition temperature (Tg) and specific heat recorded were 82.8 ^{0}C and 0.540 J/(g*K) respectively. **Figures (4.59) and (4.60)** respectively show the DSC and DDSC curves of the 5 Gy irradiated 20 wt% $AgNO_3$ composite films, there appear an endothermic peak lesser than 200 ^{0}C which can be attributed to make out moisture in the polymer composite which is

consistent with the TGA result. Onset glass transition temperature (T_g) and specific heat recorded were 33.8 ^{0}C and 0.783 J/(g*K) respectively. **Figures (4.55) and (4.56)** respectively show the DSC and DDSC curves of the 10 Gy irradiated 10 wt% $AgNO_3$ composite films, it shows an endothermic peak lesser than 200 ^{0}C which can be attributed to make out moisture in the polymer composite which is consistent with the TGA result. Onset glass transition temperature (T_g) and specific heat recorded were 73.2 ^{0}C and 0.196 J/(g*K) respectively. **Figures (4.61) and (4.62)** respectively show the DSC and DDSC curves of the 10 Gy irradiated 20 wt% $AgNO_3$ composite films, there appear an endothermic peak lesser than 200 ^{0}C which can be attributed to make out moisture in the polymer composite which is consistent with the TGA result. Onset glass transition temperature (T_g) and specific heat recorded were 43.6 ^{0}C and 0.120 J/(g*K) respectively.

A summary of the important characteristics obtained from the DSC thermograms are listed in **Table (4.11).** We observe that the glass transition values of composite films of PVA/$AgNO_3$ shift to lower temperatures with increasing dose and silver concentration, this means also shifting in heat capacity. This change in the size of (Tg); which can be attributed to a change in the amount of material detected, accompanied with the change in its location; which can be attributed to a change in the mobility of molecules indicates that there are some interactions between the components of the composite films (A. NimrodhAnanth et al., 2011). We observe that increasing radiation dose leads to a random breaking of bonds, thus degradation predominates; in other terms, chain scission started to dominate over crosslinking lowering thermal stability. PVA melting point is 230 °C for the fully hydrolyzed grades and its glass transition temperature is 85 ^{0}C (M. S. N. Salleh, et al., 2017). When samples were heated up to the melting stage, extra energy was required

by its components to vibrate and broke up the bonds out of the rigid/crystal arrangement. In general, melting stage can be observed through the present of an endothermic peak in DSC thermograms.

As illustrated before, all samples have prominent endothermic peaks indicative of crystallinity in the PVA. In DSC thermograms the onset temperature is when sample began to melt, whereas the end-point temperature is the temperature when the melting stage is completed. The temperature at the middle of the endothermic peak is taken as the melting temperature (T_m). The effect of the addition of $AgNO_3$ into the matrix, however, has led to a little change in the onset and end-point temperature as well as (T_m). Radiation dose has similar effects. **Table (4.11)** indicates that (T_g) of the PVA not only depends on the concentration of the incorporated inorganic fillers but also it should have a considerable impact from the nature of the fillers as well as the radiation dose (Mbhele et al. 2003).

5.2 Conclusion

- Functional composite material of PVA\$AgNO_3$ films with enhanced optical and thermal properties was successfully synthesized using controlled temperature and pressure by casting method alongside γ-ray irradiation.
- Gamma radiation is an effective reducing agent for Ag^+ within the PVA matrix to Ag nanoparticles having controlled particle size.
- The results indicated that $AgNO_3$ can be effectively embedded in PVA matrix and enhance its optical and electrical properties. In addition γ- irradiation is an effective technique for preparing inorganic/organic nanocomposite materials.
- The irradiation of the PVA\$AgNO_3$ films with γ-ray doses induced obvious color changes from white (non-irradiated film) to light

yellow, golden then to brown and dark brown and the color intensity increased with increasing γ-ray doses.

- X-ray Fluorescence (XRF) analysis validated that the intensity of AgLα characteristic X-ray line depends on the Ag concentration in the prepared PVA/$AgNO_3$ films with a correlation value near to 1.
- The irradiated films showed absorption band peaking at the wavelengths around 230 and 450 nm and the intensity of peaks is in direct proportion with radiation dose.
- There exist a clear linear correlation between the applied dose and the specific absorbance and the absorption coefficient of the prepared films.
- There exist a clear linear correlation between $AgNO_3$ concentration and the specific absorbance and the absorption coefficient of the prepared films.
- The surface Plasmon band was noted around 430–466 nm. Hence, the appearance of this very weak band may be related to the formation of small quantity of reduced silver nanoparticles.
- It has been observed that the concentration of sliver nanoparticles has greatly influenced the optical and electrical properties of PVA matrix.
- Values of the band gap (E_g) in case of PVA/Ag nanocomposite are found to be lower than that of Ag bulk. This is may be ascribed to the strong quantum confinement in the nanocomposites; it may also be attributed to the creation of electronic disorder which becomes prominent with increasing gamma-ray doses.
- Values of the extinction coefficient (K) linearly increase with increasing $AgNO_3$ concentrations and radiation dose.
- The overall effect of the radiation dose is increasing the value of the refractive index (n).

- Values of the optical conductivity linearly increase with increasing $AgNO_3$ concentration and radiation dose.
- Values of the dielectric constant linearly increase with increasing $AgNO_3$ concentration and radiation dose and was found to be very big. These high values of dielectric constant are very crucial in electric applications and for capacitance applications of small sizes as it gives possibilities of new devices with minimized dimensions.
- XRD patterns validated UV-Vis observations regarding the fact that the polymer matrix suffers from some kind of structural rearrangement due to gamma-irradiation treatments.
- XRD diffraction peak at $2\theta = 19.66^0$ revealed a clear crystalline peak of maximum intensity implying the more organized distribution of the $AgNO_3$ in the polymeric matrix.
- XRD studies confirmed the presence of Ag nanoparticles in the PVA matrix. In addition DSC analysis indicated the chemical interaction between the $AgNO_3$ and PVA chains.
- The obtained results corroborate towards the enhanced conducting behavior of PVA matrix with increase in the concentration of embedded Ag nanoparticles.
- Measurements of the onset temperature of thermal decomposition showed that the composite material of PVA/$AgNO_3$ was more thermally stable than its pristine components, i.e. pristine PVA and $AgNO_3$.
- Thermal stability was found to increase with increasing the radiation dose and $AgNO_3$ concentration; this was evidenced by the evaluation of the percentage residual mass which was at its maximal value for 10 Gy, 20 wt% composite films.
- Shift in the values of glass transition temperature as well as values of the specific heat indicates that there was some kind of

interaction between the polymer PVA and the additive filler $AgNO_3$, this was confirmed by XRD measurements.

- Melting temperatures of the composites increased with the increment of radiation dose and the filler $AgNO_3$ concentration.
- The synthesized PVA/$AgNO_3$ films can serve as a potential chemical radiation dosimeter and/or radiation monitoring device according to their linear relationship between the radiation doses and absorption spectra and the sensitivity of PVA/$AgNO_3$ films to γ-ray doses which showed color change.
- Various optical and electrical parameters of PVA/Ag nanocomposites are controlled with the Ag concentration and γ-Irradiation dose which can be used for specific requirements in the optical coating, filters, switches, etc.

5.3 Recommendations

This study could be considered as an initial step in studying structural, thermal and optical properties of functional hybrid materials (polymer/metal) due to their vast industrial, technological and medical applications. Every work has its limit and due to some constrains during this work such as time and the availability of equipment, here are some recommendations to be considered for future works:

- Further work is needed to assess the effect of composites preparation methodology on their thermal stability.
- Further work is required to investigate the effect of % crystallinity and particle distribution, shape and size on thermal stability.
- For its biomedical applications, mechanical characterizations such as swelling (% water uptake), tensile strength, elongation at break, stress, strain, Young modulus and refractive index are of great importance.

- PVA/$AgNO_3$ composite films can be used as a chemical radiation dosimeter to measure the γ-ray doses in radiotherapy centers in Sudan having good results and being fast, easy and cheap assessment tool.
- It can serve also as fast and cheap radiation monitoring and label for industrial applications such as food sector (food irradiation control).
- The color change of the films could be utilized as light filters and the surface Plasmon resonance could be utilized as local in vivo irradiation therapy as well as in signal magnification in case of Raman scattering.
- This work suggests possibility of using the gamma irradiated PVA/$AgNO_3$ films in different electronic and semiconductors applications such as catalysis, conducting inks, microelectronics, thick-film electrode material, and solar cells.
- Further work is needed to investigate how the film thickness is affected by the radiation dose increment and in return how all that affect the properties of the composites.
- More studies are needed to determine temperature dependence on the fluorescence of these potential dosimeters as well as determining the right storage and measurement conditions of PVA/$AgNO_3$ films.

References

AbdoMohdMeftah, ElhamGharibshahi, NayerehSoltani, W. Mahmooud Mat Yunus and Elias Saion; Structural, Optical and Electrical Properties of PVA/PANI/Nickel Nanocomposites Synthesized by Gamma Radiolytic Method.Polymers (2014), 6: 2435-2450; doi:10.3390/polym6092435.

Abthagir P., Syed K.; Dhanalakshmi.,Saraswathi R., Thermal Studies on Polyindole and Polycarbazole, synth. Met. (1998), 93 (1): 1-7.

Abthagir P.S., Saraswathi R., Sivakolunthu S.; Aging and Thermal Degradation of Poly (N-methylaniline), Thermochim.Acta . (2004), 411 (2): 109-123.

Alan, J.H., Semi-conducting and metallic polymers: the fourth generation of polymeric materials. Synth.Met.(2002), 125: 23-42.

Aleksandra N. Krkljes, Milena T. Marinovic -Cincovic, Zorica M. Kacarevic-Popovic, Jovan M. Nedeljkovic; Radiolytic synthesis and characterization of Ag-PVA nanocomposites, European Polymer Journal (2007), 43: 2171–2176.

Alireza Kharazmi et al.; Optical Properties of CdS/PVA Nanocomposite Films Synthesized using the Gamma-Irradiation-Induced Method,CHIN. PHYS. LETT. Vol. 30, No. 5 (2013) 057803.

Ali Z.I., Hossam M. Said and H.E. Ali; Effect of electron beam irradiation on the structural properties of poly(vinyl alcohol) formulations with triphenyltetrazolium chloride dye (TTC). Radiation Physics and Chemistry (2006), Vol. 75 (1), P. 53–60.

Al-Zahrany AA, Rabaeh KA, Basfer AA; Radiation induced color bleachingof methyl red in polyvinyl butyral film dosimeter. Radiat. Phys. Chem (2011), 80:1263-1267.

A. Miller; Dosimetry for Radiation Processing, Radiation Physics and Chemistry (1986), Vol. 28, No. 5-6, p. 321.

Andreo, P., Burns, D.T., Nahum, A.E., Seuntjens, J., and Attix F.H.; Fundamentals of Ionizing Radiation Dosimetry, WILEY-VCH (2017).

A.N.Goldstein, C.M. Echer, and A.P. Alivisatos; The journal of Science (1992), 256: 1425-1427.

A. NimrodhAnanth, S. Umapathy, J. Sophia, T. Mathavan and D. Mangalaraj; On the optical and thermal properties of insitu/exsitu reduced AgNP's/PVA composites and its role as a simple SPR-based protein sensor, ApplNanosci (2011) 1:87–96.

A Primer; Fundamentals of UV-visible spectroscopy, Hewlett-Packard publication number 12-5965-5123E (1996), Germany.

Arshak, K. and Korostynska, O.; Gamma Radiation-Induced Changes in the Electrical and Optical Properties of Tellurium Dioxide Thin Films, IEEE Sensors Journal (2003), 3, 717.http://dx.doi.org/10.1109/JSEN.2003.820327.

Athawale, A.A.; Bhagwat, S., Synthesis and characterization of novel copper/polyaniline nanocomposite and application as a catalyst in the Wacker oxidation reaction, J. Appl. Polym. Sci. (2003), 89: 2412–2417.

Attix, Frank Herbert; Introduction to Radiological Physics and Radiation Dosimetry, John Wiley & Sons, Inc. (1986), USA.

Avenue, Dublin, Ireland, British Journal of Radiology (2002), 75: 243-248©2002.

B. G. Steetman, S. K. Banerjee; Solid State Electronic Devices,Pearson Education Inc (2006) ISBN 0-13-149726-X.

Bhadra, S.; Singha, N.K.; Khastgir, D.; Electrochemical synthesis of polyaniline and its comparison with chemically synthesized polyaniline. J. Appl. Polym. Sci. (2007), 104: 1900–1904.

B. Karthikeyan, Spectroscopic studies on Ag–polyvinyl alcohol nanocomposite films, Physica B (2005), 364:328–332.

Blaskov V, Stambolova I, Shipochka M, Vassilev S, Kaneva N, Loukanov A, Decoloration of Reactive Black 5 Dye on TiO_2 Hybrid films Deposited by Sol-Gel Method., Scientific papers, Vol: 38, Book 5, (2011)-Chemistry.

Boone, J.M., "X-ray production, interaction and detection in diagnostic imaging" in Handbook of medical imaging Volume 1. Physics and Psychophysics, ed. Beutel J., Kundel H.L., VanMetter R.L., 1st edn, SPIE, Washington, USA (2000), pp. 3-81.

Bunn, C.W., Crystal structure of polyvinyl alcohol. Nature (1948), 161: 929-933.

Bushberg JT, Seibert JA, Leidholdt EM, Boone JM.; The essential physics of medical imaging, 2nd ed. Philadelphia, PA: Lippincott Williams & Wilkens (2002):145-173.

Carl, C. Koch.; Nanostructured Materials-Processing Properties and Potential Applications. Carl C. Koch.(2002), NY.

Chen YP, Liu SY, Yu HQ, Yin H, Li QR., Radiation induced degradation of Methyl Orange in aqueous solutions, Chemosphere (2008), 72:532–536.

Chiang, C. K., Fincher, Jr., C. R., Park, Y. W., Heeger, A. J., Shirakawa, H. &Louis, E. J., Electrical conductivity in doped polyacetylene, Physics Review Lett. (1977) 39: 1098-1101.

Choppin, G., Rydberg, J ., Liljenzin, J O., Theory and applications radiochemistry and nuclear chemistry. 2 nd. Ed. Oxford. London (1995): 175-180.

Chuang, F.-Y.; Yang, S.-M., Cerium dioxide/polyaniline core–shell nanocomposites. J. Colloid Interface Sci. (2008), 320: 194–201.

C. J. Tung1, H. C. Wang, S. H. Lo, J. M. Wu and C. J. Wang, in vivo dosimetry for external photon treatments of head and neck cancers by diodes and TLDs, Radiation Protection Dosimetry (2004), Vol. 111, No. 1: 45–50.

C. W. Lee, C. H. Chou, J. H. Huang, C. S. Hsu, T. P. Nguyen, j. Mater. Sci. Eng: B, (2008), 147: 307.

C.W. Mays, J.S. Vermaak, D. Kuhlmann-Wilsdorf, Surface Science (1968), 12:134-140.
Denaro, A. R. and Jayson, G. G.; Fundamental of radiation chemistry, Butterworths, London (1972).

D.R. Dance, S. christofides, A.D.A. Maidment, I.D. Mclean, K.H. Ng, Diagnostic Radiology Physics, A handbook for teachers and students (2014), ISBN 978–92–131010–1.

Drobny, J.G., Radiation Technology for Polymers, CRC Press, 2nd edition (2010).

Duch M. A, Ginjaume M, Chakkor H. Ortega X, Jornet N, Ribas M., Thermo-luminescence dosimetry applied to in-vivo dose measurements for total body irradiation techniques. Radiotherapy and oncology (1998) Vol. 47 (3), P: 319-324.

E.B. Podgorsak, Radiation Oncology Physics: A Handbook for Teachers and Students, international atomic energy agency, Vienna, (2005).

E.M. Antar, Effect of g-ray on optical characteristics of dyed PVA films, Journal of Radiation Research and Applied Sciences 7 (2014) 129-134.

Eman Kamal, Radiation effect on characterization and physical properties of polymer nanocomposites, a master thesis at Zagazig University, Faculty of Science, Physics Department, 2013.

EPA-402-K-07-006, Environmental Protection Agency Office of Radiation and Indoor Air, Radiation Risks and Realities: May 2006.

Evans, R. D.,The Atomic Nucleus. McGraw-Hill (1952), New York.

Farhat, In vivo dosimetry for head and neck carcinoma: determination of target absorbed dose from entrance and exit absorbed dose measurements, The European Physical Journal Applied Physics / Volume54 / Issue 01 / April 2011.

G.A. Snook, P. Kao, A.S. Best,Conducting-polymer-based supercapacitor devices and electrodes, J. Power Sources (2011), 196:1-12.

Gao C., Li S., Song H., Xie L.: Radiation induced crosslinking of ultra high molecular weight polyethylene fibers by means of electron beams. Journal of Applied Polymer Science (2005), 98: 1761–1764.

G. Carotenuto, L. Nicolais, Nanocomposites, Metal-Filled, in the Encyclopedia of Polymer Science and Technology, Wiley (2003), New York.

Glenn F. Knoll, Radiation Detection and Measurement, 4th Edition, ISBN: 978-0-470-13148-0, August – 2010.

Goto, H. A possibility for construction of an iodine cleaning system based on doping for π-conjugated polymers. Polymers (2011), 3: 875–885.
G. Wang, J. Xu, H. Chen, Biosens. Bioelectro.24 (2009) 2494.

Hall, E.J.,Lessons we have learned from our children: cancer risk from diagnostic radiology. Paediatric Radiology, vol. 32 (2002), pp: 700-706.

Han, D.; Yan, L.; Chen,W.; Li,W., Preparation of chitosan/graphene oxide composite film with enhanced mechanical strength in the wet state,Carbohydr.Polym. (2011), 83: 653–658.

Huda, W.,Review of radiologic physics, Third Editonedn, Lippincott Williams & Wilkins (2010), Philadelphia.

H. M. Zidan, Electron Spin Resonance and Ultraviolet Spectral Analysis of UV-Irradiated PVA Films Filled with MnCl2 and CrF3, Physics Department, Faculty of science at Damietta, Mansoura University (2002), P.O. 34517, New Damietta, Egypt .

H.M. Zidan, effect of AgNO3 filling and UV-irradiation on the structure and morphology of PVA films, Polymer Testing 18 (1999): 449–461.

IAEA Radiation oncology physics: A Handbook for Teachers and Students – 16.2.1 Slide 2 (9/236) (2005).

ICRU, Determination of absorbed dose in a patient irradiated by beams of x or gamma rays in radiotherapy procedures. ICRU report 24 (1976), Bethesda, Maryland.

International Committee for Radiation Protection (lCRP). Committee 3,(2001): Diagnostic Reference levels in Medical imaging.

IskandarShahrim Mustafa, NorhanisahMegatAzman, Azhar Abdul Rahman, RamzunMaizanRamli and Halimah Mohamed Kamari, Journal of Engineering Science, Vol. 9 (2013): 61–69.

Jin R, Cao Y, Mirkin C A, Kelly K L, Schatz G. C. and Zheng J., Photo induced conversion of silver nanospheres to nanoprisms. Science (2001), 294: 1901-1908.

Jiri George Drobny, Radiation Technology for Polymers, CRC Press LLC, (2003).

J. Liu, L. Zhang, H.B. Wu, J. Lin, Z. Shen, X.W.D. Lou, High-performance flexible asymmetric supercapacitors based on a new graphene foam/carbon nanotube hybrid film, Energy Environ. Sci.(2014), 7: 3709-3719.

J.R. Weertman, D. Farkas, K. Hemker, H. Kung, M. Mayo, R. Mitra, H.V. Swygenhoven, MRS Bull. (1999), 24: 44-53.

J. Schiøtz,, K.W. Jacobsen, Science 301 (2003) 1357-1359.

Kaeami, H., Mousavi, M.F. & Shamsipur, M. (2003).A new design for dry polyaniline rechargeable batteries. Power Sources (2003), 117: 255-259.

Kalef-Ezra J. A, Boziari A, Litsas J,TsekerisPkoligliatis T.,Thermoluminescence dosimetry for quality assurance in radiotherapy, Radiat Prot. Dosim (2002); Vol. 101 (1-4), P: 403-405.

Kerluke, D. R. and Cheng, S., Electron Beam Processing for Automotive Composite Applications, Proceedings of the 2nd Annual Automotive Composites Conference and Exposition of the Society of Plastics Engineers (2002).

Khanmohammadi H, Erfantalab M (2012). New 1, 2,4-triazole-based azo- azomethine dyes. Part I: Synthesis, characterization and spectroscopic studies. SpectrochimicaActa Part A: Mol. and Biomol. Spect. 86:39-43.

Khanna, P.K.; Singh, N.; Charan, S.; Viswanath, A.K., Synthesis of Ag/polyaniline nanocomposite via an in situ photo-redox mechanism, Mater. Chem. Phys. (2005), 92: 214–219.

Knoll, G.F., Radiation Detection and Measurement.John Wiley & Sons, 4th edition (2010).

Kron.T, P.M. Ostwald, C.S.Hamilton and J.W.Denham, TLD Extrapolation Measurements for Entrance and Exit Dose in Radiotherapy RadiatProt Dosimetry (1996) vol. 66 (1-4): p 323-326.

Kros, A., Van Hovel, S. W., Nolte, R.J.M., Sommerdijk, N.A. (2001). A printable glucose sensor based on a poly(pyrrole)-latex hybrid material. Sensors and Actuators (2001), 80: 229-233.

Kumar R, Prasad R, Vijay Y K, Acharya N K, Verma K C and Udayan De., Ion beam modification of CR-39 (DOP) and polyamide nylon-6 polymers, Nucl.Instrum.Methods (2003)B 212 221. Vol. 212, P: 221–227.

Lee, C.Y., Kim, H.M., Park, J.W., Gal, Y.S., Jin, J.I., Joo, J., AC electrical properties of conjugated polymers and theoretical high-frequency behavior of multilayer films. Synthetic Metals.(2001), 117: 109-113.

Lee, H.; Mensire, R.; Cohen, R.E.; Rubner, M.F., Strategies for hydrogen bonding based layer-by-layer assembly of poly (vinyl alcohol) with weak polyacids, Macromolecules (2011), 45: 347–355.

Lei, Zhongli and Fan Youhua., Preparation of silver nanocomposites stabilized by an amphiphilic block copolymer under ultrasonic irradiation, Material letters (2006), Vol. (60), pp. 2256-2260.

Lin, J. C., C. Y. Wang., Effects of surfactant treatment of silver powder on the rheology of its thick-film paste, Material Chemical Physics (1996), 45: 136-144.

Lin, C.W., Hwang, B.J. & Lee, C.R., Methanol sensors based on the conductive polymer composites from polypyrrole and poly(vinyl alcohol), Materials Chem. Phys. (1998),55: 139-144.

Li W, X Zhao, Z Huang and S Liu, Nanocellulose fibrils isolated from BHKP using ultrasonication and their reinforcing properties in transparent poly (vinyl alcohol) films, Polym Res(2013), 20 210.

L. Liu, H. Song, L. Fan, F. Wang, R. Qin, B. Dong, H. Zhao, X. Ren, G. Pan, X. Bai, Q. Dai, j.Mater. Res. Bull. 44 (2009) 1385.

Lokhovitsky, V.I. and V.V. Polikarpov, Technology of radiation emulsion polymerization, Atomizdat (1980), Moscow-Russia.

Long, N.V.; Thi, C.H.; Nogami, M.; Ohtaki, M., Novel issues of morphology, size, and structure of Pt nanoparticles in chemical engineering: surface attachment, aggregation or agglomeration, assembly, and structural changes. New J. Chem. (2012), 36: 1320–1334.

McGervey, J., Introduction to Modern Physics, second ed., Academic Press, New York (1983).

Mallakpour S., Taghavi M., The Accuracy of Approximation Equations in the Study of Thermal Decomposition Behavior of Some Synthesized Optically Active Polyamides, Iran. Polym. J. (2009), 18(11): 857-872.

Marija, G.N., Jadranka, T.S., Bowmaker, G.A., Cooney, R.P., Thompson, C. & Kilmartin, P.A., The antioxidant activity of conducting polymers in biomedical applications Current Appl. Phys. (2004), 4: 347-350.

Mbhele ZH, Salemane MG, Van Sittert CGCE, Nedeljkovic JM, Djokovic V, Luyt AS, Fabrication and characterization of silver-polyvinyl alcohol nanocomposites,Chem Mater (2003), 15:5019–5024.

M.C. Roco, Journal of Nanoparticle Research 3 (2001), 511.

M.C. Roco,, Journal of Nanoparticle Research 4 (2002), 19.

M. G. Lines, J. Alloys. Comp. 449 (2008) 242.

M. Kattan, Y. Daher and H. Alkassiri, A High-Dose Dosimeter-Based Polyvinyl Chloride Dyed with Malachite Green, Radiation Physics and Chemistry (1989), Vol. 76, No. 7, pp. 1195-1199. doi:10.1016/j.radphyschem.2006.12.004.

M.M. Abutalib, Effect of additive concentration and X-ray irradiation on the thermal and color properties of Polyvinyl alcohol, Life Sci J (2014), 11(9):512-517. (ISSN:1097-8135). http://www.lifesciencesite.com. 85.

Mohammed A. Ali Omer, Hamed A. Ismail, Mohamed E. M. Garlnabi, Ghada A. Edam, Nuha S. Mustafa, Optimization of PAV\AgNO3 Films for Measuring Entrance and Exit Radiotherapy Dose Relative to TLDs, International Journal of Science and Research (IJSR) (2015), Volume 4 Issue 3, March 2015.

Mohammed A. Ali Omer, Mohamed E M, Gar-elnabi, Alyaa, H. Ahmed, GhadaAbakerEidam and Nasr Aldeen N. Khidir, Radiochemical Properties of Irradiated PVA\AgNO3 Film by Electron Beam. International Journal of Science and Research (IJSR) (2013), India Online, Vol. 2 (9), P: 361-364.

Mohammed A. Ali Omer, Saion E., Gar-elnabiM. E. M., Balla E. A. A., DahlanKh. M., and Yousif Y. M., Gamma Radiation Synthesis and Characterization of Polyvinyl Alcohol/ Silver Nano Composites Film, J. Sc. Tech (2011), Vol. 12 (1), P: 104-110.

Mohamad El-Saied El-Nagdy, MohamadRabeaa El-Saadany, Antar El-Saied Mohamad, Dose Response and FWHM Properties of Dyed Poly Vinyl Alcohol-Irradiated with Gamma-Rays, Open Journal of Polymer Chemistry (2013), 3: 39-42.

Molyneux, Water Soluble Synthetics Polymers: Properties and Behavior, Vol.1. CRC.Press (1983), USA.

MónicaCobos, Iker De-La-Pinta, Guillermo Quindós , MaríaJesúsFernández and María Dolores Fernández, Synthesis, Physical, Mechanical and Antibacterial Properties of Nanocomposites Based on Poly(vinyl alcohol)/Graphene Oxide–Silver Nanoparticles, Polymers (2020), 12, 723; doi:10.3390/polym12030723.

Monti, O, L. A, J.T. Fourkas, D. J. Nesbitt, Diffraction-Limited Photo generation and Characterization of Silver Nanoparticles, Journal of Physical Chemistry B (2004), Vol. 108, P: 1604-1612.

Moscovitch M., personnel dosimetry using LiF:Mg,Cu,P. Radiation protection dosimetry 85 (1999), (1-4): 49-56.UNSCEAR, 1962.P.389.

Mott, N., F. and Davis E.A., Electronic Process in Non-crystalline Materials, 2nd.Edition (1979), Clarendon Press, Oxford, UK.

Motz, J. W., H. A. Olsen, H. W. Koch., Pair production by photons, Review. Model Physics (1969), 41: 581-639.

M. Streckova, E. Mudra, M. Sebek, T. Sopcak, J. Dusza and J. Kovac, Preparation and Investigations of Ni0:2Zn0:8Fe2O4 Ferrite Nanofiber Membranes by Needleless Electrospinning Method, ActaPhysicaPolonica Series a · April 2017.

M. S. N. Salleh, N. N. Mohamed Nor, N. Mohd, and S. F. Syed Draman, Water resistance and thermal properties of polyvinyl alcohol-starch fiber blend film, AIP Conference Proceedings 1809, 020045 (2017); https://doi.org/10.1063/1.4975460 Published Online: 24 February 2017.

Muhammad Attique Khan Shahid1, Bushra Bashir, Hina Bashir, Huma Bashir1 and ArfaMubashir, Dosimetric characterization and spectroscopic study of radiochromic films as natural dye dosimeters, International Journal of Chemistry and Material Science Vol. 2(2), pp. 028-045, June, 2014.

Murat Beyzadeoglu, GokhanOzyigit,CuneytEbruli, Basic Radiation Oncology ISBN: 978-3-642-11665-0 e-ISBN: 978-3-642-11666-7, 2010.

MutahirTunio, Mansoor Rafi, Shoukat Ali, Zaeem Ahmed, AsadZameer, AltafHashmi and Syed A. Maqbool, In vivo dosimetry with diodes in a radiotherapy department in Pakistan,RadiatProt Dosimetry (2011) vol. 147 (4):p 608-613.

Mutsuo, S.; Yamamoto, K.; Furuzono, T.; Kimura, T.; Ono, T.; Kishida, A., Release behavior from hydrogen-bonded polymer gels prepared by pressurization, J. Appl. Polym. Sci. (2011), 119: 2725–2729.

M. Zhao, J.C. Li, Q. Jiang, J., Alloys. Comp. 361 (2003) 160-164.

N. V. Bhat, M. M. Nate, R. M. Bhat and B. C. Bhatt, Effect of Gamma Radiation on PVA Films Doped with Some Dyes and Their Use in Dosimetric Studies, Indian Journal of Pure & Applied physics (2007), Vol. 45, No. 6, pp. 545-548.

Nabid, M.R.; Golbabaee, M.; Moghaddam, A.B.; Dinarvand, R.; Sedghi, R., Polyaniline/TiO2 nanocomposite: Enzymatic synthesis and electrochemical properties, Int. J. Electrochem. Sci. (2008), 3: 1117–1126.

Nagaraja, N., Subba Reddy, C.V. Sharma, A. K. NarasimhaRao, V. V. R., DC conduction mechanism in polyvinyl alcohol film doped with potassium thiocyanate, Journal of power source (2002),112: 326-330.

National Radiological Protection Board: Doses to Patients from Medical X-ray Examinations in the UK. (2000), NRPB.

National Radiological Protection Board: National Protocol for Patient Dose measurement in diagnostic Radiology, Dosimetry Working Party of the institute of physical Science in Medicine in, UK. (1992), NRPB.

Nouh S A and R ABahareth, Effect of electron beam irradiation on the structural, thermal and optical properties of PVA thin film, Radiation Effects Defects in Solids (2013): 168-274.

Omer M. A. A. Saion E. Gar-elnabiM. E. M., Balla E. A. A. DahlanKh. M. Yousif Y. M., Gamma Radiation Synthesis and Characterization of Polyvinyl Alcohol/ Silver Nano Composites Film, J.Sc. Tech 12. (1) 2011.

Painter et al 1997, Paul C.; Coleman, Michael M. (1997). Fundamentals of polymerscience : an introductory text, Lancaster, Pa.: Technomic Pub. Co. p. 1.ISBN 1-56676-559-5.

Pankove, J.I., 1971. Optical Processes in Semiconductors. Dover Publications Inc. N.Y. 1-127.

Parwate DV, Sarma ID, Batra RJ, Preliminary feasibility study of congo red dye as a secondary dosimeter. Rad. Meas. (2007), 42(9):1527-1529.

Patel HM, Dixit BC, Synthesis, characterization and dyeing assessment of novel acid azo dyes and mordent acid azo dyes based on 2-hydroxy-4-methoxybenzophenone-5-sulfonic acid on wool and silk fabrics, Int. J. Saudi Chem. (2012)Soc.In press.

P. Buffat, J.-P.Borel, Physical Review A 13 (1976): 2287-2298.
P.K. Mochahari et al., Study of chemically synthesized SHI irradiated CdS nanostructured films, Adv. Mater. Lett. 2015, 6(4), 354-358.

P. MAYLES, A. NAHUM, JC. ROSENWALD, Hand Book of Radiotherapy Physics Theory and Practice, (2007), ISBN-13:978-0-7503-1, ISBN-10:0-7503-0860-5.

Qing Liu, Ning Chen, ShibingBai and Wenzhi Li, Effect of silver nitrate on the thermal processability of poly(vinyl alcohol) modified by water, RSC Adv., (2018), 8, 2804.

Ramnani .S.P. JayashriBiswal, S. Sabharwal, Synthesis of silver nanoparticles supported on silica aerogel using gamma radiolysis, Radiation Physics and Chemistry (2007), 76: 1290–1294.

Ravindran, A. Singh, A. M. Raichur, N. Chandrasekaran, A. Mukherjee, Colloid. Surfac. B: Biointerfaces 76 (2010) 32–37.

Ravve, A., Introduction and physical properties of polymer, Principles of Polymer Chemistry, 2nd.Edition (2000), New York: Kluwer Academic/Plenum.

Reda, S.M.; Al-Ghannam, S.M., Synthesis and electrical properties of polyaniline composite with silver nanoparticles. Adv. Mater. Phys. Chem. (2012), 2: 75–81.

R.F. Hill, S. Brown, C. Baldock, (2008), Evaluation of the water equivalence of solid phantoms using gamma ray transmission measurements, Radiation Measurements (2008), 43: 1258 – 1264.

Rizk R. A. M., A. M. Abdul-Kader, M. Ali and Z. I. Ali, Influence of ion-beam bombardment on the optical properties of LDPE polymer blends, J. Phys. D: Applied Phys. (2008) Vol. 41, P: 1-5.

RonaldDenderehand, X-ray absorptiometry for measurement of bone mineral density on a slot-scanning X-ray imaging system, (2014).

Riyadh Ch, Ghufran AH, Shabeeb M, Hammouti B, Characterization of table sugar dosimeter for gamma-radiation dosimetry, Der Pharma Chemica (2011), 3(6): 182-188.

S.A. Baeurle, Multiscale modeling of polymer materials using field-theoretic methodologies: a survey about recent developments, Journal of Mathematical Chemistry (2009),46 (2): 363–426. doi:10.1007/s10910-008-9467-3.

Saxena, S.K., polyvinyl alcohol (PVA): Chemical and Technical Assessment (CTA) 61st JECFA, (2004).

Saphwan Al-Assaf, Xavier Coqueret, KhairulZaman Haji MohdDahlan, Murat Sen, PiotrUlanski, The Radiation Chemistry of Polysaccharides, International Atomic Energy Agency Vienna, 2016, Identifiers: IAEAL 16-01075 | ISBN 978–92–0–101516–7.

S. Bhadra, D. Khastgir, N.K. Singha, J.H. Lee, Progress in preparation, processing and applications of polyaniline, Prog. Polym. Sci. (2009), 34: 783-810.

S. Lotfy and Y.H.A. Fawzy, Characterization and enhancement of the electrical performance of radiation modified poly (vinyl) alcohol/gelatin copolymer films doped with carotene, journal of radiation research and applied sciences 7 (2014), 338e345.

ShaheenAkhtar, TaqmeemHussain, AamirShahzad, Qamar-ul-Islam, Muhammad YousufHussain and NasimAkhtar, Radiation Induced Decoloration of Reactive Dye in PVA Films for Film Dosimetry, Journal of Basic & Applied Sciences(2013), 9: 416 419.

Shuai, C.; Mao, Z.; Lu, H.; Nie, Y.; Hu, H.; Peng, S., Fabrication of porous polyvinyl alcohol scaffold for bone tissue engineering via selective laser sintering,Biofabrication(2013), 5, 015014.

Siegbahn, K., 1965. Alpha, Beta and Gamma Ray Spectroscopy, North-Holland, Amsterdam, Netherlands.

Smith, F., A. 2000. A Primer in Applied Radiation Physics.World Scientific Publishing Co. Pte.Ltd.

Sridevi, V.; Malathi, S.; Devi, C. Synthesis and characterization of polyaniline/gold nanocomposites.Chem. Sci. J. (2011): 1–26.

Stakheev A.Y., Kustov L.M., Effects of the support on the morphology and electronic properties of supported metal clusters; modern concepts and progress in 1990s, Applied Catalysts (1999) A188: 3-7.

Stejskal, J.; Gilbert, R.G., Polyaniline: Preparation of a conducting polymer (IUPAC technical report). Pure Appl. Chem. (2002), 74: 857–867.

Susilawati and ArisDoyan, Dose Response and Optical Properties of Dyed Poly Vinyl Alcohol-Trichloroacetic Acid Polymeric Blends Irradiated with Gamma-Rays, American Journal of Applied Sciences (2009), 6 (12): 2071-2077, ISSN 1546-9239.

Swinnen A, Verstraete J, Huyskens DP, Feasibility study of entrance in-vivo dose measurements with mailed thermo-luminescence detectors; Radiotherapy and Oncology (2004), Vol. 73 (1): 89-96.

Tauc, J., Amorphous and Liquid Semiconductors, Plenum Press (1974), New York. 1-196.

Thayalan, basic radiological physics: New Delhi; JaypeeBrothers' first edition (2001), ISBN 13: 9788171798544.

Vadapalli Chandrasekhar, Inorganic and Organometallic Polymers, Springer-Verlag Berlin Heidelberg, P. 1, 78, 80 (2005).

Venables K, Miles E, Aird E, Hoskin P., The use of in-vivo thermo-luminescent dosimeters in the quality assurance program for the START breast fractionation trial, Radiotherapy and Oncology (2004), Vol. 71, P: 303–310.

Vladimir Agabekov, NadezhdaIvanova, ViacheslavDlugunovich, and Igor Vostchula, Optical Properties of Polyvinyl Alcohol FilmsModified with Silver Nanoparticles, Hindawi Publishing Corporation, Journal of Nanomaterials (2012), Vol. (2012), pp. 1-5.

V. M. Harik, M. D. Salas, Trends in Nanoscale Mechanics, Kluwer Academic Publishers (2003).

V. Ravindrachary, R.F. Bhajantri, S.D. Praveena, B. Poojary, D .Dutta, P.K. Pujari, Polym. Degrad. Stab. 95 (2010) 1083-1091.

V. Singh, P. Chauhan, J. Phy. Chem. Solid. (2009), 70: 1074.

V. Yamakov, D, Wolf, S.R. Philipot, A.K. Mukherjee, H. Gleiter, Philos.j. Mag. Lette. 83 (2003) 385-393.

W. A. Jabbar, N. F. Habubi, S. S. Chiad, Optical Characterization of Silver Doped Poly (Vinyl Alcohol) Films, Journal of the Arkansas Academy of Science, vol: 64, 2010.

Wang, Y., N. Toshima,Preparation of Pd-Pt Bimetallic Colloids with ControllableCore/Shell Structures, J. Phys. Chem. B (1997), 101: 5301-5306.

Wankhede, Y.B.; Kondawar, S.B.; Thakare, S.R.; More, P.S., Synthesis and characterization of silver nanoparticles embedded in polyaniline nanocomposite, Adv. Mater. Lett.(2013), 4, doi:10.5185/amlett.2012.icnano.108.

Whiffen, D. H., Spectroscopy, 2nd. Edition (1971), Longman Group Ltd.

William R. Hendee, Ph.D. E. Russell Ritenour, Ph.D. (2002), MEDICAL IMAGING PHYSICS, ISBN 0-471-38226-4, New York, NY 10158-0012, (212) 850-6011.

W. L. McLaughlin, A. W. Boyd, K. H. Chadwick, J. C. McDonald and A. Miller, Dosimetry for Radiation Processing, Taylor & Francis, New York, (1989).

Wolfgang Demtroder, Atoms, Molecules and Photons An Introduction to Atomic, Molecular and Quantum Physics, ISBN-10 3-540-20631-0ISBN-13 978-3-540-20631-6Springer Berlin Heidelberg New York, 2006.

Yamauchi, T., Tansuriyavong, S., Doi, K., Oshima, K., Shimomura, M., Tsubokawa, N., Miyauchi, S. & Vincent, J.F.V., Preparation of composite materials of polypyrrole and electroactive polymer gel using for actuating system, Synthetic Metals.(2005), 152: 45-48.

Yano, S., Kurita K., Lwata K., Furukawa T., Kodomari M. Structure and properties of poly(vinyl alcohol)/tungsten trioxide hybrids. Polymer (2003), 44: 3515-3522.

Yoshio Waseda, Eiichiro Matsubara, KozoShinoda. X-Ray Diffraction Crystallography, Introduction, Examples and Solved Problems, ISBN 978-3-642-16634-1 e-ISBN 978-3-642-16635-8, DOI 10.1007/978-3-642-16635-8 Springer Heidelberg Dordrecht London New York (2011).

Zhu X R., Entrance dose measurements for in-vivo diode dosimetry, Comparison of correction factors for two types of commercial silicon diode detectors, Journal of applied clinical medical physics (2000), Vol. 1 (3), P: 100-107.

Zoetelief, J,. M. Fitzgerald, W. Leitzetal.1996: European protocol on dosimetry in mammography. EUR 16263 EN.